UNIVERSITY OF TURIN

PhD School in Life and Health Sciences
Molecular Medicine

XXIX Cycle
Academic Years: 2014-2017

Chronic wound management: a multidisciplinary, nonconventional, and innovative approach for antimicrobial and oxygenating nanotherapies.

Tutor: Dr. Giuliana Giribaldi
Co-tutor: Dr. Mauro Prato
Coordinator: Prof. Francesco Novelli

Nicole Finesso

Agli occhi di mia Madre.

INDEX

ABSTRACT 10
CHAPTER 1. INTRODUCTION 13
1.1. The skin 14
1.1.1. General structure and functions 14
1.1.2. The epidermis 14
1.1.3. The dermis 16
1.1.4. The subcutaneous fat layer 16
1.2. Wound Healing 16
1.2.1. Tissue repair and regeneration processes 16
1.2.2. Stages 17
1.2.2.1. Haemostasis 19
1.2.2.2. Inflammation 19
1.2.2.3. Re-epithelialisation 20
1.2.2.4. Remodelling 21
1.2.3. Chronic wounds 21
1.3. Infections 24
1.3.1. Infected wounds 24
1.3.2. MRSA 26
1.3.3. S. pyogenes 29
1.3.4. C. albicans 31
1.3.5. C. glabrata 34
1.4. Chronic wound management 36
1.4.1. Oxygen therapies 36
1.4.2. Treatments of infections 38
1.5. Nanotherapies 38
1.5.1. Current applications in biomedicine 38
1.5.2. Emerging biomaterials: chitin and chitosan species or derivatives 40
1.5.3. Micro and nanobubbles 43
1.5.4. Nanodroplets 47
CHAPTER 2. AIM OF THE STUDY 50
CHAPTER 3. MATERIALS AND METHODS 53
3.1. Materials 54
3.2. Methods 55
3.2.1. Nanobubble and nanodroplet preparation 55
3.2.2. Nanobubble and nanodroplet characterisation 55
3.2.3. *In vitro* determination of oxygen release from nanobubbles and nanodroplets 57
3.2.4. Nanobubble and nanodroplet sterilisation 57
3.2.5. Human cells, bacteria, and yeast 58
3.2.6. Confocal microscopy analysis on human keratinocytes incubated with MW cOLNBs 58

3.2.7. ATP assay 59
3.2.8. Cytotoxicity assay (LDH assay) 59
3.2.9. Cell viability assay (MTT assay) 60
3.2.10. Wound healing assay (scratch assay) 60
3.2.11. Confocal microscopy analysis on bacteria and yeasts 61
3.2.12. Microbiological assay on bacteria and yeasts 61
3.2.13. Statistical analysis 62
CHAPTER 4. RESULTS 63
4.1. Medium molecular weight chitosan nanobubbles 64
4.1.1. Medium molecular weight chitosan nanobubble physico-chemical characterisation 64
4.1.2. Mechanical interaction between medium molecular weight chitosan oxygen-loaded nanobubbles and human keratinocytes 67
4.1.3. Biocompatibility of medium molecular weight chitosan nanobubbles with human keratinocytes 69
4.1.4. Effects of hypoxia and medium molecular weight chitosan nanobubbles on the migration of human keratinocytes 71
4.1.5. Mechanical interaction between medium molecular weight chitosan nanobubbles and MRSA bacteria 73
4.1.6. Antibacterial activity of medium molecular weight chitosan nanobubbles on MRSA bacteria 75
4.1.7. Mechanical interaction between medium molecular weight chitosan nanobubbles and *C. albicans* yeasts 77
4.1.8. Antifungal activity of medium molecular weight chitosan nanobubbles on *C. albicans* yeasts 79
4.2. Medium molecular weight chitosan nanodroplets 81
4.2.1. Medium molecular weight chitosan nanodroplet physico-chemical characterisation 81
4.2.2. *In vitro* oxygen release from medium molecular weight chitosan oxygen-loaded nanodroplets 84
4.2.3. Mechanical interaction between medium molecular weight chitosan oxygen-loaded nanodroplets and human keratinocytes 86
4.2.4. Biocompatibility of medium molecular weight chitosan nanodroplets with human keratinocytes 88
4.2.5. Biocompatibility of medium molecular weight chitosan nanodroplets with human fibroblasts 90
4.2.6. Biocompatibility of medium molecular weight chitosan nanodroplets with human endothelium 92
4.2.7. Effects of hypoxia and medium molecular weight chitosan nanodroplets on the migration of human keratinocytes 94
4.2.8. Effects of hypoxia and medium molecular weight chitosan nanodroplets on the migration of human fibroblasts 96
4.2.9. Effects of hypoxia and medium molecular weight chitosan nanodroplets on the migration of human endothelium 98
4.2.10. Mechanical interaction between medium molecular weight chitosan nanodroplets and MRSA bacteria 99
4.2.11. Antibacterial activity of medium molecular weight chitosan nanodroplets on MRSA bacteria 101

4.2.12. Mechanical interaction between medium molecular weight chitosan nanodroplets and *S. pyogenes* bacteria 103
4.2.13. Antibacterial activity of medium molecular weight chitosan nanodroplets on *S. pyogenes* bacteria 105
4.2.14. Mechanical interaction between medium molecular weight chitosan nanodroplets and *C. albicans* yeasts 107
4.2.15. Antifungal activity of medium molecular weight chitosan nanodroplets on *C. albicans* yeasts 109
4.2.16. Mechanical interaction between medium molecular weight chitosan nanodroplets and *C. glabrata* yeasts 111
4.2.17. Antifungal activity of medium molecular weight chitosan nanodroplets on *C. glabrata* yeasts 113
4.3. Low molecular weight chitosan nanodroplets 115
4.3.1. Low molecular weight chitosan nanodroplet physico-chemical characterization 115
4.3.2. *In vitro* oxygen release from low molecular weight chitosan oxygen-loaded nanodroplets 118
4.3.3. Biocompatibility of low molecular weight chitosan nanodroplets with human keratinocytes 120
4.3.4. Biocompatibility of low molecular weight chitosan nanodroplets with human fibroblasts 122
4.3.5. Biocompatibility of low molecular weight chitosan nanodroplets with human endothelium 124
4.3.6. Effects of hypoxia and low molecular weight chitosan nanodroplets on the migration of human keratinocytes 126
4.3.7. Effects of hypoxia and low molecular weight chitosan nanodroplets on the migration of human fibroblasts 128
4.3.8. Effects of hypoxia and low molecular weight chitosan nanodroplets on the migration of human endothelium 130
4.3.9. Mechanical interaction between low molecular weight chitosan nanodroplets and MRSA bacteria 132
4.3.10. Antibacterial activity of low molecular weight chitosan nanodroplets on MRSA bacteria 134
4.3.11. Mechanical interaction between low molecular weight chitosan nanodroplets and S. pyogenes bacteria 136
4.3.12. Antibacterial activity of low molecular weight chitosan nanodroplets on S. pyogenes bacteria 138
4.3.13. Mechanical interaction between low molecular weight chitosan nanodroplets and *C. albicans* yeasts 140
4.3.14. Antifungal activity of low molecular weight chitosan nanodroplets on *C. albicans* yeasts 142
4.3.15. Mechanical interaction between low molecular weight chitosan nanodroplets and *C. glabrata* yeasts 144
4.3.16. Antifungal activity of low molecular weight chitosan nanodroplets on *C. glabrata* yeasts 146
CHAPTER 5. DISCUSSION 148
CHAPTER 6. CONCLUSION 160
CHAPTER 7. ACKNOWLEDGEMENTS 162

CHAPTER 8. REFERENCES 164
CHAPTER 9. PUBLICATIONS 184

FIGURE INDEX

CHAPTER 1. INTRODUCTION

Fig. 1. Structure of the human skin 15
Fig. 2. Timing and phases of wound healing 18
Fig. 3. Diabetic ulcers as examples of chronic wounds 23
Fig. 4. *S. aureus* clinical strain culture on MSA plate 27
Fig. 5. *S. pyogenes* clinical strain culture on blood agar plate 30
Fig. 6. *C. albicans* clinical strain culture on SAB agar plate 32
Fig. 7. *C. glabrata* clinical strain culture on SAB agar plate 35
Fig. 8. TOT and HBOT treatments 37
Fig. 9. Schematic representation of nanobubble structure 45
Fig. 10. Schematic representation of nanodroplet structure 48

CHAPTER 4. RESULTS

Fig. 11. Morphology and size distribution of MW cOLNBs 65
Fig. 12. MW cOLNB internalisation by human keratinocytes 68
Fig. 13. Effects of hypoxia and MW chitosan nanobubbles on human keratinocyte viability 70
Fig. 14. Effects of hypoxia and MW chitosan nanobubbles on migration and wound healing ability of human keratinocytes 72
Fig. 15. MW chitosan nanobubble adhesion to MRSA bacterial wall 74
Fig. 16. Antibacterial activity of MW chitosan nanobubbles on MRSA bacteria 76
Fig. 17. MW chitosan nanobubble internalisation by *C. albicans* yeasts 78
Fig. 18. Antifungal activity of MW chitosan nanobubbles on *C. albicans* yeasts 80
Fig. 19. Morphology and size distribution of MW cOLNDs 82
Fig. 20. Oxygen release from MW cOLNDs *in vitro* 85
Fig. 21. MW cOLND internalisation by human keratinocytes 87
Fig. 22. Effects of hypoxia and MW chitosan nanodroplets on human keratinocyte viability 89
Fig. 23. Effects of hypoxia and MW chitosan nanodroplets on human fibroblast viability 91
Fig. 24. Effects of hypoxia and MW chitosan nanodroplets on human endothelium viability 93
Fig. 25. Effects of hypoxia and MW chitosan nanodroplets on the migration and wound healing abilities of human keratinocytes 95
Fig. 26. Effects of hypoxia and MW chitosan nanodroplets on the migration and wound healing abilities of human fibroblasts 97
Fig. 27. MW chitosan nanodroplet adhesion to MRSA bacterial wall 100
Fig. 28. Antibacterial activity of MW chitosan nanodroplets on MRSA bacteria 102
Fig. 29. MW chitosan nanodroplet internalisation by *S. pyogenes* bacteria 104

Fig. 30. Antibacterial activity of MW chitosan nanodroplets on *S. pyogenes* bacteria 106
Fig. 31. MW chitosan nanodroplet internalisation by *C. albicans* yeasts 108
Fig. 32. Antifungal activity of MW chitosan nanodroplets on *C. albicans* yeasts 110
Fig. 33. MW chitosan nanodroplet internalisation by *C. glabrata* yeasts 112
Fig. 34. Antifungal activity of MW chitosan nanodroplets on *C. glabrata* yeasts. 114
Fig. 35. Morphology and size distribution of LW cOLNDs. 116
Fig.36 *In vitro* oxygen release from LW cOLNDs 119
Fig. 37. Effects of hypoxia and LW chitosan nanodroplets on human keratinocyte viability 121
Fig. 38. Effects of hypoxia and LW chitosan nanodroplets on human fibroblast viability 123
Fig. 39. Effects of hypoxia and LW chitosan nanodroplets on human endothelium viability 125
Fig. 40. Effects of hypoxia and LW chitosan nanodroplets on the migration and wound healing abilities of human keratinocytes 127
Fig. 41. Effects of hypoxia and LW chitosan nanodroplets on the migration and wound healing abilities of human fibroblasts 129
Fig. 42. Effects of hypoxia and LW chitosan nanodroplets on the migration and wound healing abilities of human endothelium 131
Fig. 43. LW chitosan nanodroplet internalisation by MRSA bacteria 133
Fig. 44. Antibacterial activity of LW chitosan nanodroplets on MRSA bacteria 135
Fig. 45. LW chitosan nanodroplet internalisation by *S. pyogenes* bacteria 137
Fig. 46. Antibacterial activity of LW chitosan nanodroplets on *S. pyogenes* bacteria. 139
Fig. 47. LW chitosan nanodroplet internalisation by *C. albicans* yeasts 141
Fig. 48. Antifungal activity of LW chitosan nanodroplets on *C. albicans* yeasts 143
Fig. 49. LW chitosan nanodroplet internalisation by *C. glabrata* yeasts 145
Fig. 50. Antifungal activity of LW chitosan nanodroplets on *C. glabrata* yeasts. 147

TABLE INDEX

CHAPTER 1. INTRODUCTION
Table 1. Comparison between TOT and HBOT approaches 37
CHAPTER 3. MATERIALS AND METHODS
Table 2. Composition of nanobubble formulation, nanodroplet, and OSS formulations 56
CHAPTER 4. RESULTS
Table 3. Physico-chemical characterisation of MW cOLNBs and MW cOFNBs. 66
Table 4. Physico-chemical characterisation of MW cOLNDs and MW cOFNDs. 83
Table 5. Physico-chemical characterisation of LW cOLNDs and LW cOFNDs 117

ABSTRACT

Background. Throughout all wound healing phases, skin cells act in an orchestrated manner, playing crucial roles to promote wound closure. Chronic wounds (CWs), including pressure, venous, and diabetes-associated ulcers, fail to proceed through an ordered and timed healing, representing a silent epidemic among the elderly and costing millions of euros per year. CWs are typically characterised by persistent tissue hypoxia, exacerbated inflammation, and impaired matrix remodelling. Moreover, CWs are often worsened by microbial infections, with antimicrobial therapies being hindered by emerging resistant strains. The known benefits of nanotechnology combined with the advantages of antimicrobial properties of natural polysaccharides such as chitosan have paved the way for the development of new oxygen-based therapies to treat infected CWs. In this context, our collaborative research network has developed and patented two platforms of innovative and cost-effective shell/core-structured oxygen nanocarriers (perfluoropentane (PFP)-cored nanobubbles and 2H,3H-decafluoropentane (DFP)-cored nanodroplets). In the present study, these carriers were alternatively shelled with two chitosan molecules of different molecular weight [medium weight (MW) or low weight (LW) chitosan, respectively]. After manufacturing, MW chitosan-shelled oxygen-loaded nanobubbles (cOLNBs), as well as MW or LW chitosan-shelled oxygen-loaded nanodroplets (cOLNDs) were comparatively characterised for morphology and physico-chemical properties. Their biocompatibility and their ability to promote wound healing in human hypoxic skin cells were challenged by using keratinocyte, fibroblast, and/or endothelial cell lines, whereas their antimicrobial activity was investigated by using methicillin-resistant *Staphylococcus aureus* (MRSA), *Streptococcus pyogenes*, *Candida albicans*, and *C. glabrata* clinical strains. For each cell type, the mechanical interaction with nanocarriers was also assessed.

Materials and Methods. After manufacturing, cOLNBs (only MW) and cOLNDs (either MW or LW), as well as control oxygen-free nanobubbles (cOFNBs) and nanodroplets (cOFNDs), were characterised for morphology and physico-chemical properties by microscopy and dynamic light scattering, respectively. *In vitro* oxygen releases from cOLNBs and cOLNDs or from control oxygen saturated-solution (OSS) were comparatively measured through an oxymeter. After sterilisation by UV-C rays, each formulation was carefully checked for microbial contamination or ROS production; if either of these was detected, the sample was discarded before use. For biological studies, human cells (HaCaT, HDF, and HMEC-1 cell lines) or microbial clinical strains (MRSA, *S. pyogenes*, and *C. albicans or glabrata*) were firstly incubated in normoxic conditions (20% O_2) up to 24 h with 10% v/v nanocarrier formulations, and preliminary analyses by confocal microscopy were conducted to evaluate the mechanical interactions between nanocarriers and human or microbial cells. Then, the investigation on biocompatibility, wound healing, and antimicrobial activity was performed. On the one hand, human skin cell populations were incubated in normoxic (20% O_2) or hypoxic (1% O_2) conditions for 24 h with 10% v/v cOLNBs or cOLNDs, cOFNBs or cOFNDs, and OSS, and biocompatibility was assessed by using LDH, MTT, and ATP assays, whereas wound healing was investigated through scratch assay. On the other hand, microbial strains were incubated in normoxic conditions for increasing times up to 24 h with 10% v/v cOLNBs or cOLNDs as well as cOFNBs or cOFNDs, and their antimicrobial activity was measured by monitoring bacterial or fungal growth over time.

Results. i) MW cOLNBs displayed spherical shell-core structures, cationic surfaces, and 700 nm average diameters, and were able to release clinically relevants amounts of oxygen *in vitro* in a time-sustained manner. After cellular internalisation, they did not show significant cytotoxicity and they effectively restored a normoxia-like migratory phenotype in hypoxic human keratinocytes. Short-term (up to 6 h) antibacterial activity against MRSA was associated with prolonged adhesion to bacterial cell walls, whereas long-term (up to 24 h) antifungal activity against *C. albicans* was associated with early cell internalisation. ii) Similarly, MW cOLNDs displayed spherical shell-core structures, cationic surfaces, and 700 nm average diameters. Interestingly, oxygen release from MW cOLNDs was higher and more prolonged with respect to cOLNBs. After cell internalisation, MW cOLNDs were not significantly toxic to human keratinocytes and fibroblasts, whereas they strongly compromised endothelial cell viability. Consequently, they proved effective in restoring a normoxia-like migratory phenotype in hypoxic keratinocytes and fibroblasts, but not in endothelial cells. Short-term antibacterial activity against MRSA was associated with prolonged adhesion to bacterial cell walls, whereas long-term antibacterial or antifungal activities against *S. pyogenes* or *C. albicans* and *glabrata*, respectively, were associated with early cell internalisation. iii) LW cOLNDs displayed morphological, physico-chemical, and oxygen-related characteristics similar to those of MW cOLNDs. However, they had smaller diameters (~400 nm) and were significantly less toxic to all the investigated human skin cell populations with respect to MW cOLNDs. They were able to restore a normoxia-like migratory phenotype not only in hypoxic human keratinocytes and fibroblasts, but also in endothelium. They were avidly internalised by MRSA, *S. pyogenes*, *C. albicans* and *C. glabrata* yeasts and inhibited the growth of all microorganisms up to 24 h of incubation with the exception of MRSA, which was inhibited only up to 6 h.

Conclusion. In the present study, three different oxygen nanocarriers (MW cOLNBs, MW cOLNDs, and LW cOLNDs) were challenged for their morphological and physico-chemical properties, oxygen release abilities, mechanical interaction with human or microbial cells, biocompatibility with human skin cells, abilities to promote wound healing, and antimicrobial properties. All carriers displayed spherical morphology, cationic surfaces, and diameters in the nanometer range. However, *in vitro* oxygen release from OLNDs appeared higher and more sustained over time than from OLNBs. Additionally, LW chitosan-shelled nanodroplets displayed lower toxicity to skin cells than MW chitosan-shelled carriers. Compared to MW cOLNBs/cOLNDs, LW cOLNDs displayed in general similar or better efficacy in promoting wound healing under hypoxic conditions and in inhibiting microbial growth in a long-term manner as a consequence of early cellular internalisation. Based on these findings, LW cOLNDs appear to be the most promising nanocarriers among those tested here to be potentially employed as innovative, nonconventional, and cost-effective medical devices for the treatment of hypoxic and infected CWs.

CHAPTER 1.
INTRODUCTION

1.1. The skin

1.1.1. General structure and functions

The skin is an organ of the tegumentary apparatus that covers the human body completely. It is the largest organ of the body and its weight represents the 16% of the whole organism[1] The skin has a mean surface of ~1.8 m^2 and its thickness ranges from 0.5 to 4 mm, depending on its distribution throughout the body and on the owner's sex[2]. This organ is composed of various tissues and consists of three different layers: from the most external, these layers are respectively named epidermis, dermis, and subcutaneous fat layer[3] (see Fig. 1A). The skin separates and protects the body from the external environment[4]. Moreover, it provides protection for the soft tissues and is involved in thermoregulation[5], sensory perception[6], secretions of sweat glandes[7], and absorption of UV rays[8].

1.1.2. The epidermis

The epidermis (see Fig. 1B) is a stratified squamous epithelium consisting of several cell types, including Langerhans cells, melanocytes, and keratinocytes (>90%)[9]. It serves mainly to form a physical barrier, to protect the organism against external agents and pathogens, and to limit fluid loss[4,9–11]. S*tratum corneum*, the outermost layer, is composed of dead anuclear corneocytes that are surrounded by a lipid matrix, generating a functional barrier[12]. Under the *stratum corneum*, the *stratum lucidum* - well visible only in the thick epidermis of palms or soles - represents a transition layer from the *stratum corneum* to the *stratum granulosum*[13]. The *stratum granulosum* contains dead keratinocytes expressing loricrin, filaggrin, and involucrin proteins[14]. Under the *stratum granulosum*, the *stratum spinosum* is composed by Langerhans cells and keratinocytes (namely spinous cells)[15]. In this context keratinocytes generate membrane-coating lipid-filled granules, called lamellar bodies, and express keratin 1 (K1) and keratin 10 (K10)[16]. Furthermore, keratinocytes adhere to the surrounding cells through adherent junctions and desmosomes. The *stratum spinosum* is tightly adherent to the innermost layer, the *stratum basale*[17].

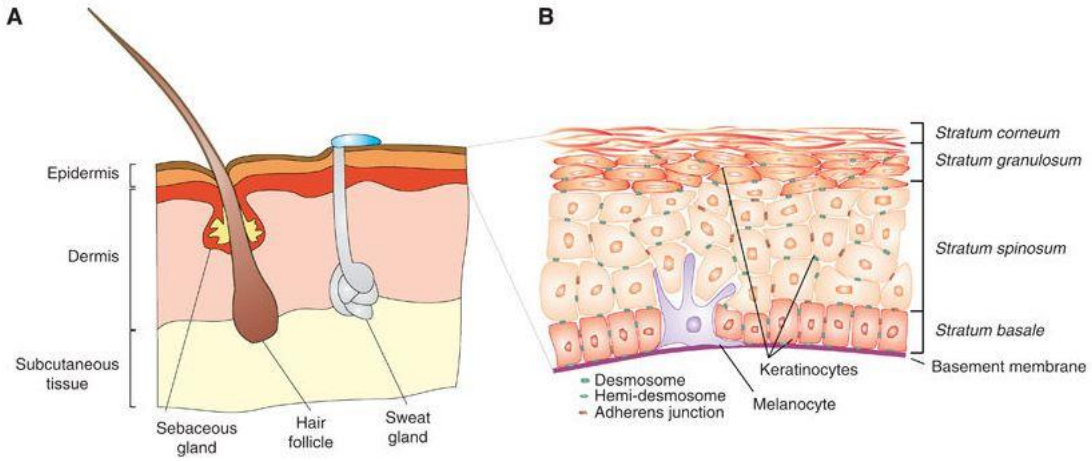

Fig. 1. Structure of the human skin. The skin is characterised by three different layers: the epidermis, the dermis, and the subcutaneous fat layer (panel A). The outermost layer, the epidermis, is a tightly regulated stratified epithelium consisting of *stratum corneum, stratum granulosum, stratum spinosum,* and *stratum basale* (panel B). Adapted from Kern et al[18].

The extracellular matrix (ECM) forms the basement membrane, a layer that separates the epidermis from the underlying dermis. ECM components are secreted by basal cells[19]. These cells are intermixed with minor populations of sensory Merkel cells, melanocytes and leukocytes[20,21].

1.1.3. The dermis

The dermis is located between the epidermis and the subcutaneous fat layer. It is a specific connective tissue composed predominantly by type I collagens fibers and elastic fibers[22]. The dermis consists of two layers: the outer papillary layer and the deeper reticular layer[23]. It feeds the epidermis and provides the skin with strength and flexibility[24]. Moreover, the dermis contains sweat and sebaceous glands, sensory cells, nerves and blood vessels[25].

1.1.4. The subcutaneous fat layer

The subcutaneous fat layer, also called adipose layer, is composed by connective tissue which is rich in adipocytes[26]. It binds the dermis to the underlying structures and serves to store energy[27]. This layer varies in thickness depending on the owner's age, sex and health status[28].

1.2. Wound Healing

1.2.1. Tissue repair and regeneration processes

The first function of the skin is to provide a protective barrier against the external environment[4]. However, when injury or illness occur, they can provoke an integrity loss in large portions of the skin, even leading to major disability or death[29]. Wound healing is a complex and highly regulated process that aims at repairing skin integrity after injury[30]. To restore tissue integrity and homeostasis, several pathways must be activated, following precise time sequences and requiring different cell types to act in concert[31].

The primary goals of wound repair processes are rapid wound closure as well as functional and aesthetical scar formation. In several wounds, only the epidermis needs to be regenerated, resulting in quick healing and minimal scar formation.

However, deep wounds penetrate throughout the dermis, triggering skin avulsion and inducing an exposure of the subcutaneous fat layer. In this case, the wound healing processes are complex and time-consuming, often leading to the formation of visible and anti-aesthetic scars[32]. Additionally, in deep wounds some serious complications such as bacterial and fungal infections are prone to develop more frequently[33].

Regardless of its depth, a wound can generally heal through two mechanisms: repair or regeneration. Repair occurs when no exact substitution of the lost or damaged tissue is needed in the injury area, thus requiring just a physiological adaptation of the organ to restore continuity[31]. On the contrary, regeneration replaces the lost or damaged tissue with an exact copy so that its morphology and function are restored[34]. Human skin cannot regenerate spontaneously, however it undergoes tissue repair processes, leading to scar formation after healing[35].

1.2.2. Stages

Wound healing is a dynamic and interactive process, involving soluble mediators, ECM proteins, as well as blood and parenchymal cells[36]. Wound healing can be divided in four overlapping phases: haemostasis, inflammation, tissue proliferation (or re-epithelialisation), and tissue remodelling[37] (see Fig. 2). After skin injury, a series of biochemical events take place in a closely orchestrated cascade to repair the damaged tissue. The duration of wound healing processes is different across individuals and it often varies depending on wound severity[38]. In order to allow cell proliferation, differentiation, and migration, a strong alteration of gene expression and phenotype of immune cells, endothelial cells, keratinocytes and fibroblasts occurs[37]. In general, these processes take place in almost all tissues after being exposed to almost any destructive stimuli. Numerous nutritional cofactors have proven to be important in wound healing, including proteins, vitamins, and minerals[39]. In particular, the intake of nutritional sources such as A and C vitamins, as well as zinc, have been suggested to ensure optimum wound healing[40].

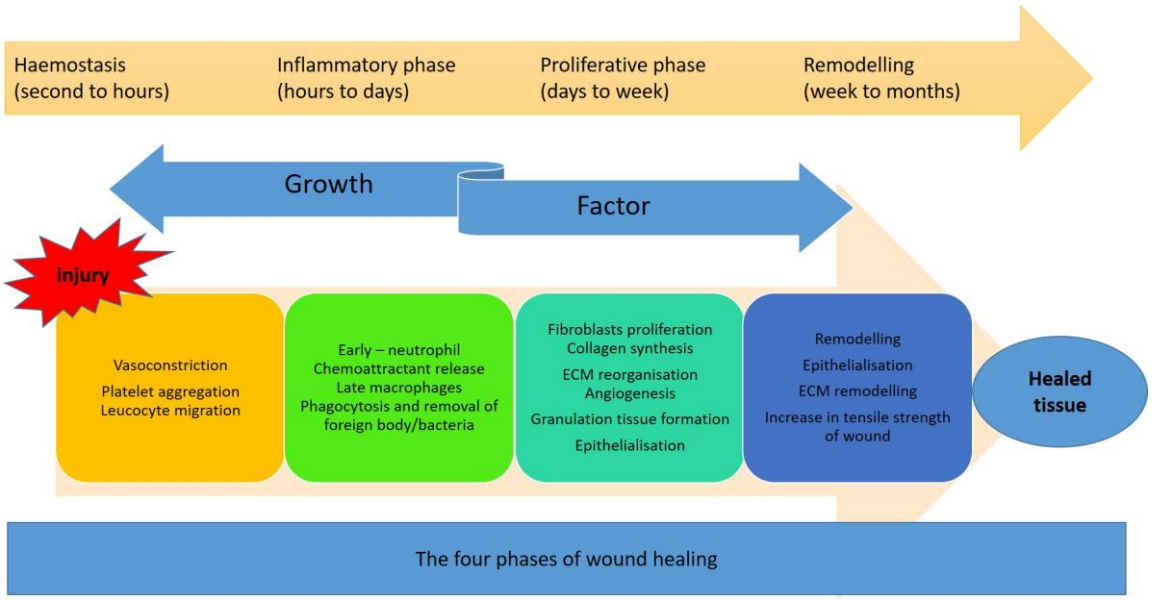

Fig. 2. Timing and phases of wound healing. As the injury occurs, wound healing processes initiate immediately. Classically, four phases are identified: haemostasis, inflammation, re-epithelialisation, and remodelling. These four stages are spatio-temporally overlapping and can even last for years. Adapted fromThiruvoth et al[41].

1.2.2.1. Haemostasis

The first stage of wound repair is haemostasis. Tissue injury causes the disruption of blood vessels and the extravasation of blood constituents. Immediately after damage, platelets aggregate and trigger clot formation together with components of the coagulation cascade[42,43].

1.2.2.2. Inflammation

The second stage of wound healing is inflammation, occurring within few hours after haemostasis. The recruitment of the immune system along with the activation of several inflammatory pathways are needed to avoid blood and fluid loss, to remove dead and devitalised tissues, and to prevent infection[29].

The blood clot re-establishes temporarily the integrity of the skin and provides a provisional ECM for cell migration. Platelets not only facilitate the formation of a haemostatic plug during the first stages of repair but also secrete several mediators of wound healing[44,45]. Numerous vasoactive mediators (including histamine, serotonin, bradykinin, C3a, and fibrinopeptides) and chemotactic factors [including inflammatoy chemokines, platelet derived growth factor (PDGF), and C5a] are generated by parenchymal cells as well as through coagulation and complement pathways[46].

The primary function of these substances is to recruit leukocytes towards the damaged site. Monocytes infiltrate the wound site in response to specific chemo-attractants, and after binding ECM proteins they differentiate into macrophages, releasing growth factors such as PDGF and vascular endothelial growth factor (VEGF)[47]. Neutrophils also infiltrate the damaged area, cleansing the tissue from foreign particles and pathogenes that have been extruded with the eschar or phagocytosed by macrophages[48]. Macrophages initiate the formation of granulation tissue by binding to specific proteins of the ECM through their integrin receptors, an action that also stimulates phagocytosis of microorganisms and ECM fragments[49]. Monocytes and macrophages express colony-stimulating factor-1 (CSF-1) and tumor necrosis factor α (TNF-α), two cytokines that are respectively essential for their survival and for triggering the inflammatory processes[50]. Macrophages and related factors are crucial for the initiation and propagation of new tissue formation in wounds, as confirmed by experiments on macrophage-depleted animals displaying defective wound repair[51].

1.2.2.3. Re-epithelialisation

The third stage of wound healing (proliferation or re-epithelialisation) is characterised by new tissue formation[52]. Wound re-epithelialisation begins within hours after injury. Keratinocytes quickly remove the clotted blood and the damaged stroma from the wound space. Subsequently, these cells undergo activation through changes in the cytoskeleton network and expression of cell surface receptors[53]. These changes include retraction of intracellular tonofilaments, dissolution of most inter-cellular desmosomes, and formation of peripheral cytoplasmic actin filaments[53,54]. Furthermore, in response to dissolution of hemidesmosomal links, the epidermis detaches from the basement membrane, resulting in an epidermal cell disunion from dermal cells[29,55]. Keratinocytes express on the surface membrane some integrin receptors that allow them to interact with ECM proteins such as fibronectin and vitronectin[56]. Both proteins are interspersed along with type I collagen in the wounded area, especially at the margin of the wound and within the fibrin clot on the damaged site.

Keratinocytes migrate and dissect the wound, separating eschar from viable tissue. ECM degradation, which is required for keratinocyte migration, depends on the production of collagenases by keratinocytes, as well as on the activation of plasmin by plasminogen activator[57,58]. Plasminogen activator (uPA) also activates some collagenases, especially matrix metalloproteinase-1 (MMP-1), thus facilitating the degradation of collagen and ECM proteins[59,60].

One or two days after the damage, skin cells at the wound margin begin to proliferate behind the actively migrating cells. As soon as re-epithelialisation begins, the proteins at the basement membrane reappear in a very ordered zip-like sequence from the edge of the wound inward while keratinocytes return to their normal phenotype once they are firmly anchored to the basement membrane and the underlying dermis through hemidesmosomal proteins, intergrins and collagan fibrils[42,61].

After a few days from injury, new blood vessels form through angiogenesis and macrophages replace the fibrin matrix with granulation tissue, also called new stroma. Angiogenesis, a complex mechanism depending on ECM degradation and on endothelial cell stimulation in the wounded area, also contributes to the formation of granulation tissue[62].

About four days after injury, new stroma starts to invade the wound space[63]. Since then, macrophages, fibroblasts, and blood vessels act in concert in the damaged area. Several growth factors secreted by macrophages, such as PDGF and transforming growth factor β (TGF- β), as well as structural molecules of the newly formed ECM ("temporary matrix"), including fibrin, fibronectin, and hyaluronic acid, stimulate the surrounding tissutal fibroblasts to proliferate, to express appropriate integrin receptors, and to migrate into the wound space[64,65]. Interestingly, PDGF was reported to accelerate the healing of chronic pressure sores and diabetic ulcers[66], whereas basic fibroblast growth factor (bFGF) was used with some success to treat chronic pressure sores[67].

1.2.2.4. Remodelling

Stimulated fibroblasts are responsible for ECM synthesis, deposition, and remodelling[68]. At this point, tissue remodeling - the fourth and final phase of wound healing - is taking place. During this last stage, the temporary matrix is gradually replaced by a collagenous matrix[29,69]. At first, fibroblasts deposite abundant collagen into the wound. Then, fibroblast-rich granulation tissue is covered by a nearly acellular scar and all remaining cells undergo apoptosis or exit the wound. Suddenly, wound begin to constrict itself.

Cells interact with ECM and cytokines to promote wound contraction. In particular, during the second week of healing, fibroblasts differentiate to myofibroblasts, displaying large bands of actin-containing microfilaments along the cytoplasmic side of the cell membrane as well as near both intercellular and cell-matrix junctions[70].

Matrix remodeling depends on continuous low-rate anabolism and collagen catabolism. Indeed, collagen ultimately forms the bulk of the mature scar, with the acellular matrix being actively remodelled from type III to type I collagen by the proteolytic action of MMPs[71].

1.2.3. Chronic wounds

Normally, wounds such as lacerations are being expected to heal within a predictable time frame. These uncomplicated wounds, which usually heal within 4-6 weeks, are known as acute wounds[72]. However, in some cases inflammation becomes persistent, causing pathological conditions and leading to chronic wound

(CW) formation. Specifically, a CW represents a break in epithelial continuity of the skin lasting more than 42 days[73]. Such a long-lasting wound has failed in one of the four stages of wound healing, usually inflammation. Bedsores, burns, and diabetes-associated vasculopathies are typical examples of CWs. A CW shows decreased levels of epidermal growth factor (EGF), FGF, TGF-β, PDGF, interleukins-1 and -6 (IL-1, IL-6), and TNF-α[74].

In diabetic ulcers (see Fig. 3) the combination of either physiological or biochemical defects leads to unsuccesful healing. These ulcers usually occur in patients who are unable to sense cutaneous pressure because of neuropathy[75]. Diabetic ulcers are also complicated by infections as a consequence of impaired granulocytic function and chemotaxis[29,76]. Other complications might rise due to prolonged inflammation, impaired neovascularisation, minor synthesis of collagen, or exacerbated levels of proteinases[77]. In these conditions, abnormalities in cell migration, proliferation, and inflammation often occurr[78]. Moreover, abnormalities in synthesis and secretion of ECM proteins or cytokines, as well as in matrix remodelling have been described[79]. Furthermore, it was recently proposed that anomalous epidermal–mesenchymal interactions and mutations in regulatory genes such as p53 might be responsible for abnormal healing processes[80,81].

CWs affect a large fraction of the population worldwide, especially among the elderly, raising a major and gathering threat to the public health and economy of developed countries, including Europe and the United States[82]. Alarmingly, it has been estimated that 1-2% of the population of developed countries will experience at least one CW during their lifetime[82]. In the Scandinavian countries, the costs related to CW management account for 2-4% of the total health care expenses[83]. In the United States alone, CWs affect 6.5 million patients[29,74,82,84,85]. Diabetic foot, pressure, and venous leg ulcers, pose a considerable economic burden, costing to the National Health Service in the United States an estimated $ 20 billion per year[86,87]. The price of managing a single full-thickness pressure ulcer is as much as $70,000, and American expenditure for treating pressure ulcers has been estimated at $11 billion per year[88,89].

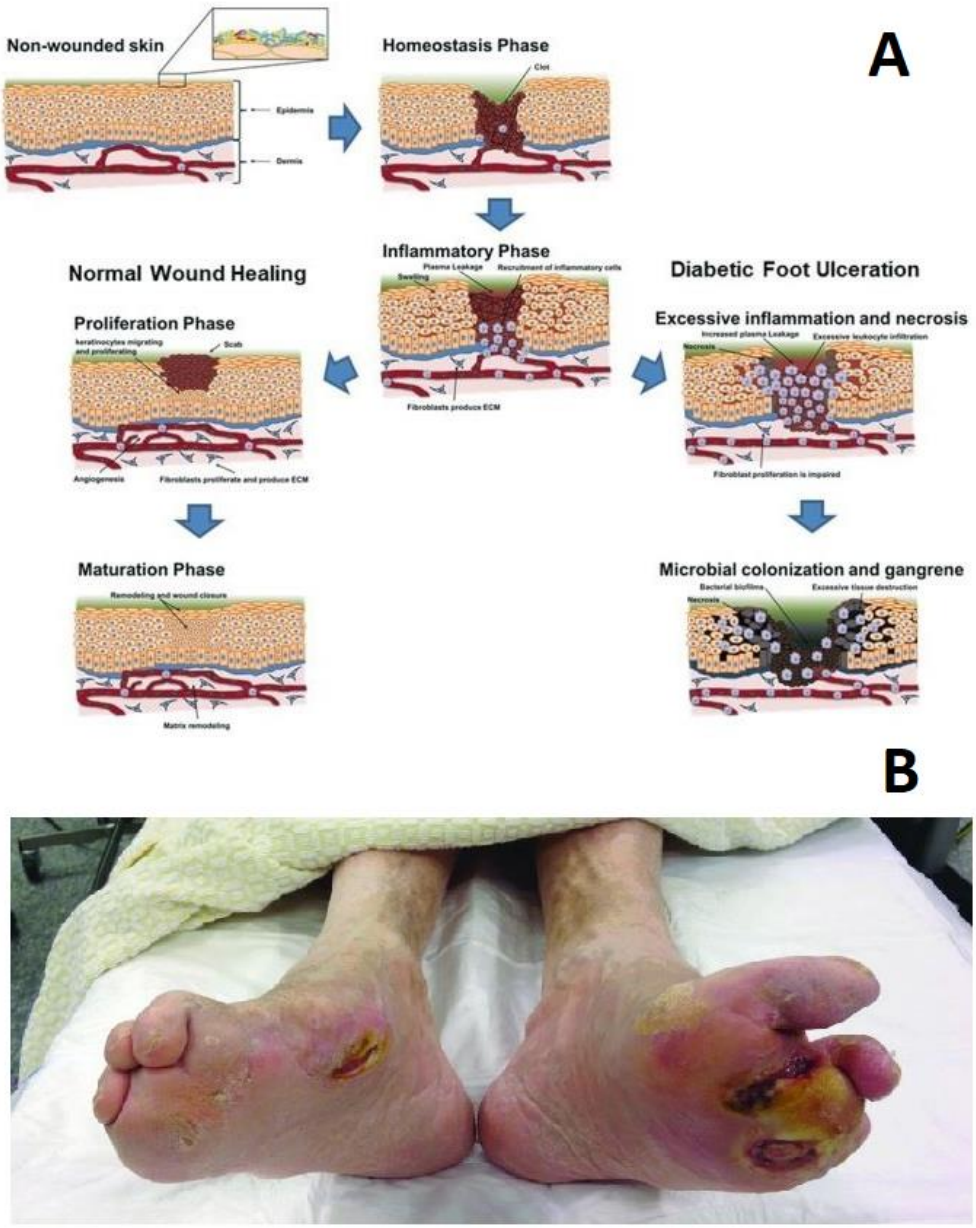

Fig. 3. Diabetic ulcers as examples of chronic wounds. Panel A. Schematic evolution of skin lesion into acute (left diagram) or chronic wound (right diagram) in a diabetic patient. Panel B. Representative image of diabetic foot ulcers. Adapted from Pereira et al[90] and Naves[91].

Some important contributors to the costs for CW management include outpatient/physician office visits, emergency department visits, hospitalisations, and amputations for diabetic foot ulcers[92,93]. The number of hospitalised patients with pressure ulcers has risen by 63% over the last ten years and approximately 60,000 deaths per year occur from hospital-acquired pressure ulcers[94].

Alarmingly, diabetes mellitus has been estimated to affect more than 371 million people worldwide, with the number of patients increasing everywhere[95]. Unfortunately also obesity, another pathology often associated with venous leg and diabetic foot ulcers, is on the rise all over the world[82,96].

1.3. Infections

1.3.1. Infected wounds

Chronic wounds are characterised by hypoxia, persistent inflammation, and unbalanced levels between proteinases and their inhibitors, both essential to accomplish the remodelling phase of healing[97–100]; furthermore, chronic wounds are often complicated by microbial infections[101]. Hospitalised patients with autoimmune diseases or immunocompromised patients are affected by local or overt infections, often worsened by the spreading of multi-resistant germs[102,103]. Notably, costly complications such as infections occur when wounds are open. Therefore, any treatments able to heal a significant percentage of wounds quickly, completely, and persistentlly would improve the clinical outcomes substantially, thus reducing the overall costs – in spite of the expenses for the therapeutics being high at the beginning[104].

The role of microorganisms in the healing processes has not been fully elucidated yet. Nevertheless, antimicrobials have been applicated topically for a long time, attempting to prevent infections in the wound area. In general, wound colonisation by bacteria is frequent and usually it is not a dangerous process[105]. A critical threshold of 10^5 colony-forming units (CFU) per mm^3 in the milieu of the wound has been proposed as the limit between normal microbial colonisation and clinically relevant infection[106,107]. Different microorganisms with distinct pathogenic degree can be isolated from the same infected wound. For this reason, infections can be differentiated from colonisation based on the evaluation of intrinsic

virulence potential to identify the pathogenic degree for each isolated bacterial strain[101].

Depending on the etiopathological agent, skin infections differ in severity, from simple pustular lesions of the integument to more spreading diseases[108]. In particular, as emerged from bacterial profiling of chronic wounds such as chronic venous leg ulcers, the most commonly isolated bacterial species (spp) are: *Staphylococcus aureus* (93.5%); *Enterococcus faecalis* (71.1%); *Pseudomonas aeruginosa* (52.2%); coagulase-negative *Staphylococcus* spp (45.7%); *Proteus* spp (43.1%); and anaerobic bacteria (39.1%)[109]. In this context, it should be noticed that *S. aureus* and *P. aeruginosa*, as well as *Streptococcus pyogenes* or S. *epidermidis*, often develop drug resistance, thus creating a serious obstacle for antimicrobial wound management, as clearly exemplified by the case of methicillin-resistant *S. aureus* (MRSA)[103,110].

During diabetic foot infection, wound healing is hampered by several factors, including low growth factor activity, reduced cellular proliferation, and elevated levels of inflammatory markers and proteases[111]. In addition, some bacteria produce specific proteases playing several roles in healing of infected wounds. In this context, the secretion of bacterial proteases has been associated with growth and potential virulence, as well as with skin attachment and penetration[97]. Bacterial proteases can also trigger the degradation of components of the complement system[112,113]. Finally, some microbial proteases play an important role in the protein degradation of human ulcer fluid and in the inhibition of fibroblast growth: for example, a MMP-like elastase produced by *P. aeruginosa* can activate the degradation of fibroblast proteins and proteoglycans as well as that of immune cell mediators in chronic wounds[114]. In conclusion, the proteases secreted by human and bacterial cells have been suggested to be crucial enzymes in wound repair, acting in a coordinated manner to keep the wound chronic[115].

Aside from bacteria, fungal infections are also often involved in worsening chronic wounds. Fungal infections, including those associated with burns or wounds, are a common cause of morbidity, mortality and cost in critical care population[116,117]. In a recent and extensive multicentric review, fungi were isolated at least once from 6.3% of burn patients, with positive cultures being obtained most commonly from the wound itself[117].

Candida spp are among the most common fungal pathogens identified in humans, with almost 96% of all opportunistic mycoses being caused by *Candida* spp.[118–121] Notably, infections triggered by *Candida* spp constitute a major threath for diabetic wounds, leading to delay in wound healing process[122]. *C. albicans* has generally been referred as the main yeast isolated in fungal infections[123,124]; nevertheless, non-*albicans Candida* (NAC) spp represent now a substantial portion of clinical isolates identified in hospitals worldwide. *C. glabrata*, *C. tropicalis*, *C. parapsilosis*, and *C. krusei* are all NAC spp with peculiar clinical relevance[121]. An increasing incidence of *C. glabrata* has been reported especially in Asia-Pacific and the European Union[125].

In healthy people, *Candida* spp trigger infection rarely. However, when either local or systemic impairment of the host immune system occurs, *Candida* yeasts are allowed to proliferate uncontrolled, causing a pathological condition named candidiasis[121,126]. Such a condition is classified into three main subgroups: cutaneous, mucous, and systemic candidiasis[121]. The number of these infections has been generally rising in the past three decades, in spite of a slight drop occurring almost ten years ago, between 2005 and 2007[125]. Several factors have increased the risk of fungal infections, including broad spectrum antibiotics, immunocompromission, cytotoxic chemotherapy, and transplantation[127–129].

In the United States, *Candida* spp are ranked fifth among hospital-acquired pathogens and cause 8% to 10% of nosocomial bloodstream infections[120,130–132]. Moreover, mortality due to nososcomial candidemia between 1997 and 2001 was 61%[133,134].

1.3.2. MRSA

S. aureus, both a commensal bacterium and a human pathogen[135], is a Gram-positive bacterium which aggregates characteristically in irregular groups like clusters of grapes[136]. One of the better-known selective media used for staphylococcal isolation and identification is mannitol-salt agar (MSA), which turns from the red to yellow[137] in the presence of a mannitol-positive colony (Fig. 4). *S. aureus* is responsible for the majority of cutaneous infections, where severe tissue hypoxia leads to final necrosis of the tissue[138–140].

Fig. 4. *S. aureus* clinical strain culture on MSA plate. Bacterial colonies show mannitol fermentation.

Neutrophils are crucial during *S. aureus* infection as they firstly act to protect organisms from pathogen invasion. Immediately after *S. aureus* entering the injured skin, neutrophils together with macrophages migrate to the infected area[141]. However, *S. aureus* is able to evade cellular responses of the host using different mechanisms[142]. For example, adhesion to surface components - the first event occurring at the beginning of diabetic foot infection - depends on bacterial expression of numerous surface proteins[135]. These receptors correspond to adhesins or microbial surface components recognising adhesive matrix molecules (MSCRAMMs)[143–147]. Moreover, a specific staphylokinase produced by *S. aureus* (Sak) seems to be related to the activation of plasminogen into plasmin, which in turn degrades fibrin clots and ECM components and activates proMMPs into MMPs[148].

Penicillin was the first antibiotic to be used for therapy against *S. aureus* infections. However, starting from the 1940s, several cases of bacterial resistance to this drug were reported[149] and a penicillin-resistant *S. aureus* strain was isolated for the first time in 1942[150]. In 1959, methicillin was developed and successfully applied to clinical practice in order to solve the calamity of penicillin-resistant *S. aureus* strains[151]. However, just two years later, British scientists isolated the first strains of MRSA[152], able to resist to most β-lactam antibiotics. At first, infections were confined to hospitals (health-associated MRSA, HA-MRSA), but since the 1990s the incidence of MRSA infections has arised in the community (community-associated MRSA, CA-MRSA), with frequent infections being reported from many countries worldwide[153]. Recently, MRSA strains were also found to colonise or infect livestock and livestock-exposed humans (livestock-associated MRSA, LA-MRSA)[154].

Complications related to HA-MRSA infections have achieved considerable dimensions in Europe[155]. HA-MRSA infections are not only resistant to beta-lactam antibiotics but they also lack sensitivity towards other antibacterial drugs[156]. For some decades, vancomycin and conventional glycopeptides have been administrated as the gold standard for therapy of MRSA infections[157]. However, the use of these antibiotics has started to decrease after the appearance of resistance cases in *Enterococcus* spp and subsequently in *S. aureus*[158,159].

Currently, the alternative therapeutic approaches to treat MRSA infections include: natural antibacterial compounds, such as β-asarone from *Acorus calamus* rhizome and mansonone F(1) from *Ulmus davidiana* var. *japonica*[160]; medical compounds originally developed for other purposes and currently studied for their possible antibacterial properties, such as bacteriocins and lysostaphin[161,162]; cationic antimicrobial peptides, such as defensins and cathelicidin[163,164]; bacteriophages[165]; photodynamic therapy[166]; and staphylococcal vaccines, including those targeting MSCRAMM adhesion proteins[167].

1.3.3. *S. pyogenes*

Streptococcus spp, constituting a significant portion of the normal microbiota of humans and animals, colonise the oral cavity and the nasopharynx mainly[168]. They are often involved in wound infections and frequently display drug-resistance, representing a serious obstacle in acute and chronic wound treatment[110]. Commonly, these Gram-positive bacteria are observed by microscopy as pairs or chains, differing from spherical to ovoid morphology and usually forming capsules[169]. They are nutritionally meticulous and they also display fermentative metabolism[170]. From a classification perspective, *Streptococcus* spp are divided serologically from groups A to V, based on the carbohydrate content of their cell wall[171]. Additionally, *Streptococci* can be grouped based on morphological differences, types of haemolysis on blood agar, biochemical reactions, different pili-associated proteins, and composition of the polysaccharidic capsule (specifically for group B *Streptococci*)[169]. The number and the severity of streptococcal infections has increased esponentially during the last decades, possibly due to the spreading of more virulent clones, the increased number of immunocompromised patients, and the abuse of intravenous drugs[172], although the exact reason for such an increase has not yet been determined.

S. pyogenes, or group A β-haemolytic *Streptococcus* (GABHS) (Fig.5), is responsible for a large percentage of human acute pharyngitis, but it also causes several cutaneous and systemic infections with variable severity and prognosis degree[173,174]. After adhesion to host tissues, *S. pyogenes* is able to elude phagocytosis, thus infiltrating and colonising the epithelial layers due to the supporting action of peculiar virulence factors[175,176].

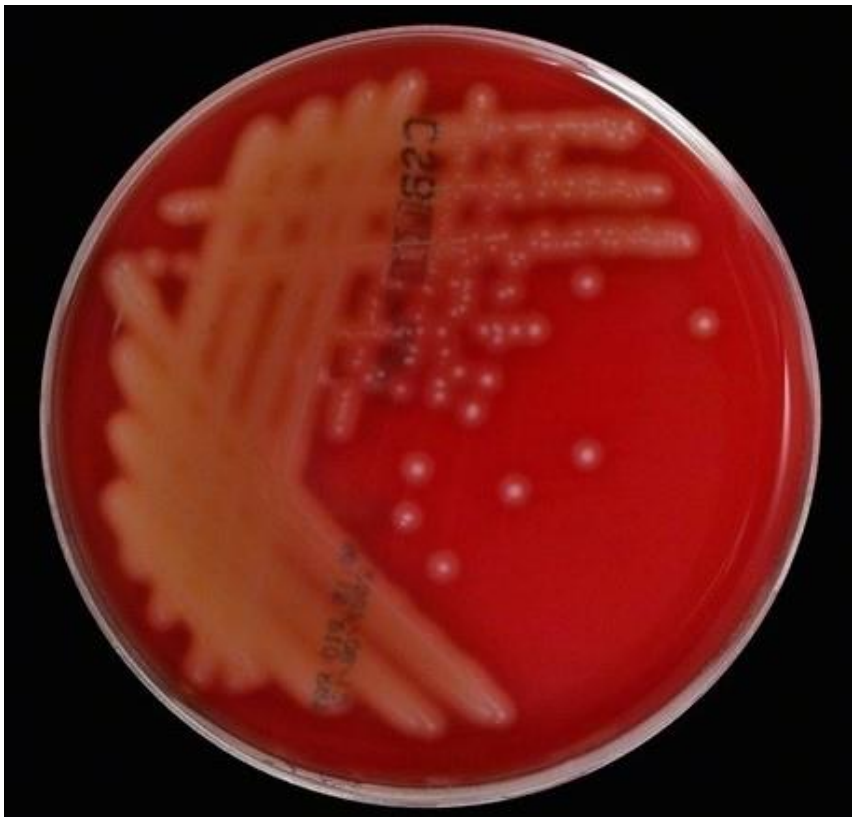

Fig. 5. *S. pyogenes* clinical strain culture on blood agar plate. Bacterial colonies display β-haemolytic activity.

Fortunately, *S. pyogenes* is sensitive to ß-lactam antibiotics, with penicillin or its derivatives (e.g. amoxicillin and ampicillin) being recommended as primary treatments for non-allergic patients[177]. For the treatment of *S. pyogenes* infections in patients allergic to penicillin and its derivatives, erythromycin is currently the best macrolide available[178]. *S. pyogenes* infections as necrotising fasciitis or toxic shock syndrome are currently addressed by using a combination of penicillin and clindamycin[179]. However, although *S. pyogenes* is not resistant to penicillin, it has become resistant to clindamycin and tetracycline[180–182]. Moreover, macrolide-resistant *S. pyogenes* strains have been identified in numerous countries in Europe and especially in Italy, where the rate of erythromycin resistance in GABHS has risen up to 30% since the 1990s[183–185]. For this reason, in the recent years the potential antimicrobial properties of several medicinal plants have been investigated: encouragingly, some phytochemicals such as polyphenols stood out for their significant antibacterial activity against *Streptococcus* spp[177].

1.3.4. *C. albicans*

Normally, *C. albicans* is a harmless commensal fungus, existing in the gastrointestinal tract of at least 70% of the healthy population[186,187]. However, *C. albicans* is also the leading global pathogen among *Candida* spp infections, causing 50%–70% of candidiasis cases[188,189]. *C. albicans* remains the most commonly isolated yeast in fungal infections, although the proportion relative to other *Candida* spp has decreased from 71% to 65% over the last 10 years[133,190].

C. albicans (Fig.6) is by far the most studied species in the fungal CTG clade[125]. Since 1994, targeted mutant strains of *C. albicans* were manufactured and their phenotypes were deeply investigated[191]. These genetic analyses improved our understanding of the pathogenic mechanisms in fungal infections, providing basic knowledge for a better comprehension of the fundamental processes responsible for yeast pathogenicity[191]. Therefore, *C. albicans* has become the model yeast for investigating the multiple leading factors in host–pathogen interactions[192,193].

C. albicans infections represent a clinical issue of growing importance worldwide, as it is the first most frequently found yeast in blood cultures from Intensive Care Unit (ICU) patients accounting for 54% of cases of Candida bloodstream infections[132,179].

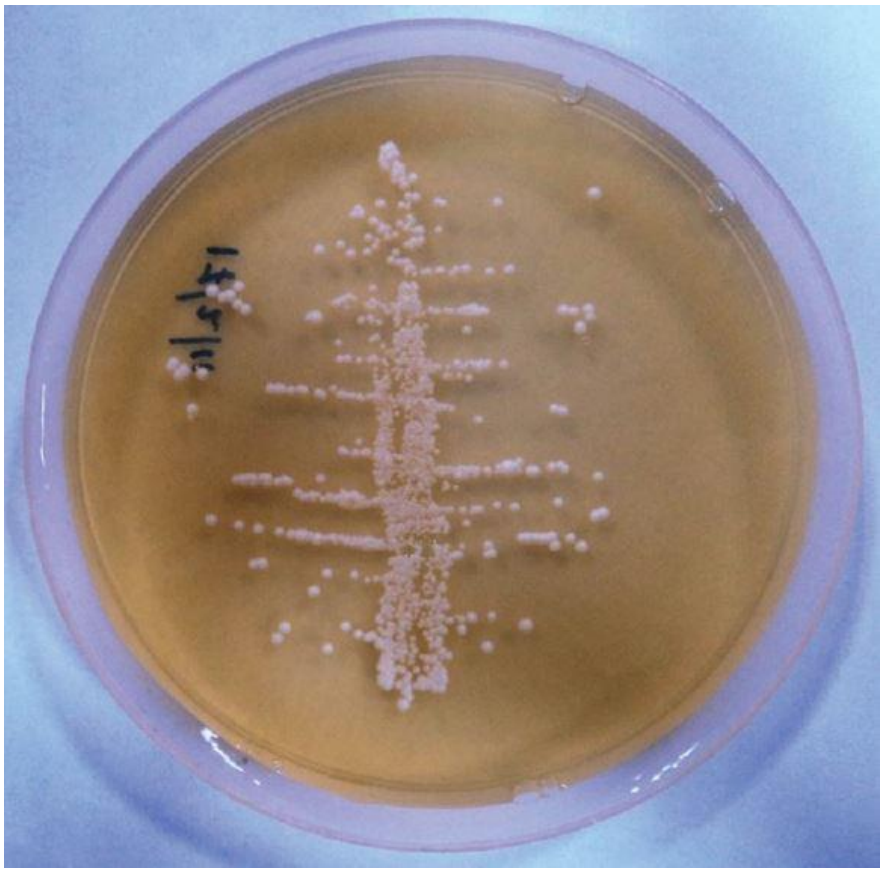

Fig. 6. *C. albicans* clinical strain culture on SAB agar plate. Representative image of yeast colonies. Adapted from Nadig et al[229].

The conversion from classic yeast growth to development of filamentous forms (hyphae and pseudohyphae)[194] – occurring with phenotypic changes, as cells switch aspect from white to opaque[195,196] - is usually associated to fungal virulence[197,198].

Hyphae were reported to be crucial for penetrating and damaging both epithelial and endothelial cells, as well as for escaping from macrophages upon phagocytosis[194,198]. In this context, the *C. albicans* hypha-specific surface protein Als3, a member of the agglutinin-like sequence (Als) protein family[199], was shown to mediate *C. albicans* endocytosis either by binding N-cadherin and E-cadherin on endothelial and epithelial cells[200–202] or by interfering with the linkage between EGF receptor and its related protein (HER2), resulting in autophosphorylation of the receptors[203]. Als3 seems to be restricted to *C. albicans* yeast[204], possibly explaining *C. albicans* preeminence among fungal infections in chronic wounds.

Exposure to antifungal drugs poses *C. albicans* under severe stress conditions, which in turn promotes the development of fungal resistance, in some cases very rapidly[205,206]. Stress was also associated to the induction of the parasexual cycle[207], resulting very high levels of aneuploidy[208]. Indeed, aneuploidy is more frequent after exposure to antimycotics, thus appearing as an essential adaptive response of *C. albicans* yeast[209,210].

So far, the number of available antimycotics for therapy is limited[211]. For decades, the gold standard chosen by clinicians and researchers have been amphotericin B deoxycholate and azoles[212,213]. Among azoles, fluconazole is primarily fungistatic[214,215]. On the other hand, itraconalzole displays fungicidal activity following to its interference with cell membrane formation[216–219]. Unfortunately, azoles have some disadvantages ranging from drug-drug interactions to hepatotoxicity, not to mention the onset of skin rashes[220–222]. Broad-spectrum azoles such as voriconazole and posaconazole as well as lipid preparations based on amphotericin B deoxycholate have recently been developed as effective alternatives to common azoles and amphotericin B deoxycholate formulations, respectively[223,224].

Echinocandins - including anidulafungin, caspofungin, and micafungin - are new drugs developed to cure fungal infections, neither showing cross-resistance to azoles nor being toxic in association with polyene drugs[225,226]. Echinocandins inhibit the synthesis of β-(1, 3)-D-glucan, a specific molecule of the fungal cell wall

that is absent in mammals[227]. Echinocandins possess a wide fungicidal spectrum, also covering *Candida* species that are resistant to triazoles[228].

1.3.5. *C. glabrata*

C. glabrata (Fig. 7) was originally known as *Cryptococcus glabratus* and described as a yeast of the human gut flora[230]. *C. glabrata* was generally considered as a human commensal, often to be found in the oral cavity[231]. Starting from the 1980s, *C. glabrata* strains were identified as causative agents of candidaemia and other deep fungal infections in immunocompromised patients[232]. Previously considered of minor interest, *C. glabrata* yeasts were included into the list of emerging pathogens just in 1995[233]. Nowadays, *C. glabrata* is considered both in Europe and North America the second pathogen after *C. albicans* to be responsible for candidaemia[234,235]. In particular, 15–25% of disseminated candidiasis are provoked by *C. glabrata* yeasts[236]. Phylogenetically, *C. glabrata* resembles more *Saccharomyces cerevisiae* (*S. cerevisiae*) than *C. albicans* or others *Candida* spp[237]. Despite its relationship with *S. cerevisiae*, which is diploid and sexual, *C. glabrata* is an obliged haploid and asexual microorganism[238–240]. Opposite to *C. albicans*[241], no evidence on switch from yeast morphology to hyphae form has ever been observed in *C. glabrata*[240]. Recently, intensive investigation on *C. glabrata* genome dynamics led to the identification of new sister spp genomes, thus contributing to better understand yeast metabolism and virulence[242,243].

C. glabrata can survive within macrophages and it can even replicate within these cells[244]. Chromatin remodelling is an essential process for the survival of *C. glabrata* upon internalisation by macrophages[245]. Other factors, such as the presence of yapsins[244] as well as the occurrence of autophagy[246] – that is the capacity to resist reactive oxygen species (ROS) production and glucose starvation – also allow *C. glabrata* to evade from the immune system. Ironically, macrophage cytokine production contributes to the following *C. glabrata* dissemination[247].

The available treatments for *C. glabrata* infections are generally similar to those for *C. albicans*, since amphotericin B deoxycholate, azoles, and echinocandins are good antimycotics for the treatment of all types of fungal infections[231]. The increase in *C. glabrata* infections has been associated with reduced susceptibility to fluconazole[231,248–250].

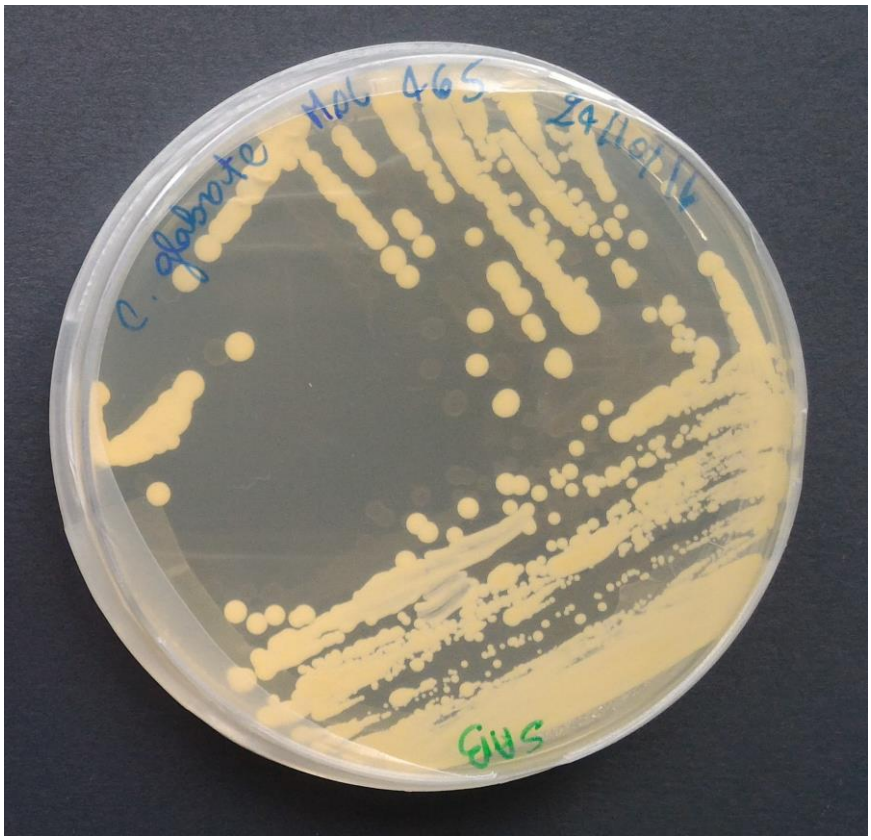

Fig. 7. *C. glabrata* clinical strain culture on SAB agar plate. Representative image of yeast colonies.

1.4. Chronic wound management

1.4.1. Oxygen therapies

The management of extreme hypoxia in chronic wounds represents a major limit to overcome. Oxygen supply and tension in the wound bed are both crucial issues for better understanding physiological wound healing. A minimum tissue oxygen tension of 20 mmHg is required for a wound to heal, however in nonhealing wounds oxygen tension runs around 5 mmHg[251,252]. Notably, when the arterial blood cannot supply cells with relevant amounts of oxygen, the risks for inflammation, infection, and scarring in wounds are enhanced[253–255]. Indeed, among the most relevant microenvironmental factors associated with tissue damage and repair, responses to hypoxia are virtually involved in all wound healing and remodelling processes, including collagen deposition, epithelialisation, fibroplasia, angiogenesis, and resistance to infections[251,252]. Another important issue revolves around medical therapy, as the effectiveness of treatments often decreases while tissue necrosis can develop in hypoxic conditions[256].

The tissutal levels of oxygen can be adequately bolstered by hyperbaric oxygen therapy (HBOT)[257–259] while an alternative therapy is represented by topical oxygen therapy (TOT)[260]. Unfortunately, either HBOT or TOT treatment display various backwards. On the one hand, HBOT approach is relatively expensive, uneasy, and even dangerous due to fire accident risks[102]. Additionally it may cause severe side effects, including myopia, brain toxicity associated with seizures, and pneumothorax[261,262]. On the other hand, TOT – which is cheaper and associates with lower toxicity – often fails to trespass effectively the *stratum corneum* and to deliver oxygen adequately to fibroblasts, keratinocytes, and inflammatory cells for restoring their functions[102,260]. Both treatments are compared in Fig. 8 and Table 1.

In the recent years, intensive research has been performed to develop new oxygen nanocarriers, including haemoglobin-based carriers and perfluorocarbon-containing formulations[263,264]. Among perfluorocarbon emulsions of the first generation, Fluosol is the only medical device approved by the Food and Drugs Administration[265] and unfortunately no perfluorocarbon-based oxygen emulsion of the second generation is currently approved for clinical uses[256].

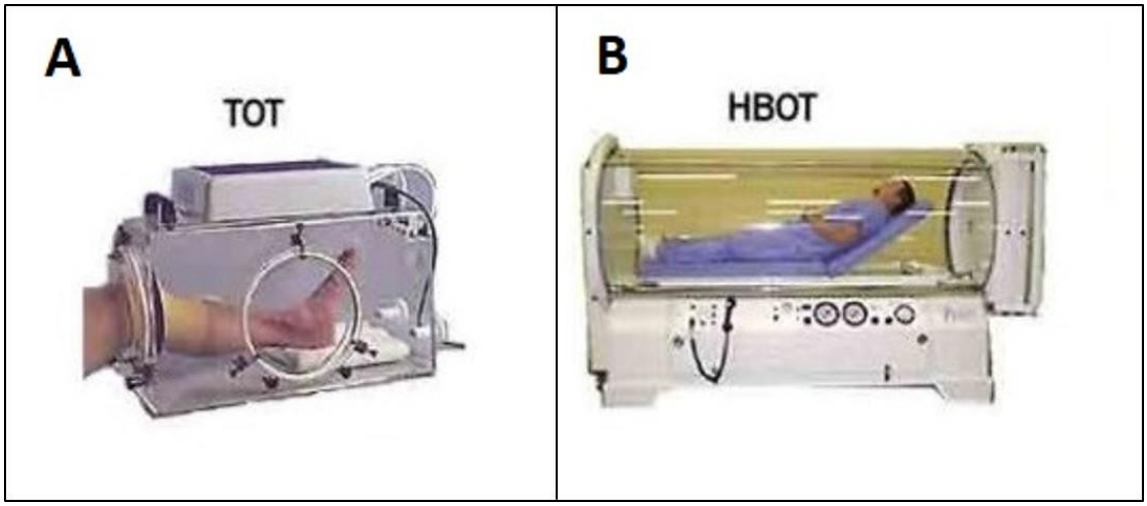

Fig. 8. TOT and HBOT treatments. Both technologies aim at using oxygen in order to promote wound healing processes. TOT is used to treat directly the wounded area by surrounding a patient's lesion with pure oxygen at pressures that must be slightly above atmospheric pressure. In contrast, HBOT is used to treat a patient systemically with oxygen at elevated pressures. Adapted from www.EO$_2$.com[226].

Modality	Topical oxygen therapy (TOT)	Hyperbaric oxygen therapy (HBOT)
Treatment at home	YES	NO
Patient mobility	NO	NO
Moisture maintenance in the wound bed	NO	possible
Direct wound treatment	YES	NO
Therapy time	~90 min/day	~90 min/day
Flow rate	5-60 L/min	up to 600 L/min

Table 1. Comparison between TOT and HBOT approaches. TOT and HBOT are compared for modality of treatment, mobility of patient, mataining of moist in the wound bed, time of treatment and flow rate of oxygen. Both technologies only offer treatment for a relatively short period of time, which means that the wound only receives supplemental oxygen for a few hours/day. Adapted from www.EO$_2$.com[226].

1.4.2. Treatments of infections

Antimicrobial wound management represents a major challenge requiring new solutions against human pathogens. In general, antibiotic and/or antimycotic therapies are considered the gold standard to treat overt infections. However, clinicians and researchers are attempting to validate alternative treatments in order to overcome the emergency of resistant microbial strains[266] and the limited effectiveness of drug delivery through dermis due to low permeability of the *stratum corneum*[267].

Drug resistance is an ubiquitous phenomenon that evolves continuously and has serious effects on human health[268]. In the recent years, antimicrobials have been largely used in both clinical and environmental contexts, however the rapidity at which resistances to antimicrobial emerge is much higher than that at which new drugs are developed[269,270]. Each year, only in the United States, antibiotic-resistant infections are responsible for $20 billion in extra-health care costs and $35 billion in societal costs[271]. In Europe, the expenses to treat these infections and to sustain extra hospital costs along with productivity losses exceed €1.5 billion euros/per year[269]. Furthermore, many antimicrobials drugs are associated with several issues reducing their efficacy, including limited solubility, short half-life, and variable adsorption[272,273]. Consequently, high dosage and frequent administration are required, affecting patient compliance and causing severe side effects[274–276].

1.5. Nanotherapies

1.5.1. Current applications in biomedicine

Nanotechnological applications cover several fields, ranging from industry to biomedicine. In particular, nanotechnologies have undergone a rapid development in the research for diagnostics and therapeutics, especially in microbiology, oncology, and immunology[277].

Over the last years, nanomedicine has become a major area of interest due to its many unique characteristics. Indeed, the achieved progresses of green nanotechnology (that is the development of eco-friendly technologies in material

synthesis)[278] combined with emerging evidence on antimicrobial, antineoplastic, and anti-inflammatory properties of several natural substances[279] have paved the way to develop a series of different and nonconventional nanoparticles (NPs) to be employed in the biomedical field.

In particular, NPs display an enormous potential as effective drug delivery systems (nanocarriers) to treat microbial infections, tumours, and inflammatory diseases since they display many advantages in comparison to conventional drugs[280]. For example, in the recent years the potential of polysaccharide-based self-aggregate NPs as delivery systems has been explored. Specifically, in aqueous media micelles or micelle-like aggregates are spontaneously formed due to the self-binding of polymeric polyamphiphiles, which minimise their interfacial free energy by associating inter or intramolecularly between hydrophobic moieties[281]. As a consequence of their hydrophobic and hydrophilic constituents, these NPs are characterised by unconventional rheological aspects, hydrodynamic radiuses in the nanometric scale, core-shell structures, and thermodynamic stability[282]. The physico-chemical properties of NPs, including their high surface-to-volume ratio, small size, stability, and controlled drug release[283] enhance their possibilities to trespass barriers such as the skin and reach biological molecules and microorganisms. Moreover, NP size, shape, and chemical properties may be adjusted in order to improve the molecular interactions and to ameliorate their primary action[284].

Several nanocarriers, including liposomes, microemulsions, and lipid nanocarriers, can be endowed with an inherent antimicrobial activity, thus synergising with the antimicrobial efficacy of the coupled antibiotic. Additionally, the direct interaction between NPs and key proteins in microbial cell membranes or walls can either inhibit the growth of pathogens or promote cell death through mechanisms different from the currently available antimicrobials[285]. Biocompatible NPs often associate to both lipophilic and hydrophilic antimicrobials and can release the loaded drug in a controlled manner with prolonged kinetics. These properties of NPs prevent the loaded drug from degradation, often leading also to a significant reduction of its side effects[286].

The design of nanocarriers may be a good approach for the release of anti-cancer drugs. NPs might be potential platforms to overcome some complications of current clinical treatments and to achieve targeted delivery into tumour

tissues[287,288]. Intriguingly, the use of nanocarriers has also been proposed recently as a promising alternative for the delivery of genes to specifically targeted tissues[289–292].

Additionally, some new nanocarriers have been shown capable to carry other molecules such as peptides or gaseous oxygen[263,264]. These findings appear extremely intriguing, since they may be exploited to produce innovative and nonconventional nanotherapies for wound management. Indeed, new treatments accelerating chronic wound closure, restoring tissue oxygen levels, and preventing microbial infections are urgently needed.

1.5.2. Emerging biomaterials: chitin and chitosan species or derivatives

A broad spectrum of materials (either natural or synthetic polymers, such as polysaccharides and lipids, as well as surfactants and dendrimers) have been exploited as components for nanocarrier manufacturing[293]. Among such a large number of molecules, a major focus was given to the investigation of polysaccharides, due to their outstanding physico-chemical and biological properties[283]. In particular, the most promising polysaccharydes to be employed as candidate biomaterials for the development of new nanomedical devices have emerged to be chitin and chitosan.

Chitin, a long-chain polymer composed of repeated units of β-D-(acetylamino)-2-deoxy-glucopyranose (N-acetyl-D-glucosamine), represents the second ubiquitous natural polysaccharide on Earth after cellulose. This very common polysaccharide can be found either in the exoskeleton or the internal structures of various invertebrates, such as crustaceans and insects[294]. Chitin is also a structural molecule of bacterial and fungal cell walls[295].

Upon N-deacetylation of chitin, chitosan is generated[296]. However, it should be noted that “chitosan” is quite a collective term, as it sums up together a wide spectrum of linear polysaccharides with different molecular weight, viscosity, and degree of deacetylation (ranging from 40% to 98%)[295]. Generally speaking, chitosan can be defined as an amino-polysaccharide composed of randomly distributed β-(1→4)-linked units of deacetylated and acetylated chitin (D-glucosamine and N-acetyl-D-glucosamine, respectively). As mentioned above, this naturally abundant and renewable cationic polysaccharide displays excellent

physico-chemical and biological properties, which are strongly influenced by its molecular weight and degree of deacetylation[297,298].

Opposite to the other main polysaccharides (cellulose, dextrin, pectin etc.), all featuring acidic characteristics, both chitin and chitosan stand out for their strongly basic nature[294]. For this reason, they are generally not soluble in any solvents but diluted organic or mineral acids[299]. The number of N-acetyl groups in chitin and chitosan strongly affects their solubility, crystallinity, and viscosity, as well as their optical properties[296]. Furthermore, the reactivity of chitin and chitosan depends on the available amino and hydroxyl groups. In particular, chitosan derivatives can be easily obtained by reacting chitosan primary amino groups as well as its primary or secondary hydroxyl groups[299]. Chitosan derivatives have been designed to improve specific properties of native chitosan[300,301]. In particular, glycol chitosan represents a paradigmatic chitosan derivative that has been widely exploited either for diagnostic or therapeutic applications in the nanomedical field[302,303].

Biocompatibility and biodegradability are peculiar biological properties of chitin and chitosan. *In vitro*, both polysaccharydes displayed low cytotoxic effects when employed to grow human skin cells, such as keratinocytes and fibroblasts[304,305]. Chitin and chitosan biocompatibility and biodegradability over time were also confirmed *in vivo* when these molecules were employed during wound care management[306]. Interestingly, chitin has received increasing attention due to its sensitivity to human lysozyme, which is responsible for the degradation of chitinous materials in bacterial cell walls[307]. On the other hand, the release of fragmented chitosan residues upon biological degradation has been associated with the activation of the immune system through direct interaction with cell surface receptors[308]. This immunoadjuvant effect may in part explain chitosan antimicrobial and antineoplastic properties, which have been largely documented in literature[309,310]. Nevertheless, chitosan species and/or derivatives are also known to exert direct bacteriostatic or fungistatic activity against several microbes (including *Staphylococcus* spp, *Streptococcus* spp, and *Candida* spp), independently from the presence or absence of activated immune cells[311,312]. Additional biological properties of chitin and chitosan species or derivatives include acceleration of bone formation, regeneration of connective gum tissue, promotion of haemostasis, depression of the central nervous system, and reduction of cholesterolaemia[294].

Due to their abundant availability and crucial physico-chemical and biological characteristics, chitin and chitosan species or derivatives have been exploited in various application fields, including food processing, wastewater treatment, agriculture, paper making, and cosmetics[294,296].

Intriguingly, chitin and chitosan, as well as their derivatives, have revealed themselves as very valuable biomaterials also in the field of biomedical research and tissue engineering[294,296,313,314]. The potential for these molecules appears tremendous, ranging from wound care management to regenerative medicine, up to nephrology or ophthalmology, as suggested by the following few examples: i) chitin and chitosan fibres proved very useful as reabsorbable sutures[315] and as dressing materials[316] for wound treatment; ii) due to its polycationic nature, the employment of chitosan in tissue engineering was associated with acceleratory effects in articular cartilage repair processes[317]; iii) the permeability of chitosan and its great tensile strength led to the development of artificial kidney membranes[318]; iv) chitosan was proposed as a promising candidate biomaterial to develop contact lenses and ocular bandages[319].

Finally, it should be highlighted that chitin and chitosan, as well as their derivatives, have acquired in the last decade an increasingly relevant role both in pharmacology and in drug technology. On the one hand, since these biocompatible and relatively inexpensive molecules display antimicrobial and antineoplastic properties, they are currently being considered for potential use as pharmacologically active principles[309,310]. On the other hand, chitosan species and derivatives have proven to be valuable eccipients for drug formulations. Indeed, chitosan is able to enhance the adsorption of hydrophobic macromolecular drugs and to improve the effectiveness of drug delivery by holding the therapeutic materials in closer proximity to its site of action, due to its mucoadhesive cationic nature. For example, chitosan NPs were reported to remain anchored to the ocular membrane for very long time periods and to be able to release high concentrations of the encapsulated drug to the target site, greatly lowering the systemic exposure[320,321]. Based on these crucial properties, chitosan could be a promising molecule for the encapsulation of antimicrobial or anticancer drugs and the development of novel nanotherapeutics[286,320,321]. Intriguingly, chitosan nanocarriers have also been proposed as potentially safe and effective adjuvants

and delivery systems for enhancing the immunogenicity of mucosally administered vaccines[322].

1.5.3. Micro and nanobubbles

According to the Law of Laplace for spherical surfaces, the difference between the outer and the inner gas pressure in bubbles (and droplets) is inversely proportional to their radius. Therefore, the smaller the bubble's radius, the higher the differential pressure of the gas, and the faster the diffusion of the gas[323]. Exploiting this law, innovative platforms of oxygen-loaded and shell/core-structured bubbles were developed[324] recently for diagnostic and therapeutic purposes. These new nonconventional spherical oxygen carriers, which can be classified either as microbubbles or as nanobubbles depending on their average diameters, were produced by using a peculiar fluorocarbon (perfluoropentane, PFP) for the inner core and alternative polysaccharydes (chitosan, dextransulfate, or dextran) for the outer shell[263,264,325–327].

Perfluorocarbons are stable and biologically inert molecules which have been employed since the 1980s in emulsified forms as key molecules for oxygen-transporting plasma substitutes[328]. Indeed, these molecules are able to dissolve more than 50 volumes percent of oxygen, with the carried gas being directly proportional to the oxygen tension[328]. As a consequence of the high strength of the bond between carbon and fluorine atoms[329], perfluorocarbons cannot be metabolised by human cells, thus being excreted unmodified from the lungs[330].

PFP is a well-known perfluorocarbon and has been widely employed to develop oxygen-transporting strategies, including microbubbles and nanobubbles. Indeed, PFP is constituted by a carbon skeleton surrounded by twelve fluorine atoms which are able to avidly bind oxygen molecules at high oxygen tensions through van deer Waals interactions[331]. Not being very strong, such a peculiar intermolecular bond allows biatomic oxygen to be also easily released at lower gas tensions[328]. In the context of micro and nanobubbles, such a release can either occur spontaneously, through passive diffusion, or it can be induced upon ultrasound (US) administration. In particular, the latter approach promotes cavitation events within the bubble, thereby destabilising its shell and promoting instant release of the gas from the inner core[264].

On the other hand, bubble shells can be manufactured with different biocompatible polysaccharides, such as chitosan or dextran as well as their derivatives (glycolchitosan, dextransulfate etc.). The biological properties of chitosan were already described in the previous section. As far as it concerns dextran, it is worth mentioning that in the recent years it has been widely studied as a potential matrix biomaterial to be used in tissue engineering, not leading to any signs of inflammation *in vivo*[332].

Based on these preconditions, in 2008 a first platform of medium weight chitosan-shelled oxygen-loaded microbubbles (MW cOLMBs) was developed by a collaborative and interdisciplinary research network, also involving a few members from our group[325]. These PFP-filled microbubbles, displaying spherical shapes, average 2.5 µm diameters, positively charged surfaces, acceptable biocompatibility rates, and high responsiveness upon US administration (which in turn promoted cavitation events and local release of oxygen), were conceived as possible therapeutic devices to counteract hypoxia in several diseases, including pre-eclampsia, inflammation, and cancer[333]. However, during the last decade, it has become increasingly clear that the size of a carrier represents a crucially limitant factor that strongly influences the range of feasible applications, with micrometric diameters making the bubbles more suitable for diagnostic rather than therapeutic purposes[334]. Indeed, nanometric dimensions are generally needed in order to trespass biological barriers or to penetrate cell membranes[335], thereby carrying out a therapeutic role within cells and tissues.

In order to obtain improved oxygen-carrying platforms that could also be suitable for therapeutic goals, further investigation by our group was aimed at minimising the size of bubbles up to the nanometric range. This led to the development of new platforms of PFP-filled oxygen carriers, namely oxygen-loaded nanobubbles (OLNBs), which were alternatively shelled with dextransulfate, dextran or MW chitosan[263,264,326], as schematised in Fig. 9.

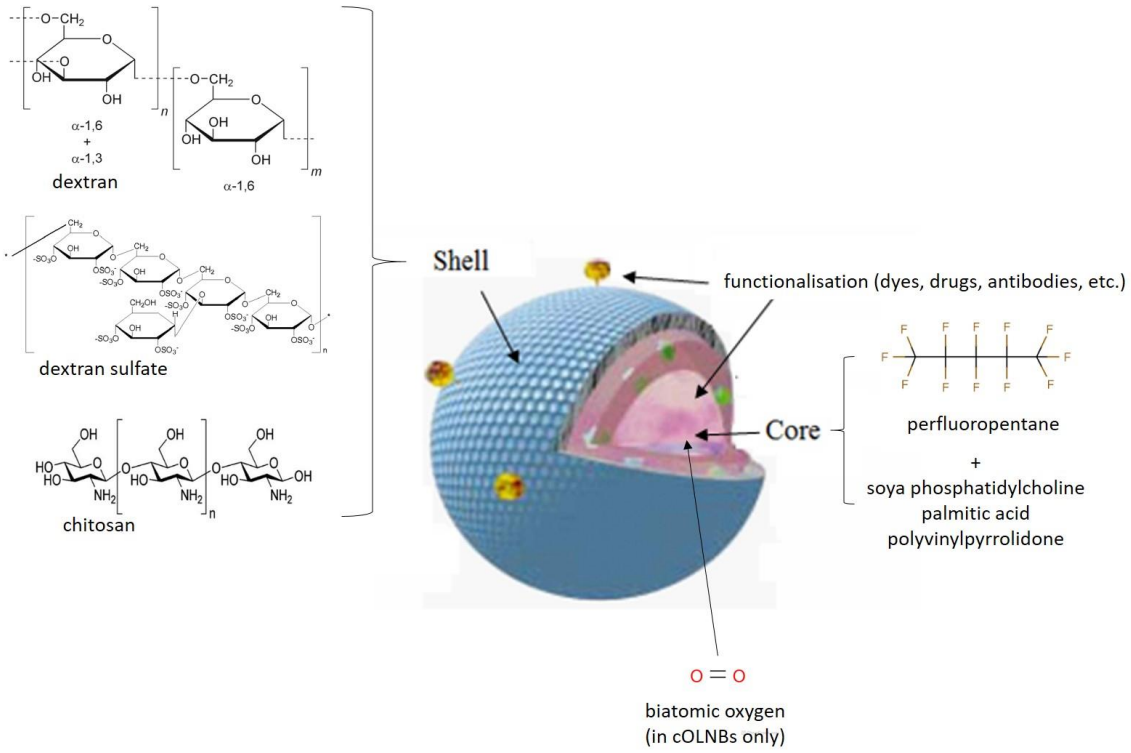

Fig. 9. Schematic representation of nanobubble structure. Nanobubbles display a typical core-shell structure with spherical morphology. The polysaccharidic shell can be alternatively constituted by dextransulfate, dextran, or chitosan. The core contains PFP as main oxygen-binding fluorocarbon as well as soya phosphatidylcholine, palmitic acid, and polyvinylpyrrolidone as complementary surfactants. When biatomic oxygen is added into the core, OLNBs are generated; otherwise, the nanobubbles are commonly known as OFNBs. Both OLNBs and OFNBs can be further functionalised by coupling additional molecules - including drugs, dyes, and antibodies - either to the shell or to the core, depending on the physico-chemical characteristics of the chosen molecules.

Dextransulfate-shelled OLNBs (dsOLNBs) displayed spherical morphology, 500 nm average diameters, and anionic surfaces, neither being associated to haemolytic activity on human erythrocytes nor to cytotoxicity to African green monkey fibroblastoid kidney cells[263]. Moreover, dsOLNBs showed efficient oxygen storing and delivering abilities, with the percentage of oxygen release being directly proportional to the degree of hypoxia in the outer environment and the release kinetics being enhanced after insonation with US[263].

Alternative polysaccharides such as dextran and MW chitosan were also employed to produce two additional types of OLNBs (dOLNBs[326] and MW cOLNBs[264,336], respectively). In particular, dOLNBs did not differ strongly from dsOLNBs for physico-chemical characteristics and effectiveness in oxygen storage and release[326]. Nevertheless, the choice of the polysaccharide appears to be crucial for further functionalisation of the carrier with additional molecules (drugs, dyes, antibodies, etc.), as either dextran or dextransulfate can be less or more suitable for coupling with other molecules due to their different charge: for instance, dextransulfate recently revealed itself as an excellent matrix to anchor vancomycin to the shell of nanobubbles[327]. On the other hand, the use of MW chitosan as a shell component led to the production of cationic OLNBs with larger diameters than dsOLNBs or dOLNBs. Nevertheless, cOLNBs appeared exquisitely efficient in releasing oxygen and in trespassing biological membranes after US administration, as a consequence of the promotion of cavitation and sonophoresis, respectively[264,336]. Additionally, the antimicrobial and anti-inflammatory properties of chitosan discussed in the previous section make it a unique polysaccharide to be exploited in OLNB production for therapeutic treatment of infected chronic wounds.

Besides polysaccharides and PFP, another couple of ingredients are also needed for nanobubble manufacturing. Indeed, soya phosphatidylcholine and palmitic acid are commonly used as surfactants to lower the surface tension between the gas (oxygen) and the liquid phases (aqueous solutions and PFP) during the preparation of nanobubble formulations, which is performed at room temperature conditions. Also, it should be noticed that nanobubbles can either be fully saturated with a specific gas (i.e. oxygen for OLNBs) or just filled with air. In the latter case, they have been conventionally named as oxygen-free nanobubbles (OFNBs) since they are not saturated with oxygen during manufacturing, although

in reality they do contain a smaller amount of oxygen (20%, that is the percentage of oxygen content in the air)[326,336].

1.5.4. Nanodroplets

In the past few years, nanobubble technology was exploited and optimised, leading to the development of a new platform of oxygen nanocarriers to be used to treat infected chronic wounds, displaying even higher efficacy than nanobubbles - yet maintaining all of their advantages.

As shown in Fig. 10, these new nanocarriers - which have been named nanodroplets[326,336] - share with nanobubbles a quite similar structure and morphology. Indeed, they are both constituted by a polysaccharidic shell and a fluorocarbon core and they both display a spherical shape. As in older nanobubbles, MW chitosan and dextran are commonly employed as shell polysaccharidic components also in newer nanodroplets while soya phosphatisylcholine and palmitic acid are used as surfactants[326,336]. However, the main fluorocarbon employed to bind biatomic oxygen within the nanodroplet's core is 2H,3H-decafluoropentane (DFP)[326,336]. Opposite to PFP (boiling point: 32° C), which is liquid during nanobubble manufacturing but becomes gaseous at body temperature, DFP (boiling point: 51° C) remains liquid at both temperatures[337], hence the name "nanodroplets" given to these new nanocarriers.

DFP, constituted by a carbon skeleton surrounded by ten fluorine and two hydrogen atoms, interacts well with surfactants[338]. Even more so, its peculiar structure allows to bind oxygen molecules not only through van der Waals forces, as for PFP, but also by establishing hydrogen intermolecular bonds[339]. As a consequence, DFP binds biatomic oxygen more effectively than PFP while its release by diffusion appears more slow and sustained over time[326,336]. Nevertheless, nanodroplets still conserve all the peculiar characteristics of nanobubbles, including nanometric size, surface charge, stability, biocompatibility, and responsiveness to US[326,336]. The latter property appears pretty crucial, since it allows the nanocarriers to trespass biological barriers through sonophoresis[340] and to discard their gaseous content instantly as a consequence of cavitation events[341].

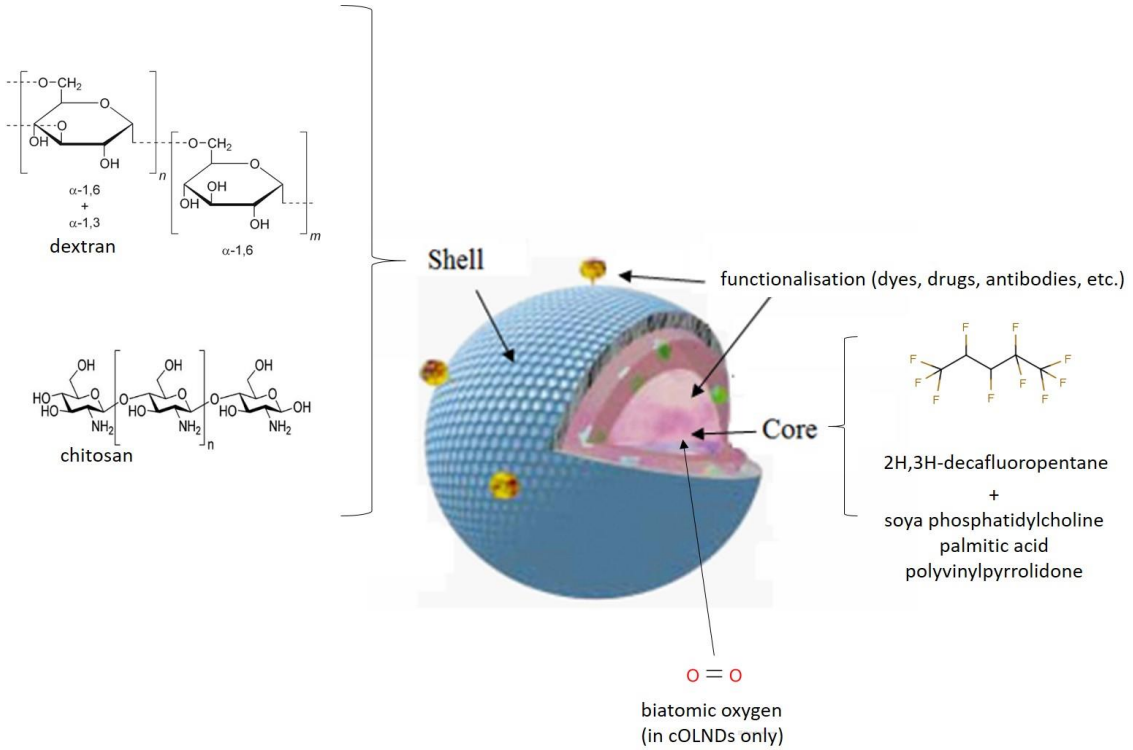

Fig. 10. Schematic representation of nanodroplet structure. As for nanobubbles (see Fig. 9), also nanodroplets display a typical core-shell structure with spherical morphology. The polysaccharidic shell is generally constituted by dextran or chitosan. The core contains DFP as main oxygen-binding fluorocarbon as well as soya phosphatidylcholine, palmitic acid, and polyvinylpyrrolidone as complementary surfactants. When biatomic oxygen is added into the core, OLNDs are generated; otherwise, the nanodroplets are commonly known as OFNDs. Both OLNDs and OFNDs can be further functionalised by coupling additional molecules - including drugs, dyes, and antibodies - either to the shell or to the core, depending on the physico-chemical characteristics of the chosen molecules.

Interestingly, US irradiation was recently reported to induce DFP evaporation[342], thus promoting the transformation of nanodroplets into nanobubbles and allowing them to undergo cavitation and sonophoresis. This is consistent with either *in vitro* or *in vivo* data showing US-dependent effective trespassing of skin layers by nanodroplets[326,336,343] along with higher and more time-sustained oxygen release from oxygen-loaded nanodroplets (OLNDs) with respect to oxygen-free nanodroplets (OFNDs)[326,336].

Due to all these intriguing properties, OLNDs have been proposed as potential therapeutic tools to treat hypoxia-associated pathologies, including chronic wounds and pre-eclampsia. In this context, a series of studies on different skin populations (human keratinocytes[344], dermal microvascular endothelial cells[345], and monocytes[346]) and placental tissues (human chorionic villous explants[347]) were conducted to investigated the effects of hypoxia and OLND on the regulation of balances between secreted gelatinases (MMP-2 and MMP-9) and their physiological inhibitors (TIMP-2 and TIMP-1, respectively). Encouragingly, either dextran- or chitosan-shelled OLNDs proved to be able to abrogate the dysregulating effects induced by hypoxia, promoting a normoxia-like phenotype in all the hypoxic cells or tissues under investigation[344–347].

CHAPTER 2.
AIM OF THE STUDY

The present work aimed at formulating, characterising and testing *in vitro* two innovative and nonconventional platforms of chitosan-shelled oxygen nanocarriers (nanobubbles and nanodroplets) as potential medical devices for the treatment of infected chronic wounds.

In the first section of the study, medium molecular weight (MW) chitosan-shelled oxygen-loaded nanobubbles (cOLNBs) and MW chitosan-shelled oxygen-free nanobubbles (cOFNBs) were challenged for their properties in the context of chronic wound potential management. The specific aims of this section were:

- to produce MW cOLNB and cOFNB formulations
- to characterise MW cOLNBs and cOFNBs for their morphology and physico-chemical properties
- to analyse the mechanical interaction between MW cOLNBs and human keratinocytes
- to check MW cOLNB and cOFNB biocompatibility with human keratinocytes in normoxia and hypoxia
- to investigate the effects of MW cOLNBs and cOFNBs on wound healing abilities of human keratinocytes in normoxia and hypoxia
- to analyse the mechanical interaction between MW cOLNBs or cOFNBs and MRSA bacteria or *C. albicans* yeasts
- to assess MW cOLNB and cOFNB antimicrobial activity against MRSA bacteria and *C. albicans* yeasts

In the second part of this work, MW chitosan-shelled oxygen-loaded nanodroplets (cOLNDs) and MW chitosan-shelled oxygen-free nanodroplets (cOFNDs) were challenged for their properties in the context of chronic wound potential management. The specific aims of this section were:

- to produce MW cOLND and cOFND formulations
- to characterise MW cOLNDs and cOFNDs for their morphology and physico-chemical properties
- to measure oxygen release from MW cOLNDs
- to analyse the mechanical interaction between MW cOLNDs and human keratinocytes

- to check MW cOLND and cOFND biocompatibility with human keratinocytes, dermal fibroblasts, and dermal microvascular endothelial cells in normoxia and hypoxia
- to investigate the effects of MW cOLNDs and cOFNDs on wound healing abilities of human keratinocytes, dermal fibroblasts, and dermal microvascular endothelial cells in normoxia and hypoxia
- to analyse the mechanical interaction between MW cOLNDs or cOFNDs and MRSA or *S. pyogenes* bacteria as well as *C. albicans* or *C. glabrata* yeasts
- to assess MW cOLND and cOFND antimicrobial activity against MRSA and *S. pyogenes* bacteria as well as *C. albicans* and *C. glabrata* yeasts

In the third section of the study, low molecular weight (LW) cOLNDs and cOFNDs were challenged for their properties in the context of chronic wound potential management. The specific aims of this section were:

- to produce LW cOLND and cOFND formulations
- to characterise LW cOLNDs and LW cOFNDs for their physicochemical properties
- to measure oxygen release from LW cOLNDs
- to check LW cOLND and cOFND biocompatibility with human keratinocytes, dermal fibroblasts, and dermal microvascular endothelial cells in normoxia and hypoxia
- to investigate the effects of LW cOLNDs and cOFNDs on wound healing abilities of human keratinocytes, dermal fibroblasts, and dermal microvascular endothelial cells in normoxia and hypoxia
- to analyse the mechanical interaction between LW cOLNDs or cOFNDs and MRSA or *S. pyogenes* bacteria as well as *C. albicans* or *C. glabrata* yeasts
- to assess LW cOLND and cOFND antimicrobial activity against MRSA or *S. pyogenes* bacteria as well as *C. albicans* and *C. glabrata* yeasts

CHAPTER 3.
MATERIALS AND METHODS

3.1. Materials

Unless otherwise stated, all materials were from Sigma-Aldrich (Saint Louis, USA). Plastics were from Costar (Corning, USA), Jet Biofil (Guangzhou, China) and VWR (Radnor, Pennsylvania); 0.9% sodium chloride saline solution was from Baxter (Bloomington, USA); 96% ethanol was from Carlo Erba (Cornaredo, Italy); Epikuron 200® (95% soya phosphatidylcholine) was from Degussa (Hamburg, Germany); palmitic acid, DFP, PFP, and polyvinylpyrrolidone (PVP) were from Fluka (Buchs, Switzerland); ultrapure water was obtained using a 1-800 Millipore system (Molsheim, France); Trypticase Soy Broth and Agar (TSB, TSA), and Sabouraud dextrose (SAB) Broth and Agar were from Oxoid SpA (Rodano, Italy); Todd Hewitt (TODD) broth was from Biolife Italiana s.r.l. (Milano, Italy); Panserin 601 medium was from PAN Biotech (Aidenbach, Germany); cell culture RPMI 1640 medium and propidium iodide were from Invitrogen-Thermo Fisher Scientific Inc. (Carlsbad, USA); cryovials were from Microbank, BioMérieux (Marcy-l'Etoile, France); CellTiter-Glo® was from Promega (Madison, USA); cell culture inserts were from Ibidi (Planegg, Germany); human dermal fibroblasts were from Cell Application Inc (San Diego, USA); plan flour fluorescent microscope was from Nikon (Minato, Japan); HQ40d model oxymeter was from Hach Lange (Derio, Spain); Ultra-Turrax SG215 homogenizer was from IKA (Staufen, Germany); Delsa Nano C analyzer was from Beckman Coulter (Brea, USA); Synergy HT microplate reader was from Bio-Tek Instruments (Winooski, USA); optical microscope AE31 was from Motic (Xiangan Qu, China); optical microscope XDS-3FL Optika (Ponteramica, Italy); Philips TEM CM10 was from Philips (Eindhoven, The Netherlands); Olympus Fluoview 200 laser scanning confocal system and inverted IX70 Olympus microscope was from Olympus America Inc. (Center Valley, USA); LSM710 inverted confocal laser scanning microscope equipped with a Plan-Neofluar 63×1.4 oil objective was from Zeiss (Oberkochen, Germany). For statistical analysis and scientific graphing: software SPSS 16.0 for Windows was from SPSS Inc. (Chicago, USA) and software Graphpad Prism version 6.00 for Windows was from Graphpad Software (San Diego, USA).

3.2. Methods

3.2.1. Nanobubble and nanodroplet preparation

In order to prepare cOLNB and cOLND formulations, a pre-emulsion was obtained adding 300 mL of an ethanol solution containing Epikuron® 200 and 1% w/v palmitic acid to PFP (for nanobubbles) or DFP (for nanodroplets) under magnetic stirring. After addition of 4.8 mL of phosphate buffered saline (PBS), the system was homogenised for 2 min using an Ultra-Turrax SG215 homogenizer. Thereafter, oxygen was added to the suspension for 2 min. Then, 0.139 % w/v aqueous solution of MW or LW chitosan was added drop-wise under magnetic stirring. To produce cOFNBs and cOFNDs the addition of oxygen was skipped. Similarly, OSS was prepared without adding any polysaccharides or fluorocarbons. For selected experiments, nanobubbles and nanodroplets were conjugated with 10% or 7% fluorescein isothiocyanate (FITC) solution overnight (confocal microscopy studies on human cells and on microbial cells, respectively). The composition of nanobubble, nanodroplet and OSS formulations is reported in Table 2.

3.2.2. Nanobubble and nanodroplet characterisation

The average diameters, polydispersity indexes and zeta potentials of the nanobubbles and nanodroplets were determined by dynamic light scattering, as described previously[263,264,326,336]. Briefly, a monochromatic light source (laser ray) was shot through a polarizer into each sample, previously diluted in de-ionised water before measurement. The scattered light then went through a second polarizer where it was collected by a photomultiplier and the resulting image (speckle pattern) was projected onto a screen. This process was repeated at short time intervals and the resulting set of speckle patterns were analyzed by an autocorrelator comparing the intensity of light at each spot over time. The most important use of the autocorrelation function (also known as photon correlation spectroscopy) is its use for size determination. The polydispersity index indicates the size distribution within a nanobubble/nanodroplet population.

Ingredients (% w/v)	cOLNBs	cOFNBs	cOLNDs	cOFNDs	OSS
chitosan	0.139	0.139	0.139	0.139	-
PFP	7011	7011	-	-	-
DFP	-	-	6868	6868	-
palmitic acid	0.015	0.015	0.015	0.015	0.015
Epikuron® 200	0.051	0.051	0.051	0.051	0.051
PVP	0.070	0.070	0.070	0.070	0.070
ethanol	3.989	3.989	3.989	3.989	3.989
filtered PBS	88.868	88.868	88.868	88.868	88.868
O_2^*	YES	NO	YES	NO	YES

Table 2. Composition of nanobubble, nanodroplet, and OSS formulations. * O_2 is merely indicated for its presence or absence in the solution (YES or NO), as it was addd in excess to reach saturation.

For the zeta potential determination, samples from each formulation were placed in an electrophoretic cell, where an electric field of 15 V/cm was applied. Each sample was analysed at least in triplicate. The measured electrophoretic mobility was converted into zeta potential value using the Smoluchowsky equation[348]. The morphology of nanodroplet and nanobubble formulations was assessed by optical microscopy and by transmitting electron microscopy (TEM), as described previously[263,264,326,336]. Nanobubble and nanodroplet suspensions were dropped onto a Formwar-coated copper grid and air-dried before observation.

3.2.3. *In vitro* determination of oxygen release from nanodroplets

In vitro oxygen release from MW and LW cOLND formulations was investigated using the dialysis bag technique. The donor phase, consisting of 3 mL of MW or LW cOLND formulation, was placed in a dialysis bag (cellulose membrane, molecular weight of 12–14,000 Da), hermetically sealed and immersed in 45 mL of the receiving phase. The receiving phase consisted of hypoxic 0.9% (w/v) NaCl (saline) solution. The oxygen concentration of the receiving phase was previously reduced (0.5 mg/L) with a N_2 purge in order to mimic hypoxic conditions. Then, the oxygen release kinetics from MW or LW cOLND into the receiving phase was monitored for 6 hours, using an oximeter, displaying an accuracy of 0.01 mg/L. The oxymeter was calibrated in air, waiting for stable temperature and humidity conditions to be reached before each measurement.

3.2.4. Nanobubble and nanodroplet sterilisation

Nanobubble and nanodroplet formulations were sterilised through UV-C exposure for 20 min. Thereafter, UV-C-treated materials were incubated with cell culture RPMI 1640 medium in a humidified CO_2/air-incubator at 37° C up to 72 h, not displaying any signs of microbial contamination when checked by optical microscopy. UV-C-sterilised samples underwent further analyses to exclude ozone and singlet oxygen generation by spectrophotometric assay and EPR studies, respectively. No ozone was detected in nanobubble and nanodroplet formulations after UV-C sterilisation (data not shown). Moreover, UV-C sterilisation procedure was not accompanied by ROS production (data not shown).

3.2.5. Human cells, bacteria, and yeasts

HaCaT cell line, immortalised from a 62-year old Caucasian male donor[349], was used as source of human keratinocytes. HDF cell line of normal healthy human foreskin or adult skin was used as source of human dermal fibroblasts[350]. HMEC-1, a long-term cell line of dermal microvascular endothelial cells immortalized by SV 40 large T antigen[351] was used as source of human endothelium. HaCaT cells were grown as monolayers in Dulbecco's Modified Eagle Medium - high glucose (DMEM HG) supplemented with 10% foetal bovine serum (FBS), 100 U/ml penicillin, 100 µg/ml streptomycin and 2 mM L-glutamine. HDF cells were grown as monolayers in DMEM supplemented with 10% foetal calf serum (FCS), 100 U/ml penicillin, 100 µg/ml streptomycin and 2 mM L-glutamine. HMEC-1 cells were grown as monolayers in MCDB 131 medium supplemented with 10% foetal calf serum (FCS), 10 ng/ml of EGF, 1 µg/ml of hydrocortisone, 2mM L-glutamine, 100 units/ml of penicillin, 100 µg/ml of streptomycin and 20 mM HEPES buffer, pH 7.4. Cells were grown in a humidified CO_2/air-incubator at 37° C.

Clinical strains of MRSA, *S. pyogenes*, *C. albicans* and *C. glabrata* from human ulcerated wounds were cultured at 37° C. Bacteria were cultured on Mannitol salt agar and Todd Hewitt agar, respectively. Both yeasts were cultured on Sabouraud dextrose agar. Young colonies (18-24 h) were picked up to approximately 3-4 McFarland standard and inoculated into cryovials containing both cryopreservative fluid and porous beads to allow microorganisms to adhere. After inoculation, cryovials were kept at -80° C for extended storage.

3.2.6. Confocal microscopy analysis on human keratinocytes

HaCaT cells ($6x10^4$ cells/ml) were seeded and incubated under normoxic condition (20% O_2) in humidified CO_2/air-incubator at 37° C overnight. Then, cells were left untreated or treated with 10% v/v FITC-labelled MW cOLNB or cOLND suspensions for 24 hours in normoxia. After incubation with FITC-labelled nanobubbles, human cells were fixed with 1% paraformaldehyde (PFA) PBS solution for 15 min. Then cells were incubated with 15 µg/ml PI to visualise nucleic acids. Alternatively, after incubation with FITC-labelled nanodroplets, cells were incubated with 4',6-diamidino-2-phenylindole (DAPI) staining to visualise cells nuclei. Confocal images were acquired by a LSM710 inverted confocal laser scanning microscope equipped with a Plan-Neofluar 63×1.4 oil objective that

allowed a field view of at least 5 cells. A wavelength of 488 nm was used to detect MW cOLNBs and MW cOLNDs, and of 460 nm to detect the labelled nuclei. The acquisition time was 400 ms. Confocal images were taken using FITC and TRITC filters.

3.2.7. Adenosine triphosphate assay

The CellTiter-Glo® Luminescent Cell Viability Assay is a homogeneous method of determining the number of viable cells in culture based on quantification of detected adenosine triphosphate (ATP), an indicator of metabolically active cells. Briefly, cells were seeded in multi-wells in their supplemented cell culture medium and incubated in a humidified CO_2/air-incubator at 37° C overnight to allow the cellular adhesion. The day after, cells were incubated in absence or presence of 10% v/v MW cOLNBs/cOFNBs (only HaCaT cells) either in normoxic (20 % O_2) or hypoxic (1 % O_2) conditions, in a humidified CO_2/air-incubator at 37° C. After 24 h, cells reached about 90% of confluence and CellTiter-Glo® Luminescent Cell Viability Assay was performed following manufacturer's instructions.

3.2.8. Lactate dehydrogenase assay

The potential cytotoxic effects of nanobubbles and nanodroplets were measured as the release of lactate dehydrogenase (LDH) from cells into the extracellular medium. Cells were seeded in 6 multiwell plates (1.5 x 10^5 cells/ml) in their supplemented cell culture medium and incubated in a humidified CO_2/air-incubator at 37° C overnight to allow cellular adhesion. The day after, cells were incubated in absence or presence of 10% v/v MW cOLNBs/cOFNBs (HaCaT cells only), MW cOLNDs/cOFNDs (HaCaT, HDF, and HMEC-1 cells), and LW cOLNDs/cOFNDs (HaCaT, HDF, and HMEC-1 cells) either in normoxic (20 % O_2) or hypoxic (1 % O_2) conditions, in a humidified CO_2/air-incubator at 37° C. After 24 h, cells (~ 5 x 10^5 cells/ml of culture medium) reached about 90% of confluence and 1 ml of cell supernatants were collected and centrifuged at 13000g for 30 min. Cells were washed with fresh medium, detached with scraper, washed with PBS, resuspended in 1 ml of 82.3 mM triethanolamine solution, pH 7.6 (TRAP), and sonicated on ice with a 10s burst. Five µl of cell lysates and 50 µl of cell supernatants were diluted with TRAP and supplemented with 0.5 mM sodium pyruvate and 0.25 mM nicotinamide adenine dinucleotide reduced form (NADH)

(300 µl as a final volume). The reaction was monitored by measuring the absorbance at 340 nm (37° C) with Synergy HT microplate reader. After determining the intracellular and extracellular LDH activities, expressed as µmol of oxidized NADH/min/well, cytotoxicity was eventually calculated as the net ratio between extracellular and total (intracellular + extracellular) LDH activities.

3.2.9. 3-(4,5-dimethylthiazol- 2-yl)-2,5-diphenyltetrazolium bromide assay

Cell viability was evaluated using 3-(4,5-dimethylthiazol- 2-yl)-2,5-diphenyltetrazolium bromide (MTT) assay. Cells were seeded in 96 multiwell plates (10^5 cells/ml) in their supplemented cell culture medium and incubated in a humidified CO_2/air-incubator at 37° C overnight to allow cellular adhesion. Then, cells were incubated in their supplemented medium for 24 h without or with 10% v/v MW cOLNBs/cOFNBs (only HaCaT cells), MW cOLNDs/cOFNDs (HaCaT, HDF, and HMEC-1 cells), and LW cOLNDs/cOFNDs (HaCaT, HDF, and HMEC-1 cells) either in normoxic (20 % O_2) or hypoxic (1 % O_2) conditions, in a humidified CO_2/air-incubator at 37° C. After 24 h, cells (~ 1.6 x 10^5 cells/ml of culture medium) reached about 90% of confluence. Medium was discarded and 20 µl of 5 mg/ml MTT in PBS were added to cells for 3 additional hours at 37° C. After plate centrifugation and cell supernatant discarding, the dark blue formazan crystals were dissolved using 100 µl of sodium dodecyl solphate (SDS). The plates were read on Synergy HT microplate reader at a test wavelength of 550 nm and at a reference wavelength of 650 nm. Data are expressed as percentage of viability.

3.2.10. Wound healing assay

Cell abilities to perform wound healing were assessed through a specific *in vitro* biological assay, commonly known as scratch assay[345]. Briefly, cells were cultured in their supplemented culturing medium to confluence density. Subsequently, cells were seeded (3 x 10^4 cells/ml) in 24 multi-well plate and incubated for 24 h at 37° C. Then cells were starved with 2% supplemented medium o/n. Subsequently, cells (2 x 10^4 cells/insert) were inoculated into cell culture Ibidi inserts, a specific type of supports composed by a 2-well silicone insert with a defined cell-free gap. Cells were incubated for 24 h, to allow cellular adhesion. Then, supports were removed and cells were incubated in absence or presence of 10% v/v MW cOLNB/cOFNB, MW cOLND/cOFND, and LW cOLND/cOFND suspensions or

OSS in normoxic (20% O_2) and hypoxic (1% O_2) conditions for 16 h. Live imaging was then performed using Nikon Plan Fluor fluorescent microscope (magnification 20X). Pictures were taken using Nikon Eclipse TI-E objective. ImageJ (1.48 v) was used to analyse pictures. Briefly, wound areas were delimited using the free-hand selection tool; then, the measurement tool was employed to edit the data window listing the area in μm^2 for each scratch.

3.2.11. Confocal microscopy analysis on bacteria and yeasts

Nanobubbles and nanodroplets were conjugated with 10% FITC solution overnight and sterilised under UV-C radiation for 20 min.

MRSA and *S. pyogenes* bacteria (10^9 CFUs/ml) were incubated without or with 10% v/v FITC-labelled MW cOLNBs/cOFNBs, MW cOLND/cOFNDs, and LW cOLNDs/cOFNDs for 3 and 24 h with agitation at 37° C. At each incubation time, bacteria and different formulation suspensions (50 µl) were transferred on glass slides, heat-fixed, and subsequently stained with 5 µg/ml PI in humid chamber at 37° C for 15 min. Bacteria were fixed with mounting solution and covered by cover slips. Confocal fluorescent images were taken using FITC and TRITC filters.

C. albicans and *C. glabrata* yeasts (10^8 CFUs/ml) were stained with 10 µg/ml PI and incubated without or with 10% v/v FITC-labelled MW cOLNBs/cOFNBs, MW cOLND/cOFNDs, and LW cOLNDs/cOFNDs for 3 and 24 h with agitation at 37° C. At each incubation time, 100 µl suspensions from yeasts and different formulations were transferred on glass slides. Yeasts were fixed with mounting solution and covered by cover slips. Confocal fluorescent images were taken using FITC and TRITC filters.

3.2.12. Microbiological assay on bacteria and yeasts

MRSA and *S. pyogenes* bacteria [10^4 Colony Forming Units (CFUs)/ml] were incubated in trypticase soy broth or TODD broth respectively alone (growth control) or with 10% v/v OSS, 0.139% MW or LW chitosan solution, MW cOFNB/cOLNB, MW cOLND/cOFND, and LW cOLND/cOFND formulations in sterile sampling tubes for 2, 3, 4, 6, and 24 h at 37° C. At each incubation time, serial ten-fold dilutions from each sample were prepared in 0.9% NaCl saline solution and 100 µl of each dilution was spread on TSA or TODD agar medium to

determine the number of CFU/ml and incubated in a humidified CO_2/air-incubator at 37° C for 24 h.

C*. albicans* and *C. glabrata* yeasts (10^5 CFUs/ml) were incubated in SAB broth and experiments were performed as described above for bacteria. At each incubation time, each dilution was spread on SAB agar medium to determine the number of CFU/ml and incubated at 37° C for 24 h.

3.2.13. Statistical analysis

Each condition was performed at least in duplicate for every experiment. At least three independent experiments were performed for every investigational study. Numerical data are shown as means ± standard errors of the means (SEM) for inferential results or as means ± standard deviations (SD) for descriptive results[352]. Imaging data are shown as representative pictures. All data were analysed for significance by a one-way analysis of variance (ANOVA) followed by Tukey's post hoc test.

CHAPTER 4.
RESULTS

4.1. Medium molecular weight chitosan nanobubbles

4.1.1. Medium molecular weight chitosan nanobubble physico-chemical characterisation

After manufacturing, MW cOLNBs and MW cOFNBs were characterised for morphology by optical microscopy and TEM, as well as for average diameters, polydispersity indexes, and zeta potentials by dynamic light scattering.

MW cOLNBs displayed spherical shapes (Fig. 11, panels A and B: optical microscopy and TEM images, respectively) and sizes in the nanometer range, with average diameters of 700 nm (Fig. 11, panel C). Moreover, MW cOLNBs displayed cationic zeta potentials with values around +37 mV. The physico-chemical characteristics of all nanobubble formulations tested in this study are summarised in Table 3.

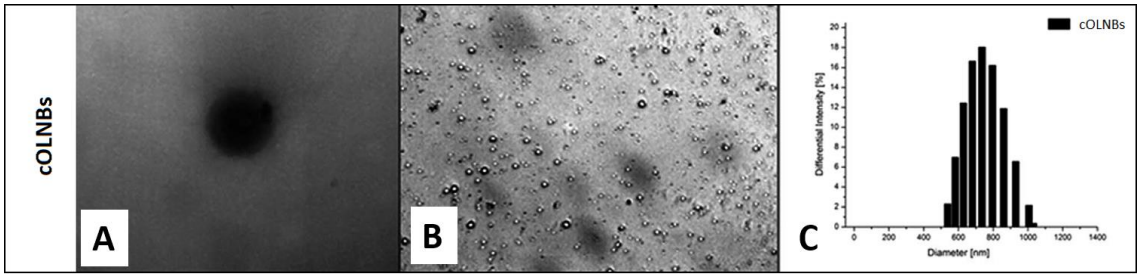

Fig. 11. Morphology and size distribution of MW cOLNBs. MW cOLNBs were checked for morphology by TEM and optical microscopy, and for size distribution by dynamic light scattering. Results are shown as representative images from ten different preparations. Panel A. MW cOLNB image by TEM. Magnification: 52000X. Panel B. MW cOLNBimage by optical microscopy. Magnification: 630X. Panel C. MW cOLNBs size distribution by dynamic light scattering.

Nanocarrier	MW cOLNB	MW cOFNB
Outher shell polysaccharide	MW chitosan	MW chitosan
Inner core fluorocarbon	PFP	PFP
Fluorocarbon boiling point	32° C	32° C
Diameter (nm ± SD)	745,20 ± 117,89	320,40 ± 100,90
Polydispersity index	0,19	0,10
Zeta potential (mV ± SD)	+ 39,20 ± 1,00	+ 38,65 ± 1,00

Table 3. Physico-chemical characterisation of MW cOLNBs and MW cOFNBs.
MW cOLNB/cOFNB formulations were characterised for diameters, polydispersity index, and zeta potential by dynamic light scattering. Results are shown as means ± SD from ten different preparations for each formulation.

4.1.2. Mechanical interaction between medium molecular weight chitosan oxygen-loaded nanobubbles and human keratinocytes

The mechanical interaction between MW cOLNBs and human keratinocytes was investigated through analysis by confocal microscopy. HaCaT cells ($6x10^4$ cells/ml) were left untreated or treated with 10% v/v FITC-labelled MW cOLNBs under normoxic conditions. After 24 h, human keratinocytes were fixed and then incubated with PI to visualise nucleic acids.

As shown in Fig. 12 (panel f), MW cOLNBs were avidly internalised by human keratinocytes.

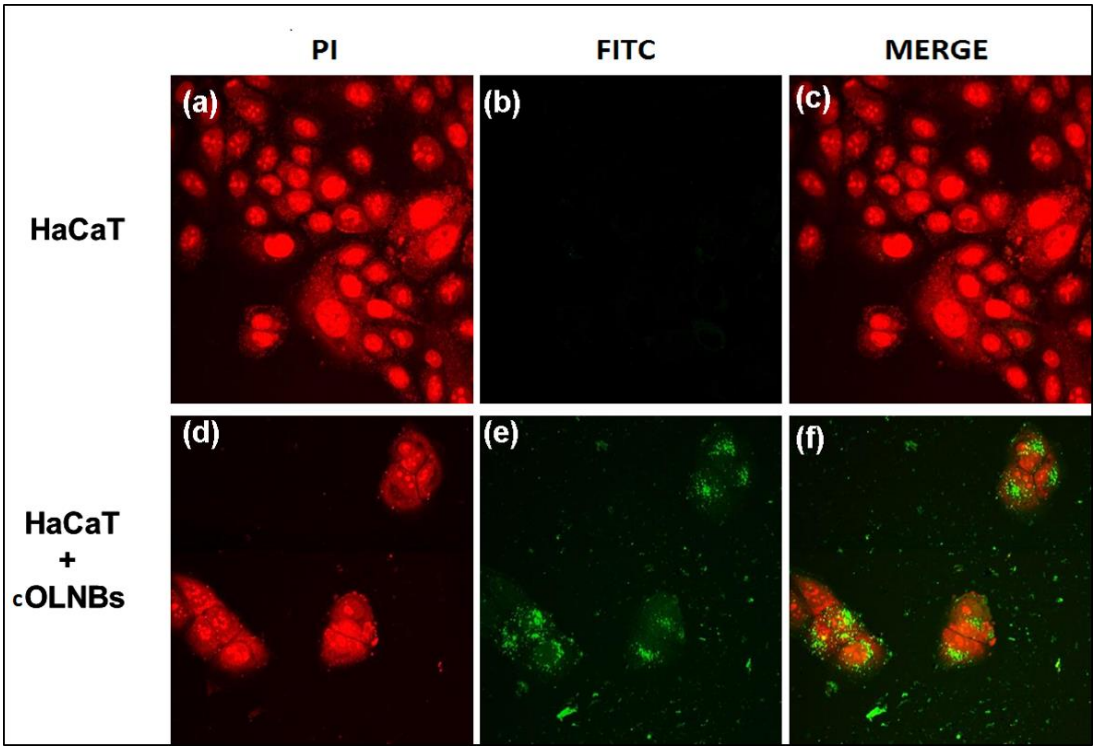

Figure 12. MW cOLNB internalisation by human keratinocytes. HaCaT cells ($6x10^4$ cells/ml) were left untreated or treated with FITC-labelled MW cOLNBs for 24 h in normoxia (20% O_2). After PI staining, cells were checked by confocal microscopy. Results are shown as representative images from three independent experiments. Panels a-c (red, green, merged): control cells; panels d-f (red, green, merged): OLNB-treated cells. Red: cell nuclei after PI staining. Green: FITC-labelled MW cOLNBs. Magnification: 60X.

4.1.3. Biocompatibility of medium molecular weight chitosan nanobubbles with human keratinocytes

The biocompatibility of MW cOLNBs and cOFNBs with normoxic and hypoxic human keratinocytes was evaluated by using a series of complementary biochemical assays. In particular, cell metabolic activity was measured by ATP assay, treatment cytotoxicity was analysed by LDH assay, and cell viability was checked by MTT assay. HaCaT cells (5×10^5 cells/ml for ATP studies, 5×10^5 cells/ml for LDH studies, and 1.6×10^5 cells/ml for MTT studies) were incubated for 24 h in presence or absence of 10% v/v MW cOLNBs or cOFNBs either in normoxic (20 % O_2) or hypoxic (1 % O_2) conditions.

As shown in Fig. 13 (results from ATP (A), LDH (B), and MTT (C) assays, respectively), hypoxia displayed significant toxicity, affecting HaCaT cell metabolism and viability. However, the values obtained upon MW cOLNB treatment either in normoxia or in hypoxia were not significantly different in comparison with their respective controls. A slight toxicity of MW cOFNDs was observed after measuring LDH release, but was not confirmed by ATP and MTT assays.

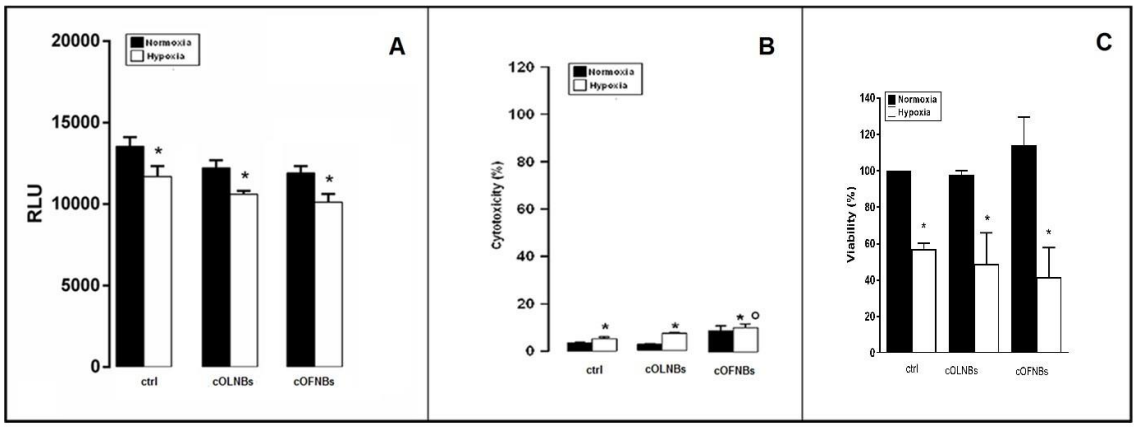

Fig. 13. Effects of hypoxia and MW chitosan nanobubbles on human keratinocyte viability. HaCaT cells (5 x 10^5 cells/ml for ATP studies, 5 x 10^5 cells/ml for LDH studies, and 1.6 x 10^5 cells/ml for MTT studies) were left untreated or treated with MW cOLNBs and MW cOFNBs for 24 h in normoxia (20% O_2, black columns) or hypoxia (1% O_2, white columns). After collection of cell supernatants and lysates, ATP production was measured through ATP assay (panel A), cytotoxicity percentage through LDH assay (panel B), and cell viability percentage was measured through MTT assay (panel C). Results are shown as means + SEM from three independent experiments. Data were also evaluated for significance by ANOVA: * vs normoxic control cells: $p<0.05$; ° vs hypoxic control cells: $p<0.05$.

4.1.4. Effects of hypoxia and medium molecular weight chitosan nanobubbles on the migration of human keratinocytes

HaCaT cell abilities to migrate and to promote wound healing under hypoxic conditions after treatment with nanobubbles, as well as OSS, was evaluated through scratch assay. Cells (3 x 10^5 cells/ml) were allowed to grow within cell culture well inserts purposely made to generate a standardised cell-free gap within the well for 24 h. Then, cells were incubated in absence or presence of 10% v/v MW cOLNBs, MW cOFNBs and OSS in normoxic and hypoxic conditions for 16 h.

As shown in Fig. 14, hypoxia slowed down the migration of human keratinocytes with respect to normoxic conditions. Additional treatment with MW cOLNBs fully abrogated hypoxia-dependent dysregulation of cell migration, whereas MW cOFNBs and OSS did not.

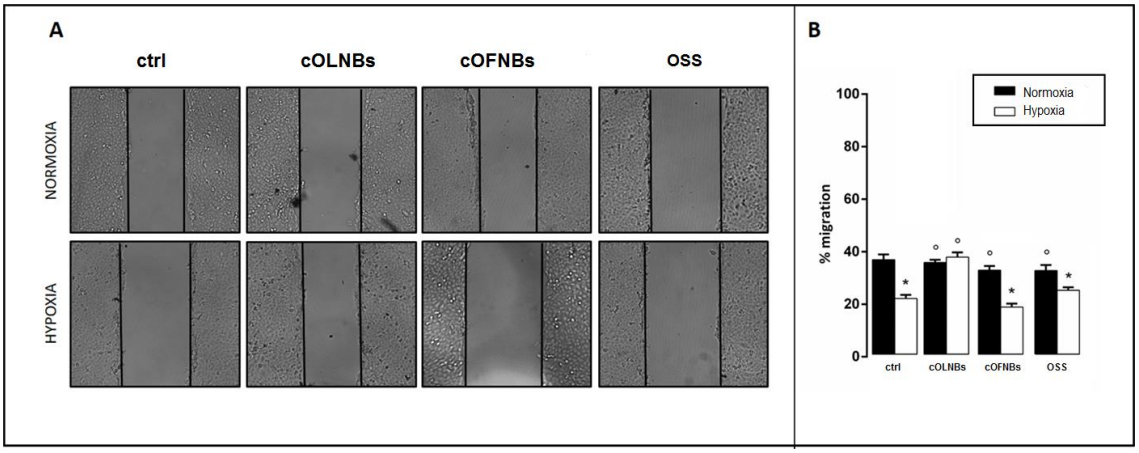

Fig. 14. Effects of hypoxia and MW chitosan nanobubbles on the migration and wound healing abilities of human keratinocytes. HaCaT cells (3 x 10^5 cells/ml) were seeded in two confluent monolayers, divided by a scratch of 500 µm, and incubated for 16 h in normoxia (20% O_2) or hypoxia (1% O_2) with/without 10% v/v MW cOFNBs, MW cOLNBs or OSS. Thereafter, scratch lengths were photographed and measured. Panel A: representative images. Panel B: means + SEM of scratch lengths. Results are from three independent experiments performed in triplicates. Data were also evaluated for significance by ANOVA: * vs normoxic untreated cells: $p<0.01$; ° vs hypoxic untreated cells: $p<0.01$.

4.1.5. Mechanical interaction between medium molecular weight chitosan nanobubbles and MRSA bacteria

The mechanical interaction between MW cOLNBs or cOFNBs and MRSA bacteria was investigated through analysis by confocal microscopy. MRSA bacteria (10^9 CFU/ml) were left untreated or treated with 10% v/v FITC-labelled MW cOLNBs or OFNBs under normoxic conditions. After 3 h and 24 h, bacteria were fixed and stained with PI.

After 3 hours of incubation, nanobubbles seemed to physically interact with MRSA wall (data not shown). Even after 24 hours of incubation, both MW cOLNBs and cOFNBs appeared to still adhere to the bacterial wall, without being internalised by MRSA (Fig. 15).

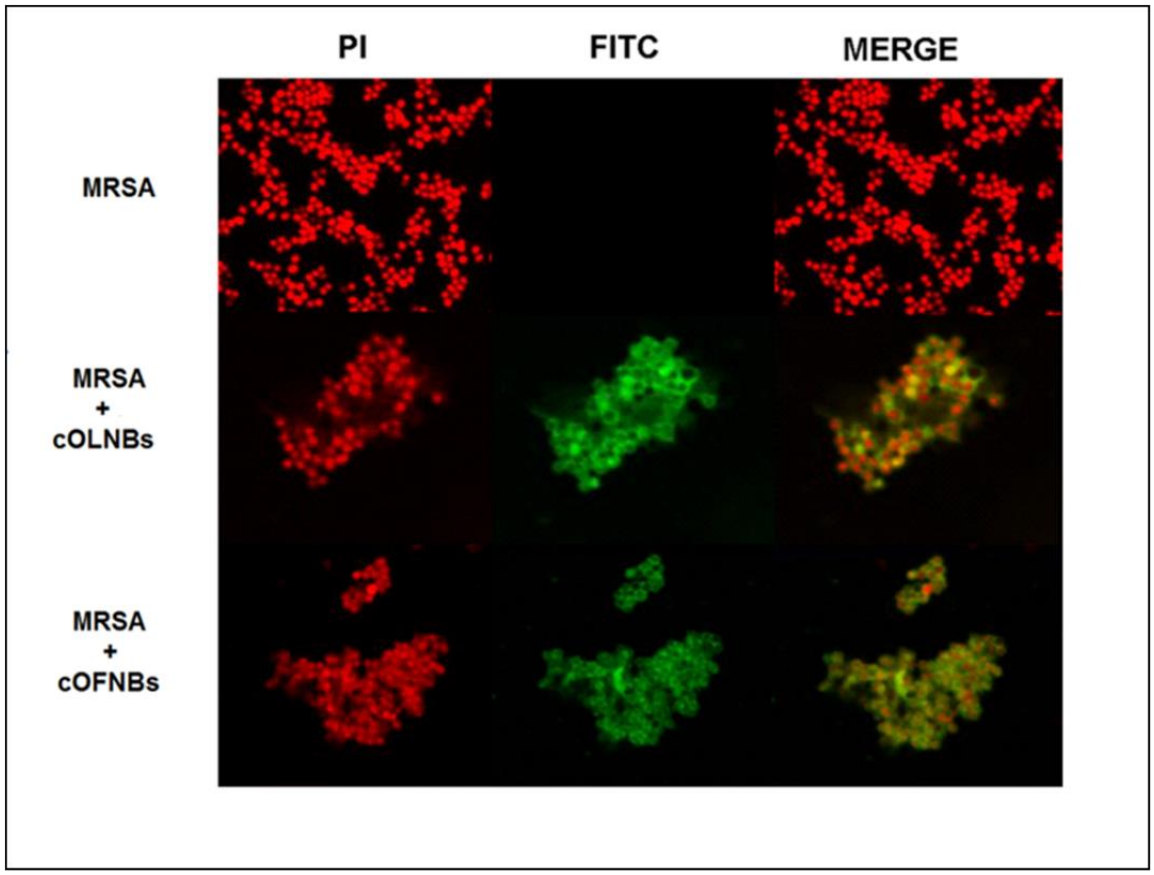

Fig. 15. MW chitosan nanobubble adhesion to MRSA bacterial wall. MRSA bacteria (10^9 CFUs/ml) were left alone or incubated with 10% v/v FITC-labelled MW cOLNBs/cOFNBs for 24 h. After staining bacteria with PI, confocal fluorescent images were taken using FITC and TRITC filters. Data are shown as representative images from three independent experiments. Magnification: 100X. Red: PI. Green: FITC.

4.1.6. Antibacterial activity of medium molecular weight chitosan nanobubbles on MRSA bacteria

The antibacterial properties of MW chitosan nanobubbles against MRSA were evaluated through a microbiological assay. MRSA bacteria (10^4 CFUs/ml) were incubated alone or in presence of 10% v/v OSS, free MW chitosan solution (0.139% m/v), MW cOFNBs, or MW cOLNBs. The bacterial growth was monitored for 2, 3, 4, 6 and 24 h.

As shown in Fig. 16, both MW cOLNBs and MW cOFNBs, as well as free MW chitosan solution, significantly inhibited MRSA growth up to 6 hours of incubation, especially between 4 and 6 hours, whereas OSS did not affect MRSA growth. At these observational timepoints, no significant differences were observed among treatments with MW cOLNBs, MW cOFNBs, and chitosan alone. The bacterial growth did not appear to be affected by any treatments after 24 h of incubation.

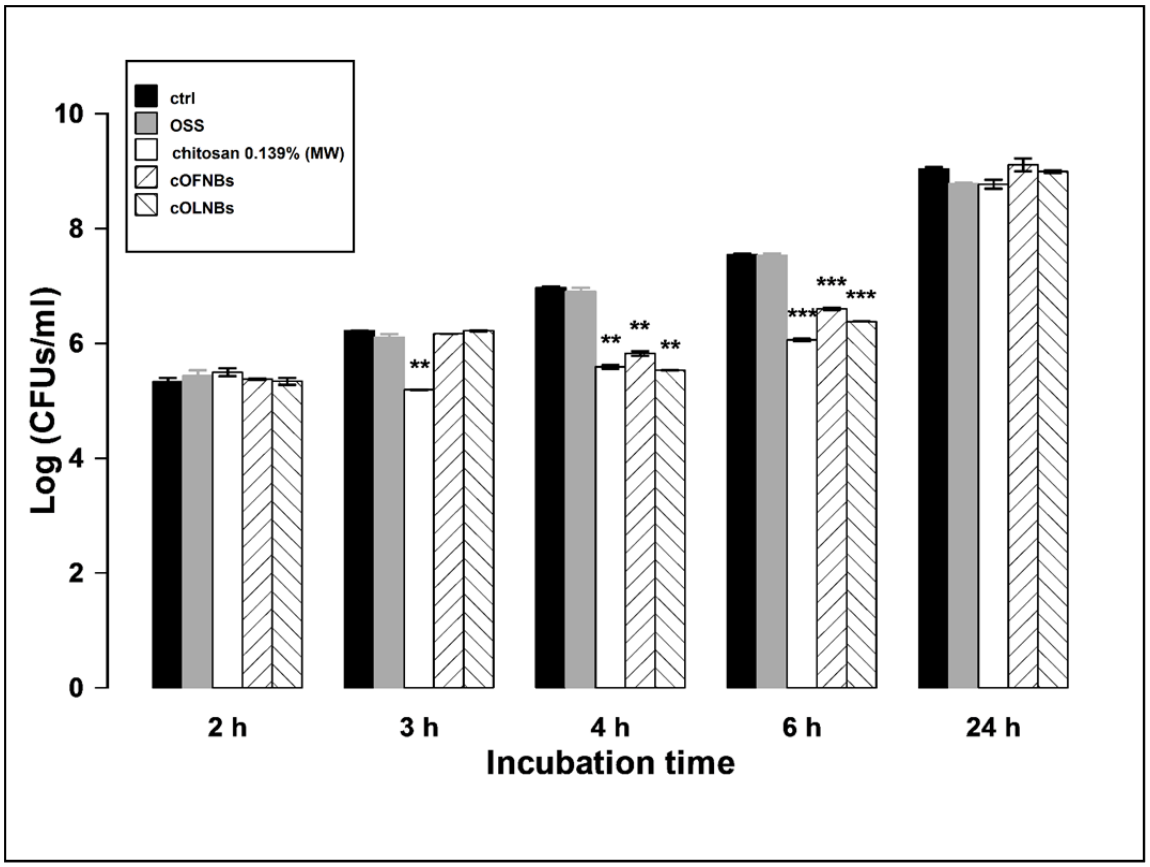

Fig. 16. Antibacterial activity of MW chitosan nanobubbles on MRSA bacteria. MRSA bacteria (10^4 CFUs/ml) were incubated alone or with 10% v/v OSS, free MW chitosan solution (0.139% m/v), MW cOFNB suspension, or MW cOLNB suspension in sterile conditions at 37°C and their growth was monitored for 2, 3, 4, 6 and 24 h. At each incubation time, the samples were spread on TSA agar medium to determine the CFUs/ml. Results are shown as means ± SEM from three independent experiments and expressed as Log CFUs/ml. Data were evaluated for significance by ANOVA: vs controls: 3-4 h, ** p<0.01; 6 h, *** p=0.0001.

4.1.7. Mechanical interaction between medium molecular weight chitosan nanobubbles and *C. albicans* yeasts

The mechanical interaction between MW cOLNBs or cOFNBs and *C. albicans* yeasts was investigated through analysis by confocal microscopy. *C. albicans* yeasts (10^8 CFUs/ml) were left untreated or treated with 10% v/v FITC-labelled MW cOLNBs or MW cOFNBs under normoxic conditions. After 3 h and 24 h, yeasts were fixed and stained with PI.

As shown in Fig. 17, both formulations appeared to have been avidly uptaken and internalised by yeasts already at the earlier observational time-point (3 h). Consistently, cOLNB/OFNB internalisation by yeasts was also observed at the later time-point (24 h) of incubation (data not shown).

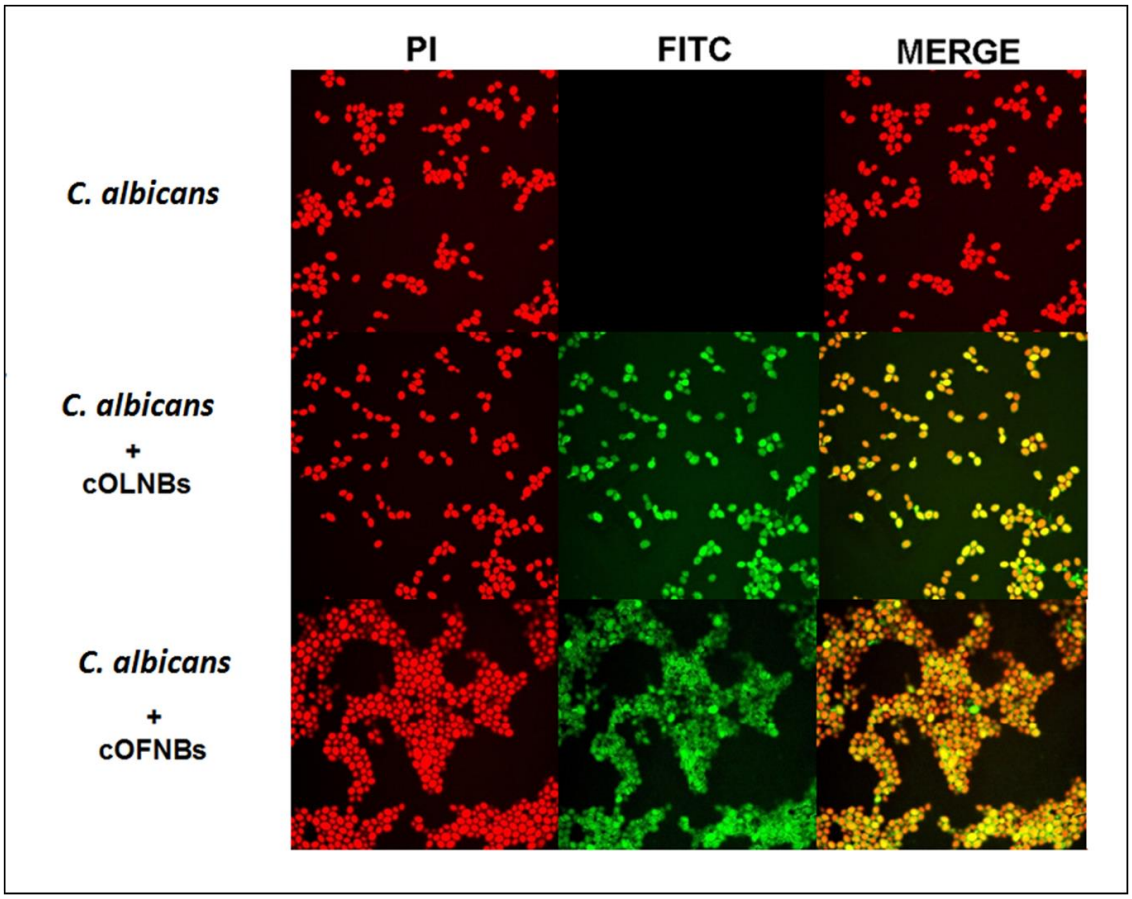

Fig. 17. MW chitosan nanobubble internalisation by *C. albicans* yeasts. *C. albicans* yeasts (10^8 CFUs/ml) were left alone or incubated with 10% v/v FITC-labelled MW cOLNBs or cOFNBs for 3 h. After staining yeasts with PI, confocal fluorescent images were taken using FITC and TRITC filters. Data are shown as representative images from three independent experiments. Magnification: 100X. Red: PI. Green: FITC.

4.1.8. Antifungal activity of medium molecular weight chitosan nanobubbles on *C. albicans* yeasts

The antifungal properties of MW chitosan nanobubbles against *C. albicans* were evaluated through a microbiological assay. *C. albicans* yeasts (10^5 CFUs/ml) were incubated alone or in presence of 10% v/v OSS, free MW chitosan solution (0.139% m/v), MW cOFNBs, or MW cOLNBs. The fungal growth was monitored for 2, 3, 4, 6 and 24 h.

As shown in Fig. 18, both MW cOLNBs and MW cOFNBs, as well as free MW chitosan solution, significantly inhibited *C. albicans* growth up to 24 hours of incubation, with no significant differences being observed among these three treatments at any observational timepoints. On the contrary, OSS did not affect fungal growth at any times.

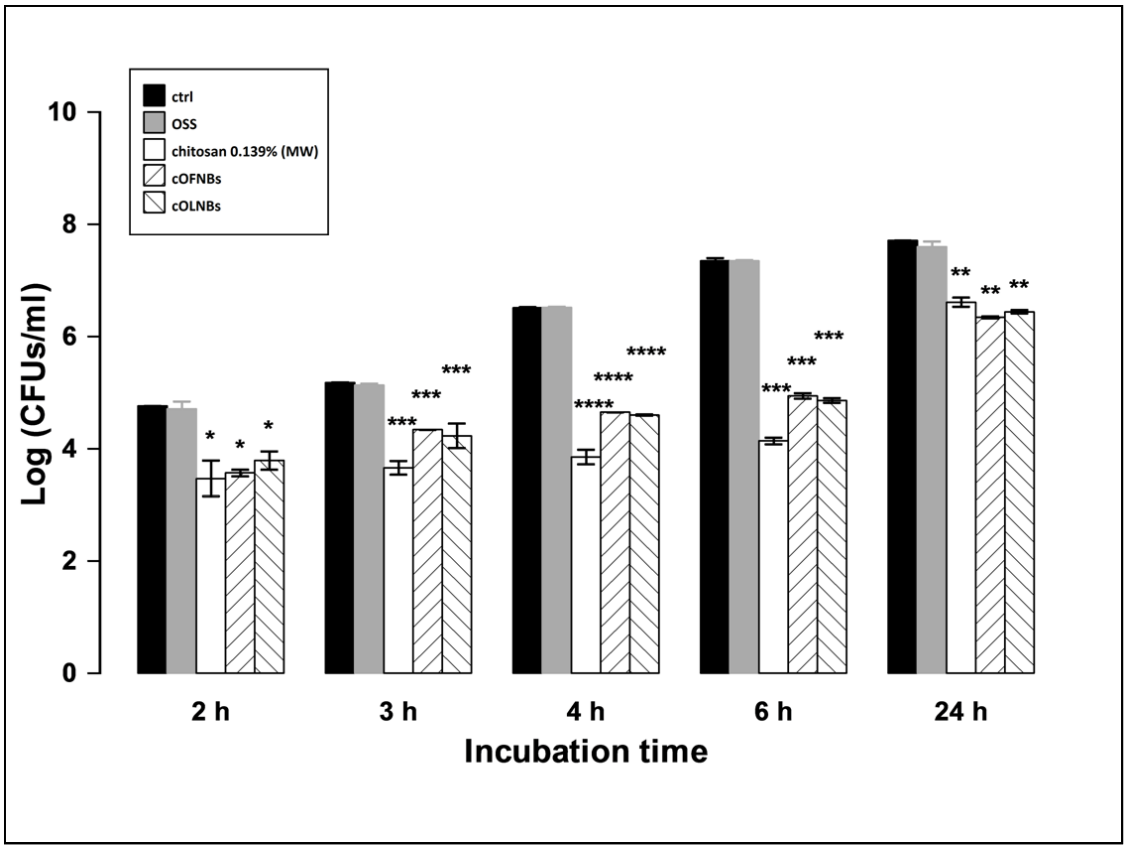

Fig. 18. Antifungal activity of MW chitosan nanobubbles on *C. albicans* yeasts. *C. albicans* yeasts (10^5 CFUs/ml) were incubated alone or with 10% v/v OSS, free MW chitosan (0.139% m/v) solution, MW cOFNB suspension, or MW cOLNB suspension in sterile conditions at 37°C and their growth was monitored for 2, 3, 4, 6 and 24 h. At each incubation time, the samples were spread on SAB agar medium to determine the CFUs/ml. Results are shown as means ± SEM from three independent experiments and expressed as Log CFUs/ml. Data were evaluated for significance by ANOVA: vs controls: 2 h, * p<0.05; 3-6 h, *** p=0.0001; 4 h, **** p<0.0001; 24 h, ** p<0.01.

4.2. Medium molecular weight chitosan nanodroplets

4.2.1. Medium molecular weight chitosan nanodroplet physico-chemical characterisation

After manufacturing, MW cOLNDs and MW cOFNDs were characterised for morphology by optical microscopy and TEM, as well as for average diameters, polydispersity indexes, and zeta potentials by dynamic light scattering.

MW cOLNDs displayed spherical shapes (Fig. 19, panel A and B: optical microscopy and TEM images, respectively) and sizes in the nanometer range, with average diameters of 700 nm (Fig. 19, panel C). Moreover, MW cOLNDs displayed cationic zeta potentials with values around +35 mV. The physico-chemical characteristics of MW nanodroplet formulations tested in this study are summarised in Table 4.

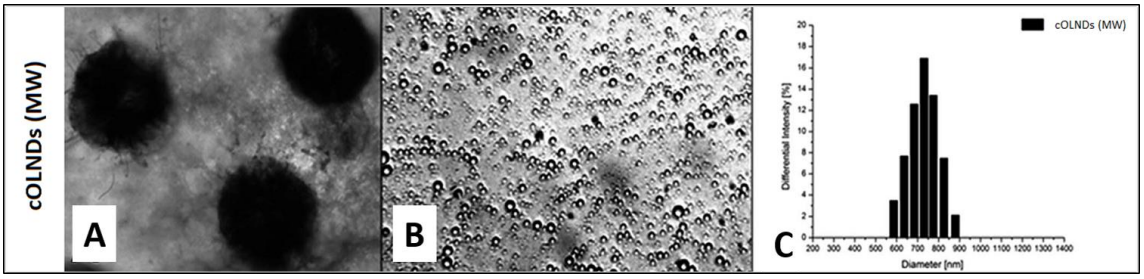

Fig. 19. Morphology and size distribution of MW cOLNDs. MW cOLNDs were checked for morphology by TEM and optical microscopy, and for size distribution by dynamic light scattering. Results are shown as representative images from ten different preparations. Panel A. MW cOLND image by TEM. Magnification: 15 500X. Panel B. MW cOLNDs image by optical microscopy. Magnification: 630X. Panel C. MW cOLND size distribution by dynamic light scattering.

Nanocarrier	MW cOLND	MW cOFND
Outher shell polysaccharide	MW chitosan	MW chitosan
Inner core fluorocarbon	DFP	DFP
Fluorocarbon boiling point	51° C	51° C
Diameter (nm ± SD)	726,55 ± 123,07	332,70 ± 101,10
Polydispersity index	0,24	0,11
Zeta potential (mV ± SD)	+ 35,38 ± 1,00	+ 34,97 ± 1,00

Table 4. Physico-chemical characterisation of MW cOLNDs and MW cOFNDs.
MW cOLND/cOFND formulations were characterised for diameters, polydispersity index, and zeta potential by dynamic light scattering. Results are shown as means ± SD from ten different preparations for each formulation.

4.2.2. *In vitro* oxygen release from medium molecular weight chitosan oxygen-loaded nanodroplets

In vitro oxygen release from MW cOLND formulations was monitored by an oxymeter up to 6 h through dialysis bag technique.

At the initial observational timepoint (0 min), the oxygen concentration in the receiving saline solution was previously reduced to 0.5 mg/L, to mimic sever hypoxic conditions. Already after 15 minutes, MW cOLNDs proved to be able to release oxygen into the environment and the oxygen concentration in the hypoxic solution reached the value of 3.5 mg/L. For all the observational period (6 h), oxygen delivery from MW cOLNDs continuously increased as well as related oxygen concentration in the receiving solution (up to ~ 6 mg/L). MW cOLNDs effectively released clinically oxygen amounts in a time-sustained manner *in vitro*. These results are shown in Fig. 20.

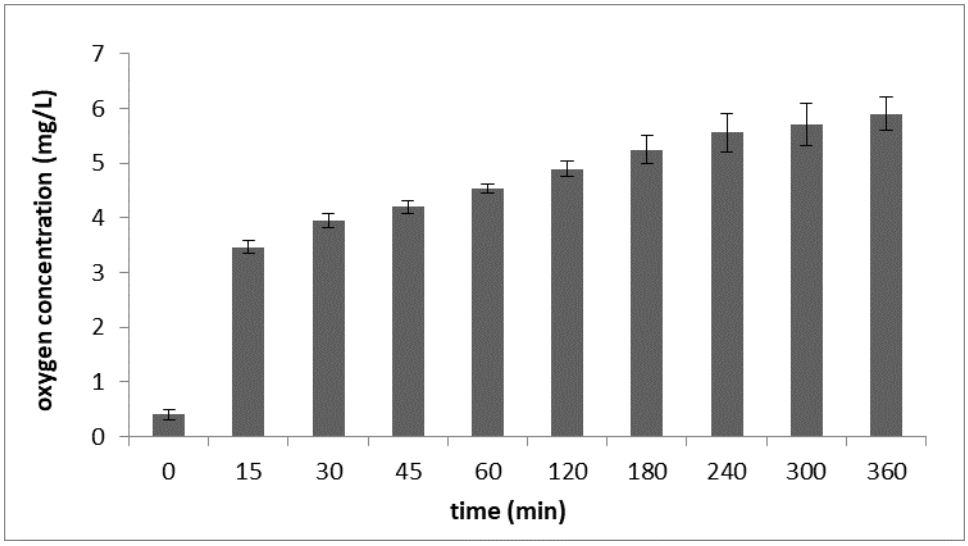

Fig. 20. *In vitro* oxygen release from MW cOLNDs. Oxygen release from MW cOLNDs were monitored for 15, 30, 45, 60, 120, 180, 240, 300, and 360 min by an oxymeter through dialysis bag technique. The donor solution (consisting of 3 ml of MW cOLNDs) was placed in a dialysis bag sealed and immersed in 45 ml of the receiving saline solution (oxygen concentration at 0 min = 0.5 mg/L). Results are shown as means ± SEM from three independent experiments.

4.2.3. Mechanical interaction between medium molecular weight chitosan oxygen-loaded nanodroplets and human keratinocytes

The mechanical interaction between MW cOLNDs and human keratinocytes was evaluated using a confocal microscopy approach. HaCaT cells ($5x10^5$ cells/ml) were left untreated or treated with 10% v/v FITC-labelled MW cOLNDs for 24 h under normoxic conditions. After incubation, keratinocytes were incubated with DAPI staining to visualise nucleic acids.

As shown in Fig. 21 (panel f), MW cOLNDs were avidly uptaken by human keratinocytes.

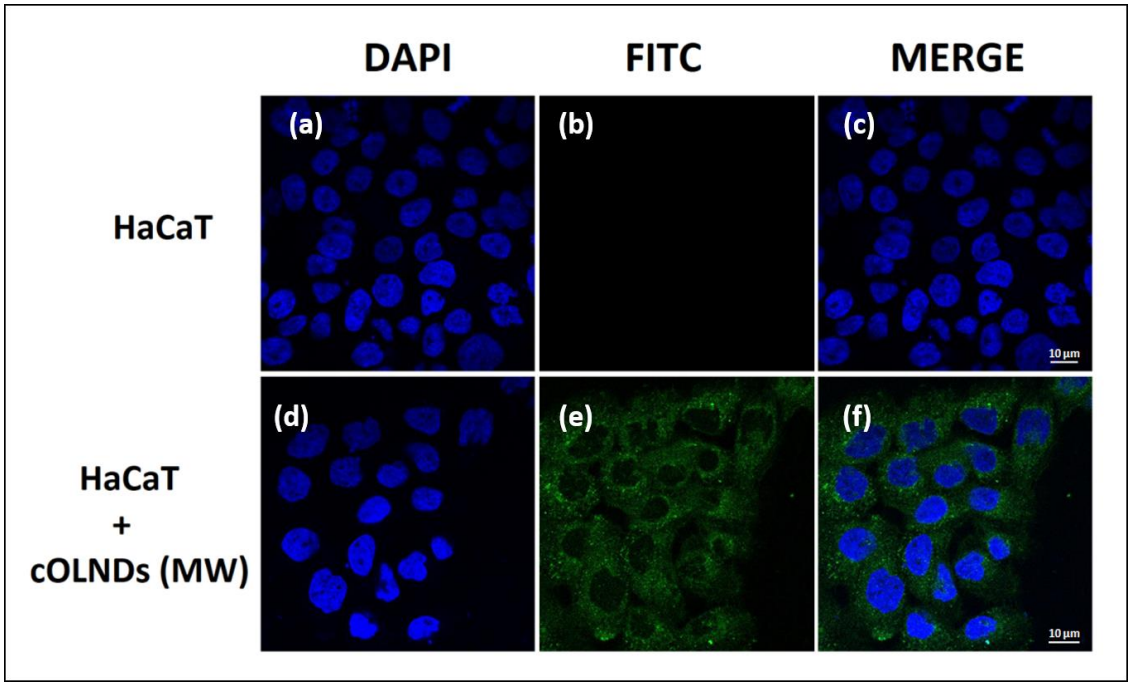

Fig. 21. MW cOLND internalisation by human keratinocytes. Human cells ($5x10^5$ cells/ml) were left untreated or treated with FITC-labelled MW cOLNDs for 24 h in normoxia (20% O_2). After DAPI staining, cells were checked by confocal microscopy. Results are shown as representative images from three independent experiments. Panels a-c (blue, green, merged): control cells; panel d-f (blue, green, merged): MW OLND-treated cells. Blue: cell nuclei after DAPI staining. Green: FITC-labelled MW cOLNDs. Magnification: 63x.

4.2.4. Biocompatibility of medium molecular weight chitosan nanodroplets with human keratinocytes

The biocompatibility of MW cOLNDs and cOFNDs with normoxic and hypoxic human keratinocytes was evaluated through LDH and MTT assays. In particular, treatment cytotoxicity was analysed by LDH assay while cell viability was checked by MTT assay. Briefly, HaCaT cells (5 x 10^5 cells/ml for LDH studies, 1.6 x 10^5 cells/ml for MTT studies) were incubated for 24 h alone or in presence of 10% v/v MW cOFNDs or MW cOLNDs either under normoxic (20% O_2) and hypoxic (1% O_2) conditions.

As shown in Fig. 22, MW cOFNDs strongly reduced viability of cells, either in normoxic or hypoxic conditions. In contrast, MW cOLNDs did not reduce human keratinocytes viability while MW cOFNDs were toxic (~50%) to human keratinocytes, either in normoxia or hypoxia.

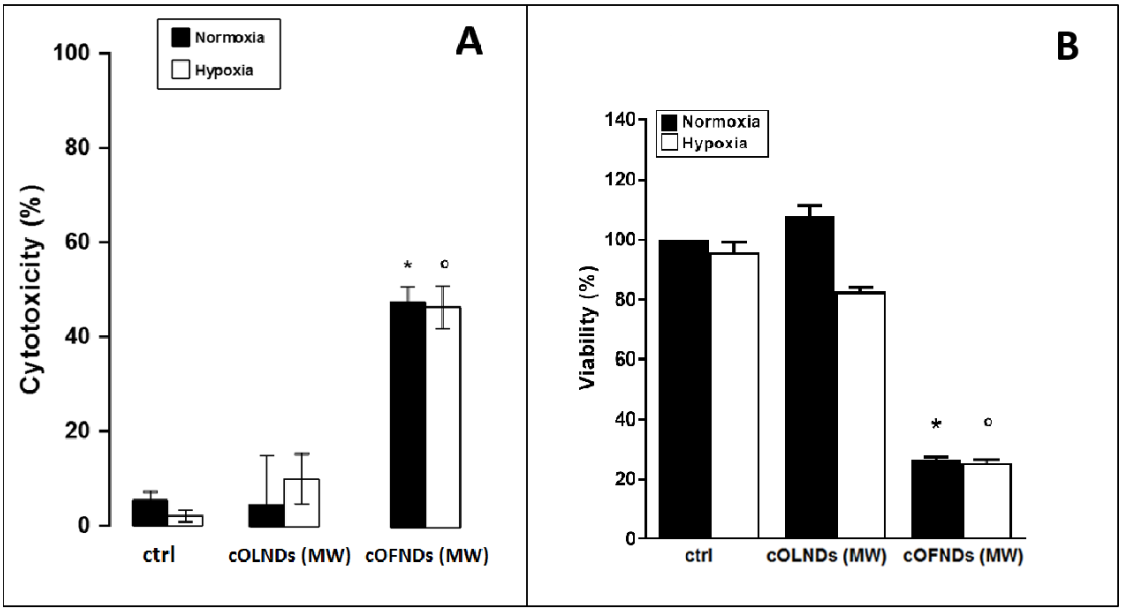

Fig. 22. Effects of hypoxia and MW chitosan nanodroplets on human keratinocyte viability. HaCaT cells (5 x 10^5 cells/ml for LDH studies and 1.6 x 10^5 cells/ml for MTT studies) were left untreated or treated with MW cOFNDs and MW cOLNDs for 24 h in normoxia (20% O_2, black columns) or hypoxia (1% O_2, white columns). After collection of cell supernatants and lysates, cytotoxicity percentage was measured through LDH assay (panel A), whereas cell viability percentage was measured through MTT assay (panels B). Results are shown as means+ SEM from three independent experiments. Data were also evaluated for significance by ANOVA: * vs normoxic control cells: $p<0.05$; ° vs hypoxic control cells: $p<0.05$.

4.2.5. Biocompatibility of medium molecular weight chitosan nanodroplets with human fibroblasts

MW chitosan nanodroplet biocompatibility with normoxic and hypoxic human fibroblasts was evaluated through LDH and MTT assays. In particular, treatment cytotoxicity was analysed by LDH assay while cell viability was checked by MTT assay. Briefly, HDF cells (5 x 10^5 cells/ml for LDH studies, 1.6 x 10^5 cells/ml for MTT studies) were incubated for 24 h alone or in presence of 10% v/v MW cOLNDs or cOFNDs in normoxia (20% O_2) and hypoxia (1% O_2).

Hypoxia did not significantly affect HDF cell viability. MW cOLNDs, as well as MW cOFNDs, did not display any significant toxicity on human fibroblasts either under normoxic or hypoxic conditions. These data were confirmed by both assays (Fig. 23, panel A and B). Even more so, the treatment with MW OLNDs promoted a reduction of cytotoxicity compared to untreated fibroblasts under hypoxic conditions (Fig. 23, panel A).

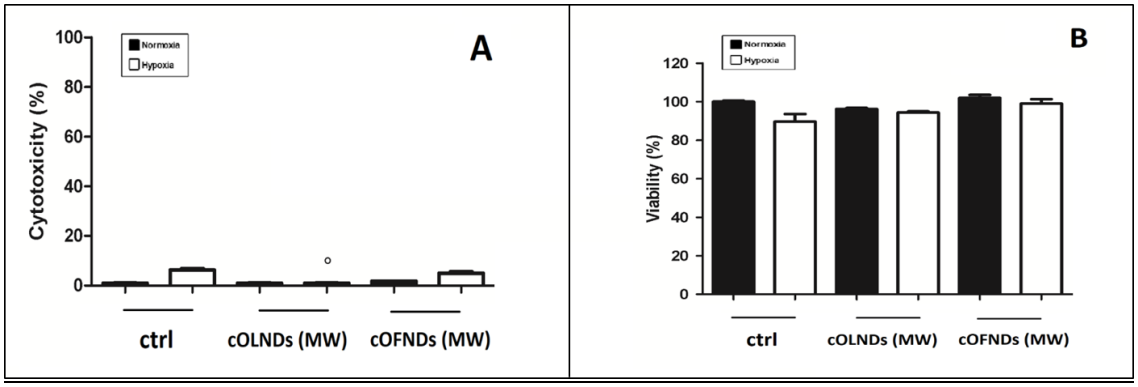

Fig. 23. Effects of hypoxia and MW chitosan nanodroplets on human fibroblast viability. HDF cells (5 x 10^5 cells/ml for LDH studies, 1.6 x 10^5 cells/ml for MTT studies) were left untreated or treated with MW cOLNDs and MW cOFNDs for 24 h in normoxia (20% O_2, black columns) or hypoxia (1% O_2, white columns). After collection of cell supernatants and lysates, cytotoxicity percentage was measured through LDH assay (panel A), whereas cell viability percentage was measured through MTT assay (panels B). Results are shown as means+ SEM from three independent experiments. Data were also evaluated for significance by ANOVA: ° vs hypoxic control cells, p<0.05.

4.2.6. Biocompatibility of medium molecular weight chitosan nanodroplets with human endothelium

The biocompatibility of MW cOLNDs and MW cOFNDs on human HMEC-1 endothelium was investigated through LDH and MTT studies. In particular, treatment cytotoxicity was analysed by LDH assay while cell viability was checked by MTT assay. Human endothelium (5 x 10^5 cells/ml for LDH assay, 1.6 x 10^5 cells/ml for MTT assay) was incubated for 24 h without or with 10% v/v MW cOLNDs or MW cOFNDs either in normoxic (20% O_2) or in hypoxic conditions (1% O_2).

According to results from analysis by LDH assay (Fig. 24, panel A), hypoxia mildly compromised the health of control cells, although it did not affect total cell viability, as emerged from investigation by MTT assay (Fig. 24, panel B). The treatment with MW cOFNDs appeared to be more toxic to cells compared to controls and reduced their viability strongly, both in normoxia and hypoxia. MW cOLNDs appeared less toxic than MW cOFNDs, however the presence of oxygen within the nanodroplets was not sufficient to counteract the loss of viability induced by nanodroplets themselves.

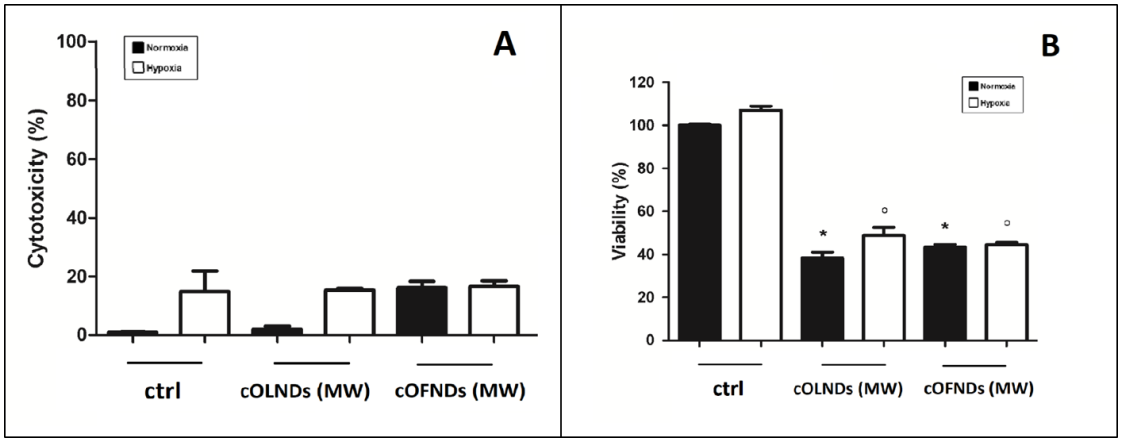

Fig. 24. Effects of hypoxia and MW chitosan nanodroplets on human endothelium viability. HMEC-1 endothelium (5 x 10^5 cells/ml for LDH studies, 1.6 x 10^5 cells/ml for MTT studies) were left untreated or treated with MW cOLNDs and MW cOFNDs for 24 h in normoxia (20% O_2, black columns) or hypoxia (1% O_2, white columns). After collection of cell supernatants and lysates, cytotoxicity percentage was measured through LDH assay (panel A), whereas cell viability percentage was measured through MTT assay (panels B). Results are shown as means+ SEM from three independent experiments. Data were also evaluated for significance by ANOVA: * vs normoxic control cells: $p<0.05$; ° vs hypoxic control cells, $p<0.05$.

4.2.7. Effects of hypoxia and medium molecular weight chitosan nanodroplets on the migration of human keratinocytes

The migration and related wound healing abilities of HaCaT cells treated with MW nanodroplets or OSS under hypoxic conditions was evaluated through scratch assay. Cells (3 x 10^5 cells/ml) were allowed to grow within cell culture inserts purposely made to generate a standardised cell-free gap within the well for 24 h. Then, cells were incubated in absence or presence of 10% v/v MW cOFNDs, MW cOLNDs and OSS in normoxic and hypoxic conditions for 16 h.

As shown in Fig. 25, hypoxia slowed down the migration of human keratinocytes with respect to normoxic conditions. Additional treatment with MW cOLNDs fully abrogated hypoxia-dependent dysregulation of cell migration, whereas MW cOFNDs and OSS did not.

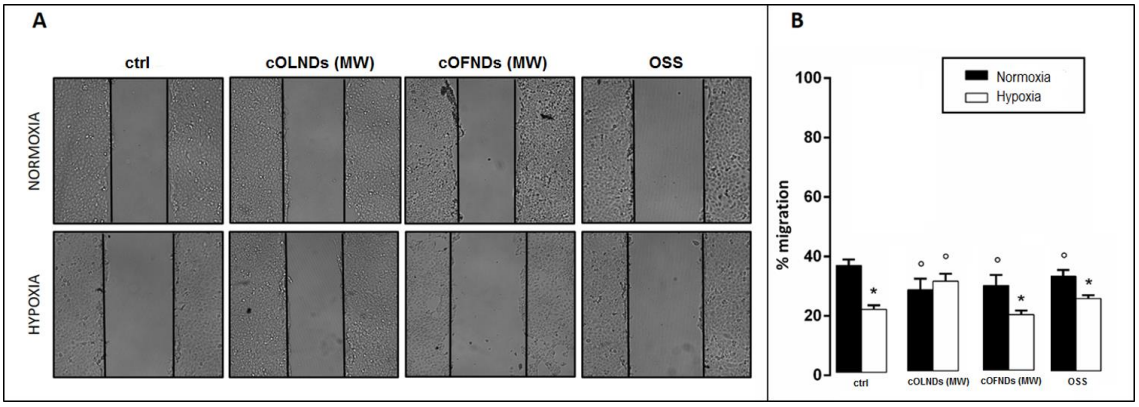

Fig. 25. Effects of hypoxia and MW chitosan nanodroplets on the migration and wound healing abilities of human keratinocytes. HaCaT cells (3 x 10^5 cells/ml) were seeded in two confluent monolayers, divided by a scratch of 500 µm, and incubated for 16 h in normoxia (20% O_2) or hypoxia (1% O_2) with/without 10% v/v MW cOFNDs, MW OLNDs or OSS. Thereafter, scratch lengths were photographed and measured. Panel A: representative images. Panel B: means + SEM of scratch lengths. Results are from three independent experiments performed in triplicates. Data were also evaluated for significance by ANOVA: * vs normoxic untreated cells: $p<0.01$; ° vs hypoxic untreated cells: $p<0.01$.

4.2.8. Effects of hypoxia and medium molecular weight chitosan nanodroplets on the migration of human fibroblasts

The migration and related wound healing abilities of human fribroblasts treated with MW nanodroplets or OSS under hypoxic conditions was evaluated through scratch assay. Cells (3 x 10^5 cells/ml) were allowed to grow within cell culture inserts purposely made to generate a standardised cell-free gap within the well for 24 h. Then, fibroblasts were incubated in absence or presence of 10% v/v MW cOLNDs, MW cOFNDs, and OSS in normoxic and hypoxic conditions for 16 h.

As shown in Fig. 26, hypoxia slowed down the migration of HDF cells with respect to normoxic conditions. Additional treatment with MW cOLNDs fully abrogated hypoxia-dependent dysregulation of cell migration, whereas MW cOFNDs and OSS did not.

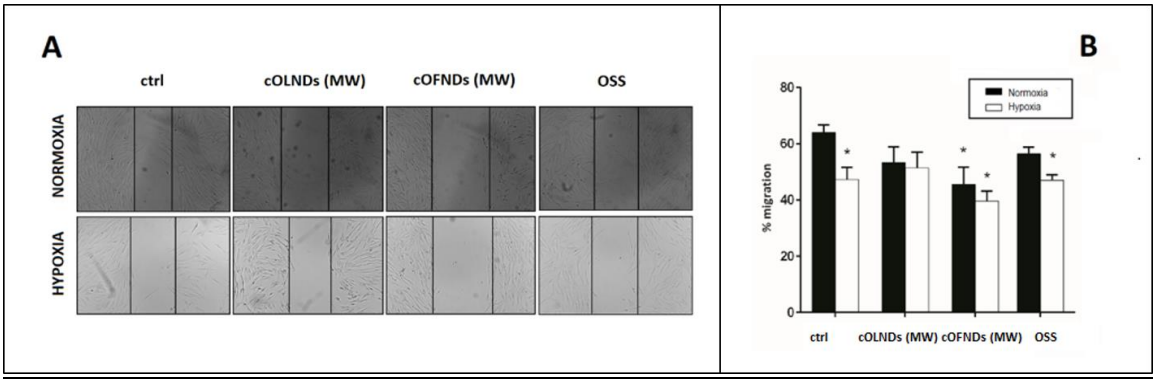

Fig. 26. Effects of hypoxia and MW chitosan nanodroplets on the migration and wound healing abilities of human fibroblasts. HDF cells (3 x 10^5 cells/ml) were seeded in two confluent monolayers, divided by a scratch of 500 µm, and incubated for 16 h in normoxia (20% O_2) or hypoxia (1% O_2) with/without 10% v/v MW cOLNDs, MW cOFNDs or OSS. Thereafter, scratch lengths were photographed and measured. Panel A: representative images. Panel B: means + SEM of scratch lengths. Results are from three independent experiments performed in triplicates. Data were also evaluated for significance by ANOVA: * vs normoxic untreated cells, p<0.01.

4.2.9. Effects of hypoxia and medium molecular weight chitosan nanodroplets on the migration of human endothelium

The effects of hypoxia and MW chitosan nanodroplets on the migration and related wound healing abilities of HMEC-1 cells were evaluated through scratch assay. HMEC-1 cells (3×10^5 cells/ml) were allowed to grow within cell culture inserts purposely made to generate a standardised cell-free gap within the well for 24 h. Then, cells were incubated in absence or presence of 10% v/v MW cOLNDs, MW cOFNDs, and OSS in normoxic and hypoxic conditions for 16 h.

Hypoxia strongly compromised the migration abilities of HMEC-1 and OSS did not alter significantly the values obtained from normoxic and hypoxic controls. However, as already described in paragraph 4.2.6, further treatments with MW cOLNDs or MW cOFNDs strongly affected cell viability. Due to the high percentage of cell mortality, wound healing properties could not be analysed in those samples. For this reason, no data are shown here. Nevertheless, the effects of hypoxia and OSS on HMEC-1 migration are going to be shown in the third and last part of the Results section. If interested in checking them now, the reader might well choose to jump momentarily to paragraph 4.3.8 and then come back here to go on with the reading.

4.2.10. Mechanical interaction between medium molecular weight chitosan nanodroplets and MRSA bacteria

The mechanical interaction between MW cOLNDs or MW cOFNDs and MRSA bacteria was investigated through analysis by confocal microscopy. MRSA bacteria (10^9 CFU/ml) were incubated without or with 10% v/v FITC-labelled MW cOLNDs or MW cOFNDs under normoxic conditions. After 3 h and 24 h, bacteria were fixed and stained with PI.

After 3 hours of incubation, nanodroplets seemed to physically interact with MRSA wall (data not shown). Even after 24 hours of incubation, MW cOLNDs, as well as MW cOFNDs, appeared to still adhere to the bacterial wall, without being uptaken by MRSA (Fig. 27).

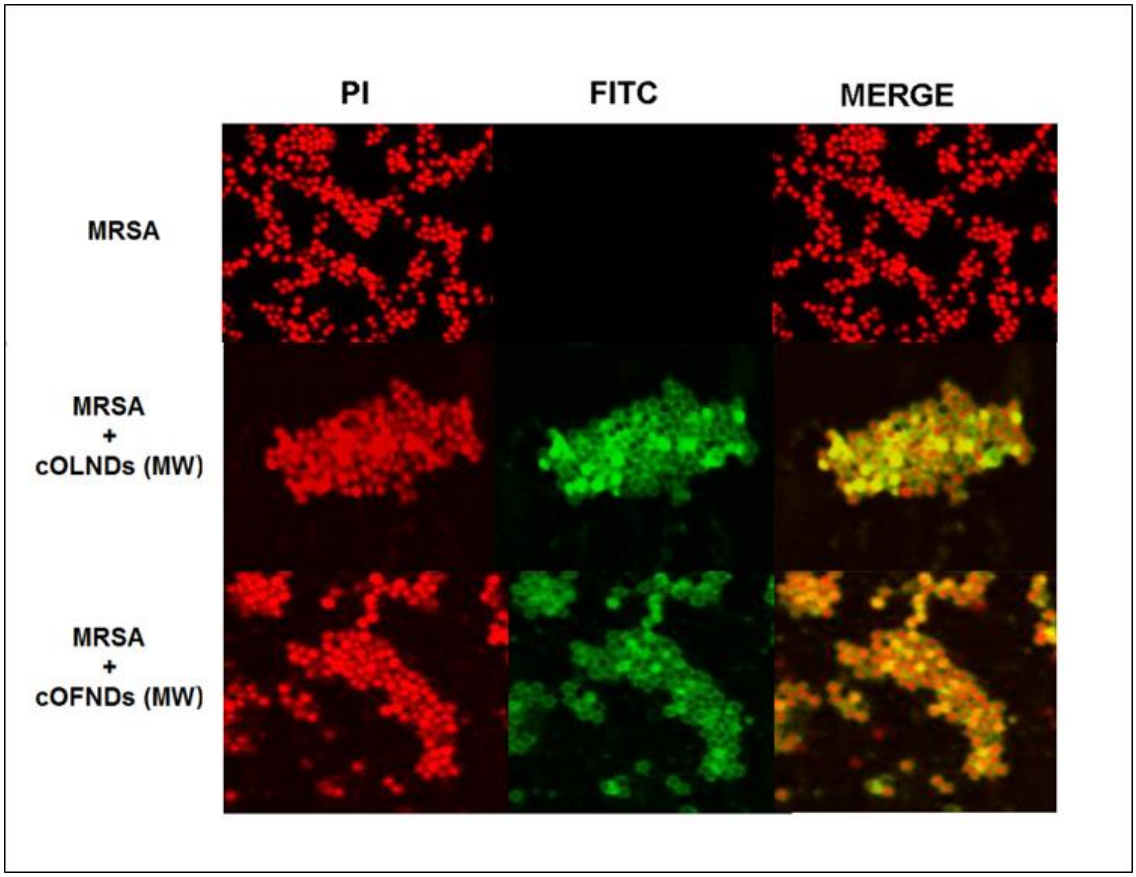

Fig. 27. MW chitosan nanodroplet adhesion to MRSA bacterial wall. MRSA bacteria (10^9 CFUs/ml) were left alone or incubated with 10% v/v FITC-labelled MW cOLNDs or MW cOFNDs for 24 h. After staining bacteria with PI, confocal fluorescent images were taken using FITC and TRITC filters. Data are shown as representative images from three independent experiments. Magnification: 100X. Red: PI. Green: FITC.

4.2.11. Antibacterial activity of medium molecular weight chitosan nanodroplets on MRSA bacteria

The antibacterial properties of MW chitosan nanodroplets against MRSA were evaluated through a microbiological assay. MRSA bacteria (10^4 CFU/ml) were incubated without or with 10% v/v OSS, free MW chitosan solution (0.139% m/v), MW cOFNDs, and MW cOLNDs. The bacterial growth was monitored for 2, 3, 4, 6 and 24 h.

As shown in Fig. 28, bacterial growth was significantly inhibited by both MW cOLNDs and MW cOFNDs, as well as by free MW chitosan solution but not by OSS, up to 6 hours of incubation, more notably at 6 hours. At these observational timepoints, no significant differences were observed among treatments with MW cOLNDs, MW cOFNDs, and chitosan alone. After 24 hours, any treatments did not affect bacterial growth.

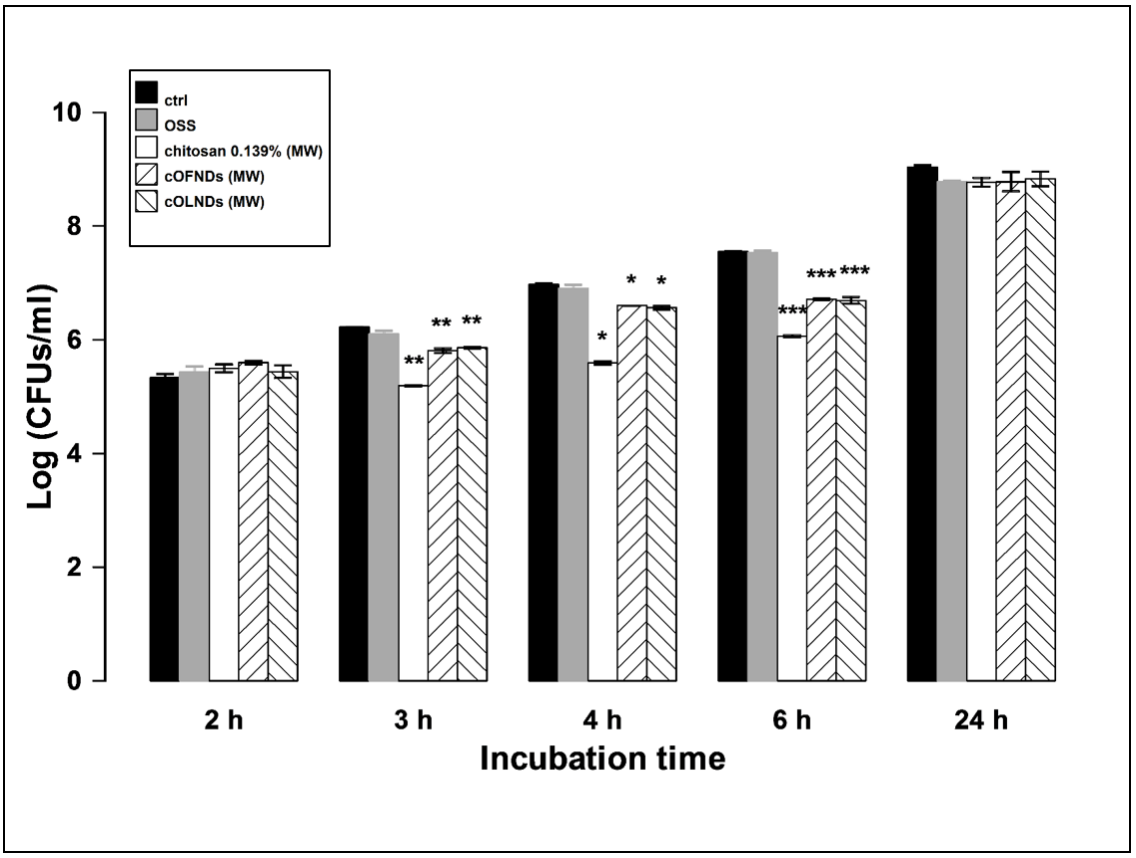

Fig. 28. Antibacterial activity of MW chitosan nanodroplets on MRSA bacteria. MRSA bacteria (10^4 CFUs/ml) were incubated alone or with 10% v/v OSS, free MW chitosan solution (0.139% m/v), MW cOFND suspension, and MW cOLND suspensions in sterile conditions at 37°C and their growth was monitored for 2, 3, 4, 6 and 24 h. At each incubation time, the samples were spread on TSA agar medium to determine the CFUs/ml. Results are shown as means ± SEM from three independent experiments and expressed as Log CFUs/ml. Data were evaluated for significance by ANOVA: vs controls: 3 h, ** p<0.01; 4 h, * p<0.05; 6 h, *** p=0.0001.

4.2.12. Mechanical interaction between medium molecular weight chitosan nanodroplets and *S. pyogenes* bacteria

The mechanical interaction between MW cOLNDs or MW cOFNDs and *S. pyogenes* bacteria was investigated through analysis by confocal microscopy. *S. pyogenes* bacteria (10^9 CFU/ml) were incubated without or with 10% v/v FITC-labelled MW cOLNDs or MW cOFNDs under normoxic conditions. After 3 h and 24 h, bacteria were fixed and stained with PI.

As shown in Fig. 29, both formulations appeared to have been uptaken and internalised by bacteria already at earlier observational time-point (3 h). Consistently, MW cOLND/cOFND internalisation by *S. pyogenes* bacteria was also observed at the later time-point (24 h) of incubation (data not shown).

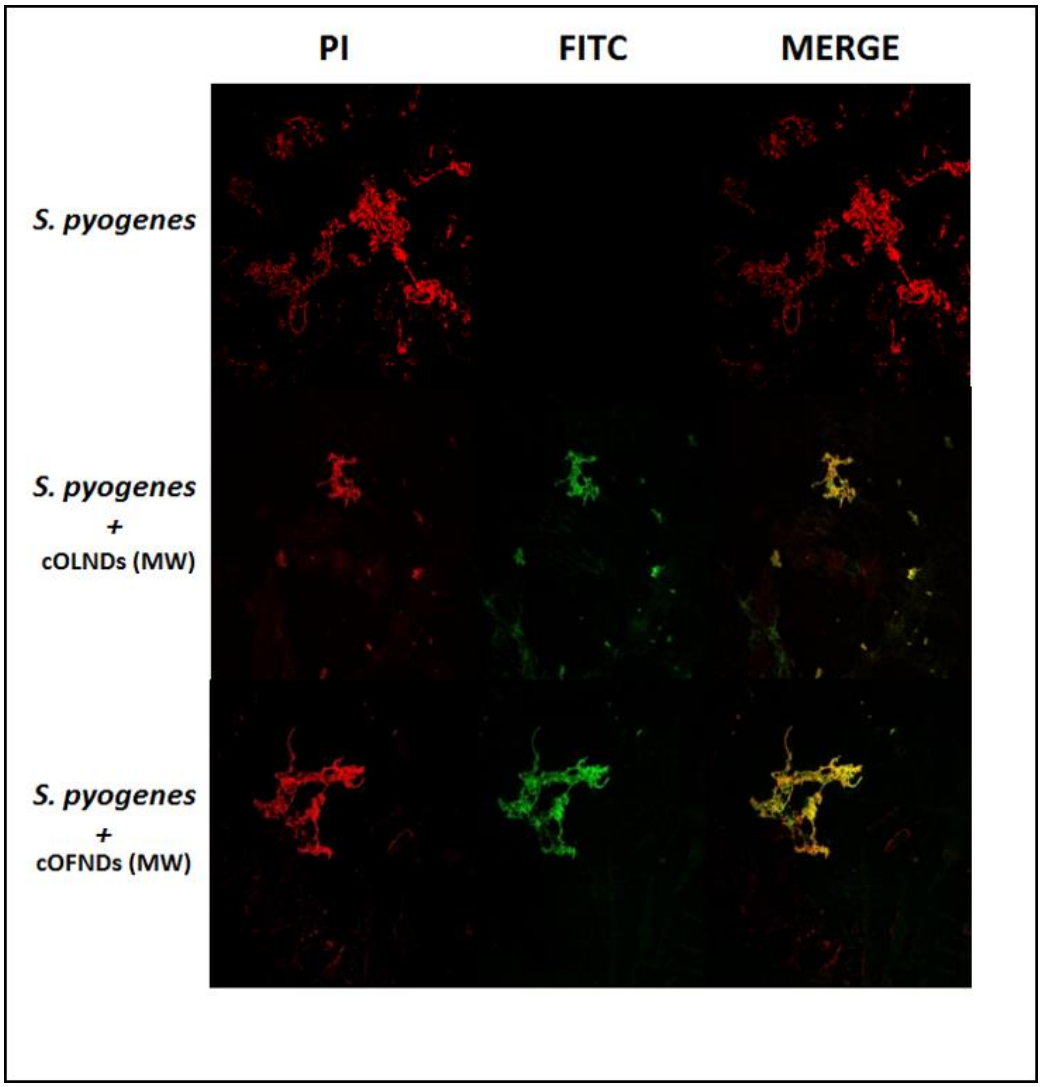

Fig. 29. MW chitosan nanodroplet internalisation by *S. pyogenes* bacteria. *S. pyogenes* bacteria (10^9 CFUs/ml) were left alone or incubated with 10% v/v FITC-labelled MW cOLNDs or MW cOFNDs for 3 h. After staining bacteria with PI, confocal fluorescent images were taken using FITC and TRITC filters. Data are shown as representative images from three independent experiments. Magnification: 100X. Red: PI. Green: FITC.

4.2.13. Antibacterial activity of medium molecular weight chitosan nanodroplets on *S. pyogenes* bacteria

The antibacterial properties of MW chitosan nanodroplets against *S. pyogenes* bacteria were evaluated through a microbiological assay. *S. pyogenes* bacteria (10^4 CFU/ml) were incubated without or with 10% v/v OSS, free MW chitosan solution (0.139% m/v), MW cOFNDs and MW cOLNDs. The bacterial growth was monitored for 2, 3, 4, 6 and 24 h.

As shown in Fig. 30, both MW cOLNDs and MW cOFNDs, as well as free MW chitosan solution, significantly inhibited *S. pyogenes* growth up to 24 hours of incubation, with no significant differences being observed among these three treatments at any observational timepoints. On the contrary, OSS did not affect bacterial growth at any times.

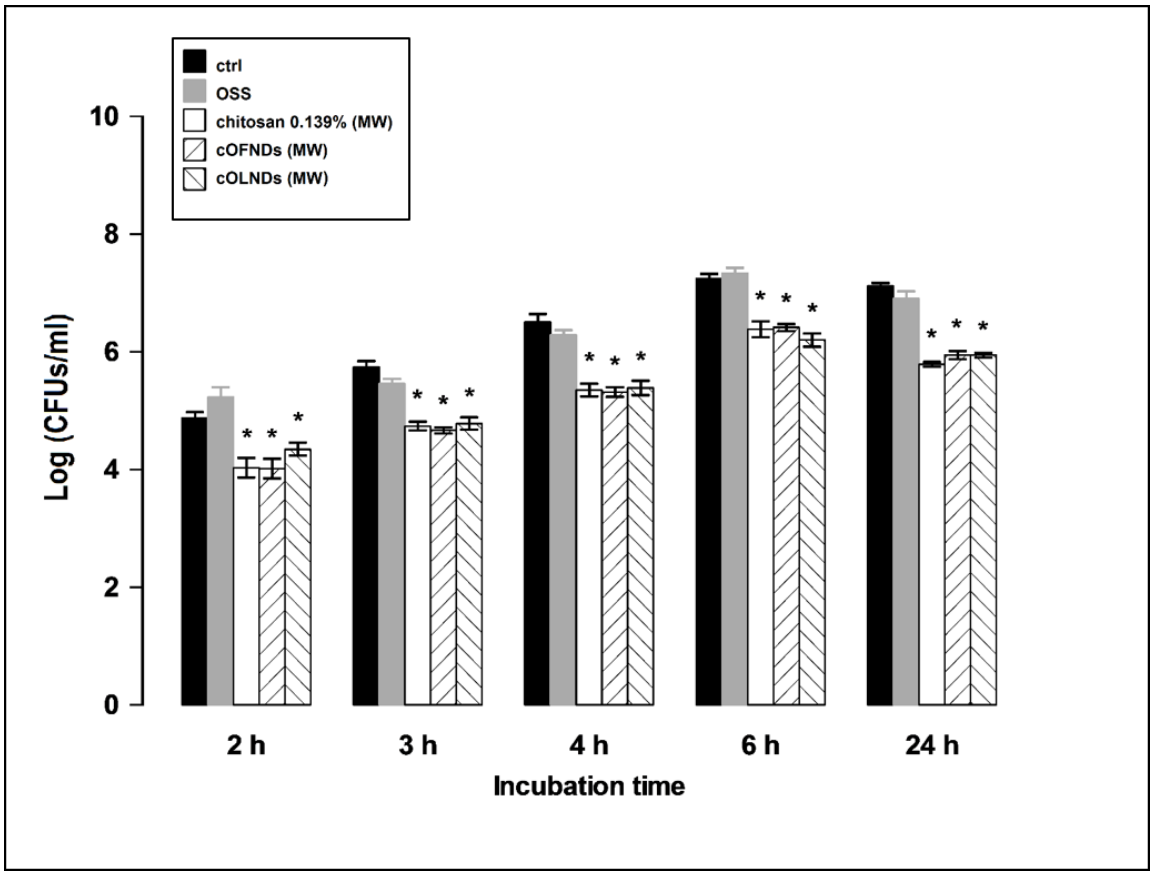

Fig. 30. Antibacterial activity of MW chitosan nanodroplets on *S. pyogenes* bacteria.
S. pyogenes bacteria (10^4 CFUs/ml) were incubated alone or with 10% v/v OSS, free MW chitosan solution (0.139% m/v), MW cOFND suspension, and MW cOLND suspension in sterile conditions at 37°C and their growth was monitored for 2, 3, 4, 6 and 24 h. At each incubation time, the samples were spread on TODD agar medium to determine the CFUs/ml. Results are shown as means ± SEM from three independent experiments and expressed as Log CFUs/ml.Data were evaluated for significance by ANOVA: vs controls: 2-3-4-6-24 h, * p<0.05.

4.2.14. Mechanical interaction between medium molecular weight chitosan nanodroplets and *C. albicans* yeasts

The mechanical interaction between MW cOLNDs or cOFNDs and *C. albicans* yeasts was investigated through analysis by confocal microscopy. *C. albicans* yeasts (10^8 CFUs/ml) were left untreated or treated with 10% v/v FITC-labelled MW cOLNDs or MW cOFNDs under normoxic conditions. After 3 h and 24 h, yeasts were fixed and stained with PI.

As shown in Fig. 31, both formulations appeared to have been avidly uptaken and internalised by yeasts already at the earlier observational time-point (3 h). Consistently, cOLND/OFND internalisation by yeasts was also observed at the later time-point (24 h) of incubation (data not shown).

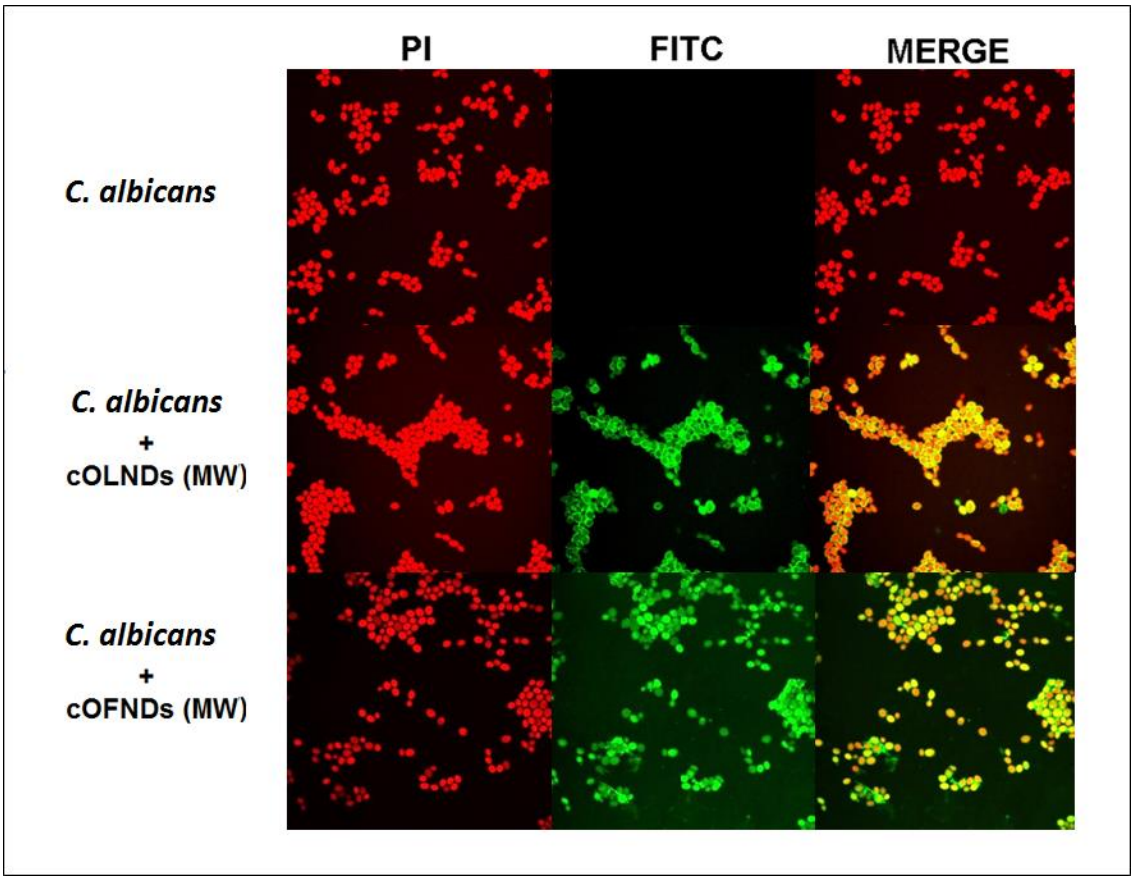

Fig. 31. MW chitosan nanodroplet internalisation by *C. albicans* yeasts. *C. albicans* yeasts (10^8 CFUs/ml) were left alone or incubated with 10% v/v FITC-labelled MW cOLNDs or MW cOFNDs for 3 h. After staining yeasts with PI, confocal fluorescent images were taken using FITC and TRITC filters. Data are shown as representative images from three independent experiments. Magnification: 100X. Red: PI. Green: FITC.

4.2.15. Antifungal activity of medium molecular weight chitosan nanodroplets on *C. albicans* yeasts

The antifungal properties of MW chitosan nanodroplets against *C. albicans* were evaluated through a microbiological assay. *C. albicans* yeasts (10^5 CFUs/ml) were incubated alone or in presence of 10% v/v OSS, free MW chitosan solution (0.139% m/v), MW cOFNDs, or MW cOLNDs. The fungal growth was monitored for 2, 3, 4, 6 and 24 h.

As shown in Fig. 32, both MW cOLNDs and MW cOFNDs, as well as free MW chitosan solution, significantly inhibited *C. albicans* growth up to 24 hours of incubation, more notably between 4 and 6 hours of treatments. On the contrary, OSS did not affect fungal growth at any times.

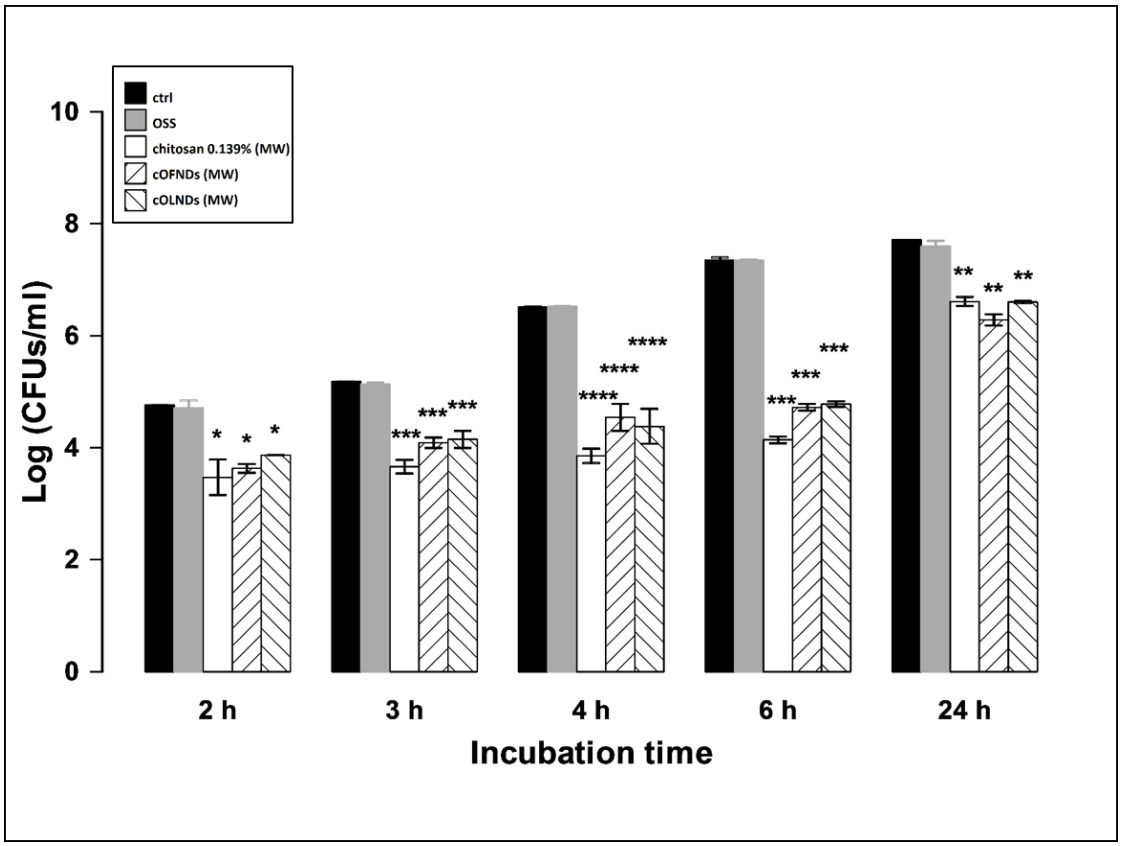

Fig. 32. Antifungal activity of MW chitosan nanodroplets on *C. albicans* yeasts.
C. albicans yeasts (10^5 CFUs/ml) were incubated alone or with 10% v/v OSS, free MW chitosan (0.139% m/v) solution, MW cOFND suspension, and MW cOLND suspension in sterile conditions at 37°C and their growth was monitored for 2, 3, 4, 6 and 24 h. At each incubation time, the samples were spread on SAB agar medium to determine the CFUs/ml. Results are shown as means ± SEM from three independent experiments and expressed as Log CFUs/ml. Data were evaluated for significance by ANOVA: vs controls: 2 h, * p<0.05; 3-6 h, *** p=0.0001; 4 h, **** p<0.0001; 24 h, ** p<0.01.

4.2.16. Mechanical interaction between medium molecular weight chitosan nanodroplets and *C. glabrata* yeasts

The mechanical interaction between MW cOLNDs or cOFNDs and *C. glabrata* yeasts was investigated through analysis by confocal microscopy. *C. glabrata* yeasts (10^8 CFUs/ml) were left untreated or treated with 10% v/v FITC-labelled MW cOLNDs or MW cOFNDs under normoxic conditions. After 3 h and 24 h, yeasts were fixed and stained with PI.

As shown in Fig. 33, both formulations appeared to have been avidly uptaken and internalised by yeasts already at the earlier observational time-point (3 h). Consistently, cOLND/OFND internalisation by yeasts was also observed at the later time-point (24 h) of incubation (data not shown).

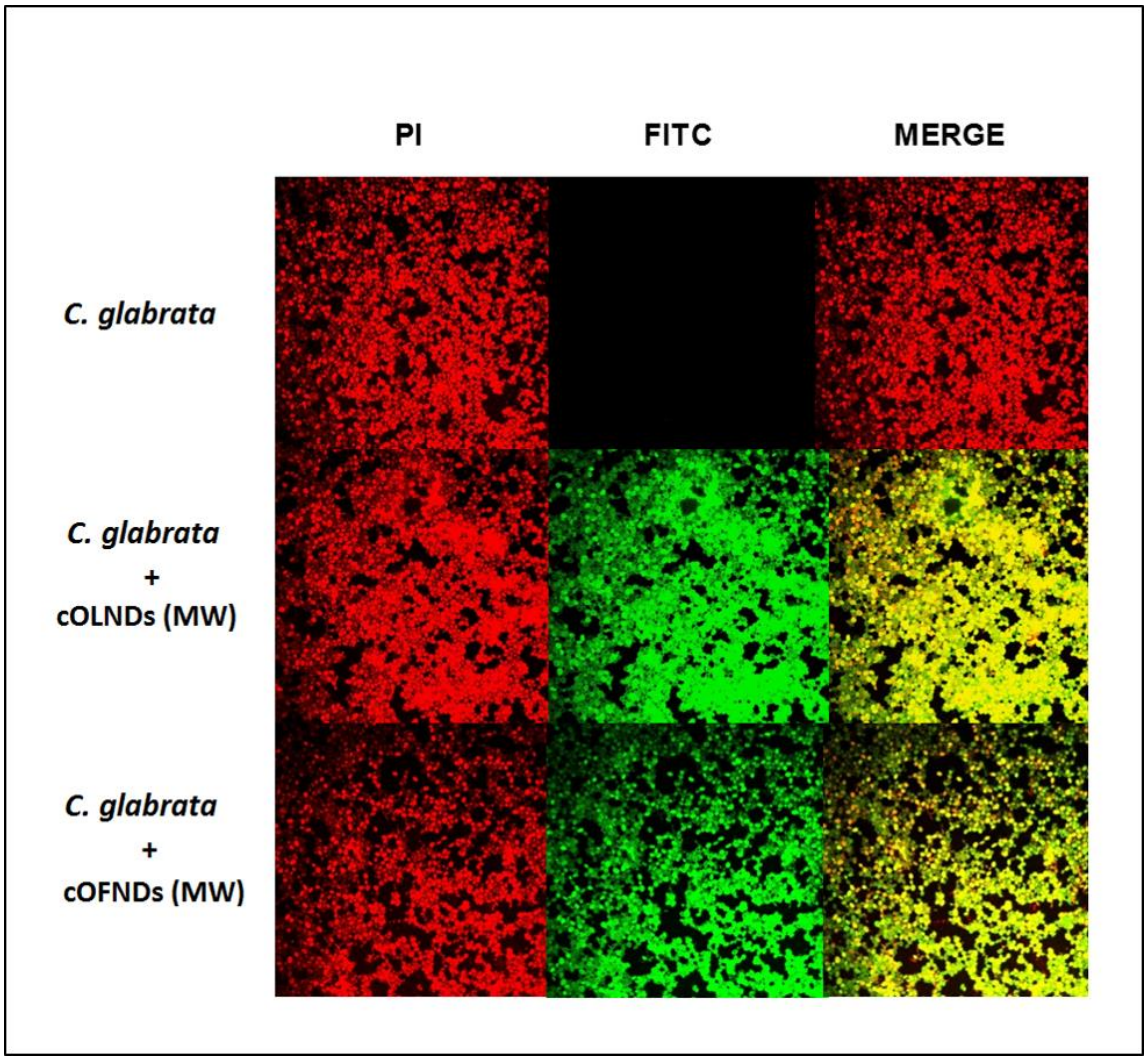

Fig. 33. MW chitosan nanodroplet internalisation by *C. glabrata* yeasts. *C. glabrata* yeasts (10^8 CFUs/ml) were left alone or incubated with 10% v/v FITC-labelled MW cOLNDs or MW cOFNDs for 3 h. After staining yeasts with PI, confocal fluorescent images were taken using FITC and TRITC filters. Data are shown as representative images from three independent experiments. Magnification: 100X. Red: PI. Green: FITC.

4.2.17. Antifungal activity of medium molecular weight chitosan nanodroplets on *C. glabrata* yeasts

The antifungal properties of MW chitosan nanodroplets against *C. glabrata* were evaluated through a microbiological assay. *C. glabrata* yeasts (10^5 CFUs/ml) were incubated alone or in presence of 10% v/v OSS, free MW chitosan solution (0.139% m/v), MW cOFNDs, or MW cOLNDs. The fungal growth was monitored for 2, 3, 4, 6 and 24 h.

As shown in Fig. 34, both MW cOLNDs and MW cOFNDs, as well as free MW chitosan solution, significantly inhibited *C. albicans* growth up to 24 hours of incubation. On the contrary, OSS did not affect fungal growth at any times.

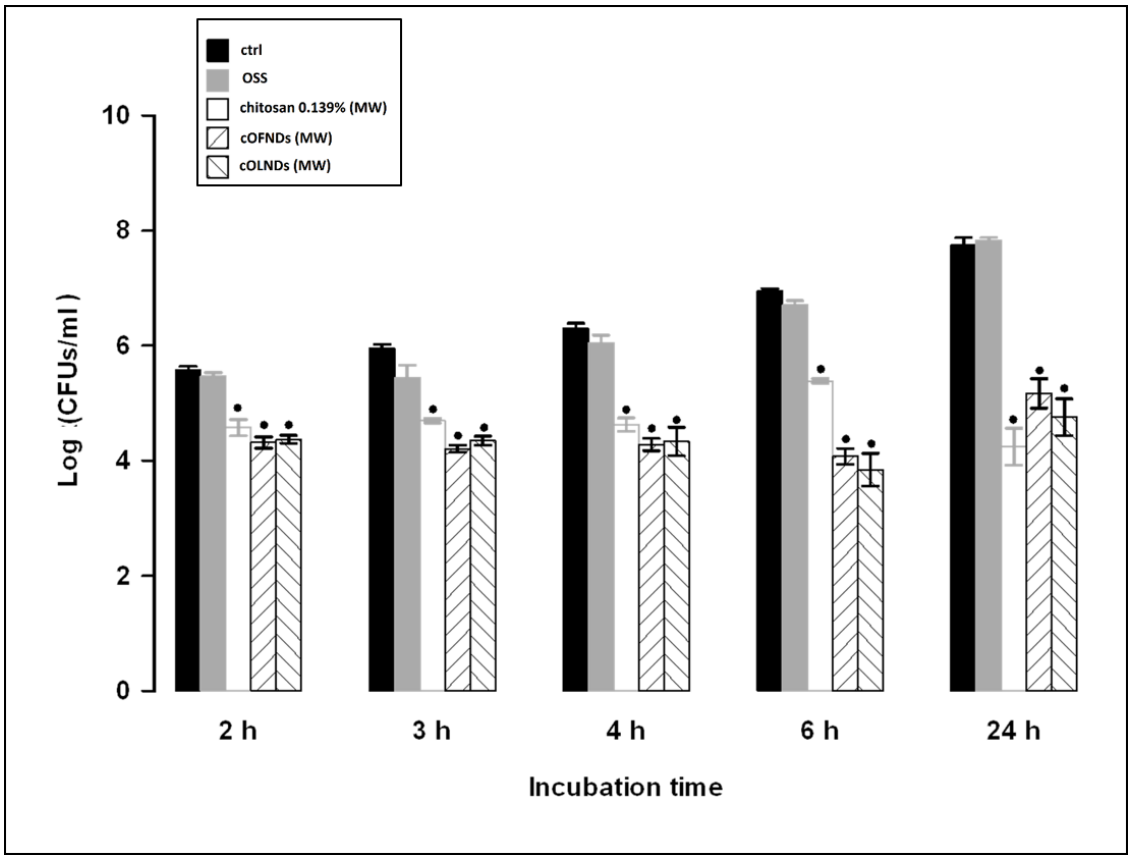

Fig. 34. Antifungal activity of MW chitosan nanodroplets on *C. glabrata* yeasts.
C. glabrata yeasts (10^5 CFUs/ml) were incubated alone or with 10% v/v OSS, free MW chitosan (0.139% m/v) solution, MW cOFND suspension, and MW cOLND suspension in sterile conditions at 37°C and their growth was monitored for 2, 3, 4, 6 and 24 h. At each incubation time, the samples were spread on SAB agar medium to determine the CFUs/ml. Results are shown as means ± SEM from three independent experiments and expressed as Log CFUs/ml. Data were evaluated for significance by ANOVA: vs controls: 2-3-4-6-24 h, * p<0.05.

4.3. Low molecular weight chitosan nanodroplets

4.3.1. Low molecular weight chitosan nanodroplet physico-chemical characterisation

After manufacturing, LW cOLNDs and LW cOFNDs were characterised for morphology by optical microscopy and TEM, and for average diameters, polydispersity indexes, and zeta potentials by dynamic light scattering.

LW cOLNDs displayed spherical shapes (Fig. 35, panel A and B: TEM and optical microscopy images, respectively) and sizes in the nanometre range, with average diameters of 400 nm (Fig. 35, panel C). Furthermore, LW cOLNDs displayed cationic zeta potentials with values around +30 mV. The physico-chemical characteristics of LW chitosan nanodroplet formulations tested in this study are summarised in Table 5.

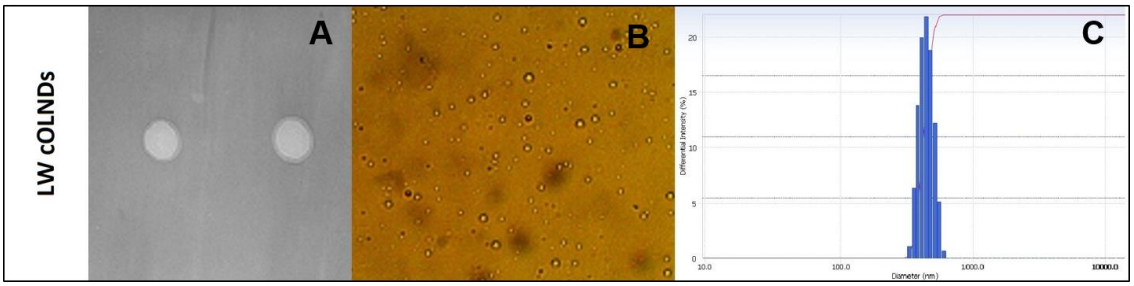

Fig. 35. Morphology and size distribution of LW cOLNDs. LW cOLNDs were checked for morphology by TEM and by optical microscopy, and for size distribution by dynamic light scattering. Results are shown as representative images from ten different preparations. Panel A. LW cOLND image by TEM. Magnification: 28 500X. Panel B. LW cOLNDs image by optical microscopy. Magnification: 600X. Panel C. LW cOLND size distribution by dynamic light scattering.

Nanocarrier	LW cOLND	LW cOFND
Outher shell polysaccharide	LW chitosan	LW chitosan
Inner core fluorocarbon	DFP	DFP
Fluorocarbon boiling point	51° C	51° C
Diameter (nm ± SD)	443,80 ± 28,60	414,30 ± 33,80
Polydispersity index	0,23	0,24
Zeta potential (mV ± SD)	+ 29,00 ± 1,00	+ 29,50 ± 1,00

Table 5. Physico-chemical characterisation of LW cOLNDs and LW cOFNDs.
LW cOLND/cOFND formulations were characterised for diameters, polydispersity index, and zeta potential by dynamic light scattering. Results are shown as means ± SD from ten different preparations for each formulation.

4.3.2. *In vitro* oxygen release from low molecular weight chitosan oxygen-loaded nanodroplets

In vitro oxygen release from LW cOLND formulations was monitored by an oxymeter up to 6 h through dialysis bag technique.

At the intial observational timepoint (0 min), the oxygen concentration in the receiving saline solution was previously reduced to 0.5 mg/L, to mimic sever hypoxic conditions. Already after 15 minutes, LW cOLNDs proved to be able to release oxygen into the environment and the oxygen concentration in the hypoxic solution reached the value of ~ 3 mg/L. For all the observational period (6 h), oxygen delivery from LW cOLNDs continuously increased as well as related oxygen concentration in the receiving solution (up to ~ 6 mg/L). LW cOLNDs effectively released clinically oxygen amounts in a time-sustained manner *in vitro*. These results are shown in Fig. 36.

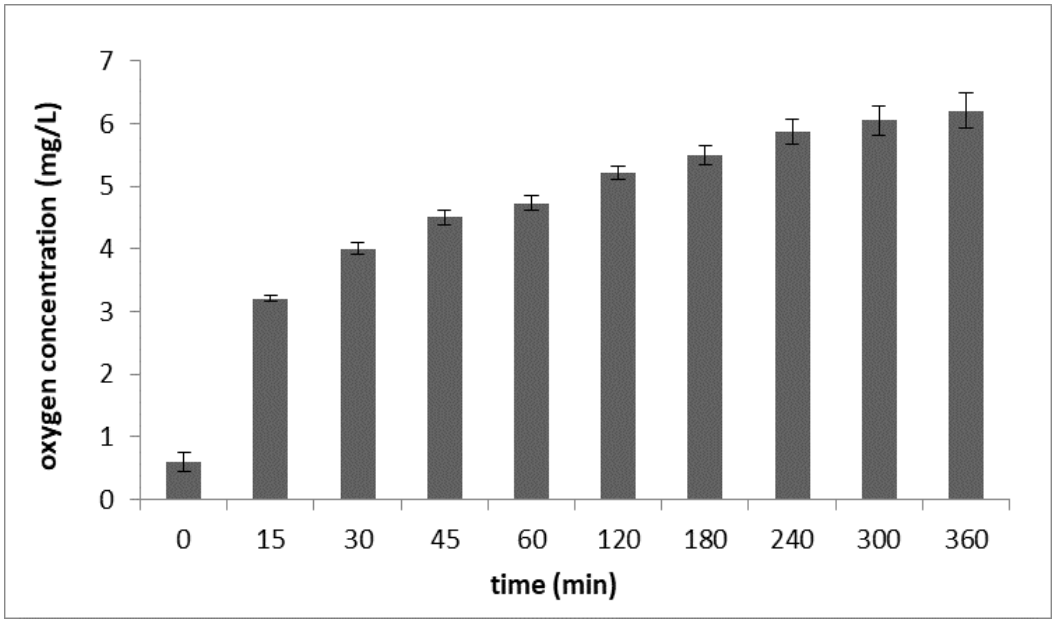

Fig. 36. *In vitro* oxygen release from LW cOLNDs. *In vitro* Oxygen release from LW cOLNDs were monitored for 15, 30, 45, 60, 120, 180, 240, 300, and 360 min by an oxymeter through dialysis bag technique. The donor solution (consisting of 3 ml of LW cOLNDs) was placed in a dialysis bag sealed and immersed in 45 ml of the receiving saline solution (oxygen concentration at 0 min = 0.5 mg/L). Results are shown as means ± SEM from three independent experiments.

4.3.3. Biocompatibility of low molecular weight chitosan nanodroplets with human keratinocytes

The biocompatibility of LW cOLNDs and LW cOFNDs with HaCaT keratinocytes was challenged through LDH and MTT assays. LW chitosan nanodroplet toxicity was analysed by LDH assay while cell viability was checked by MTT assay. Briefly, HaCaT cell line (5×10^5 cells/ml for LDH studies, 1.6×10^5 cells/ml for MTT studies) was incubated for 24 h in absence or in presence of 10% v/v LW cOLNDs and LW cOFNDs under normoxic (20% O_2) and hypoxic (1% O_2) conditions.

Hypoxia didn't influence viability of untreated human keratinocytes, as shown in Fig. 37 (panel B). LW cOLNDs and LW cOFNDs were not toxic to HaCaT cells either in normoxia or hypoxia (Fig. 37, panel A). These results are not totally confirmed by MTT assay. LW cOLNDs and LW cOFNDs reduced HaCaT keratinocyte viability in hypoxic condition (Fig.37, panel B).

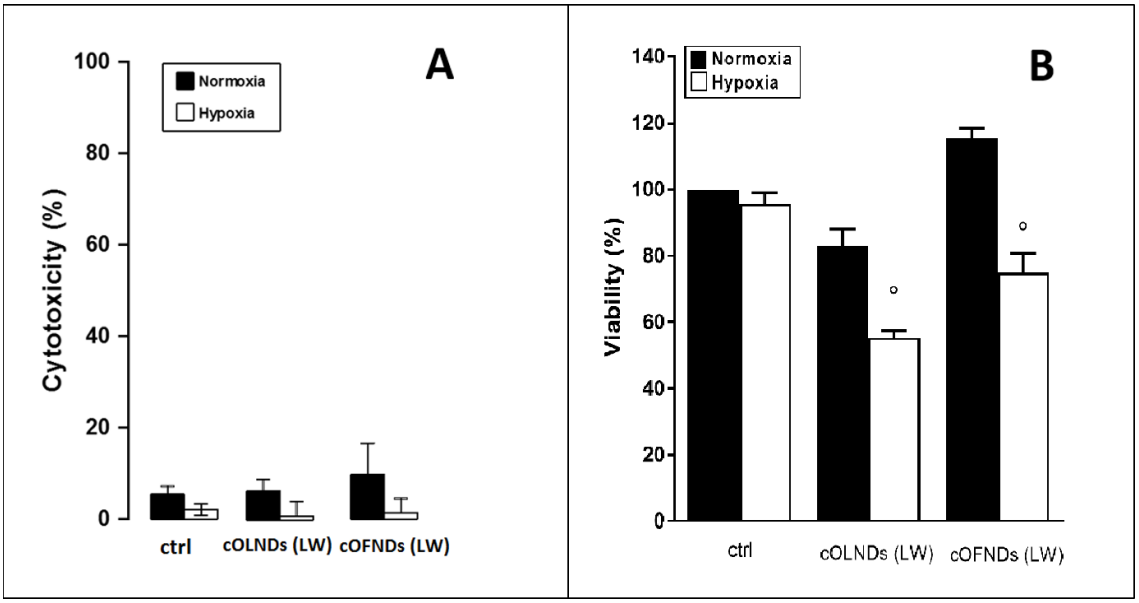

Fig. 37. Effects of hypoxia and LW chitosan nanodroplets on human keratinocyte viability. HaCaT cells (5 x 10^5 cells/ml for LDH studies, 1.6 x 10^5 cells/ml for MTT studies) were left untreated or treated with LW cOLNDs and LW cOFND for 24 h in normoxia (20% O_2, black columns) or hypoxia (1% O_2, white columns). After collection of cell supernatants and lysates, cytotoxicity percentage was measured through LDH assay (panel A), whereas cell viability percentage was measured through MTT assay (panels B). Results are shown as means+ SEM from three independent experiments. Data were also evaluated for significance by ANOVA: ° vs hypoxic control cells, p<0.05.

4.3.4. Biocompatibility of low molecular weight chitosan nanodroplets with human fibroblasts

LW chitosan nanodroplet biocompatibility with normoxic and hypoxic human fibroblasts was evaluated through LDH assay and MTT assay. In particular, treatment cytotoxicity was analysed by LDH assay while cell viability was checked by MTT assay. HDF cells (5 x 10^5 cells/ml for LDH studies, 1.6 x 10^5 cells/ml for MTT studies) were incubated for 24 h without or with 10% v/v LW cOLNDs and LW cOFNDs under normoxic (20% O_2) and hypoxic (1% O_2) conditions.

Hypoxia did not influence the viability of untreated or treated HDF cells. LW cOLNDs and LW cOFNDs were not toxic to HDF cells in both conditions. These data are confirmed by both studies as shown in Fig. 38, panel A and B. Additional treatments with LW OLNDs and LW cOFNDs reduced cytotoxicity to fibroblasts compared to cytotoxicity related to untreated fibroblasts under hypoxic conditions (Fig. 38, panel A).

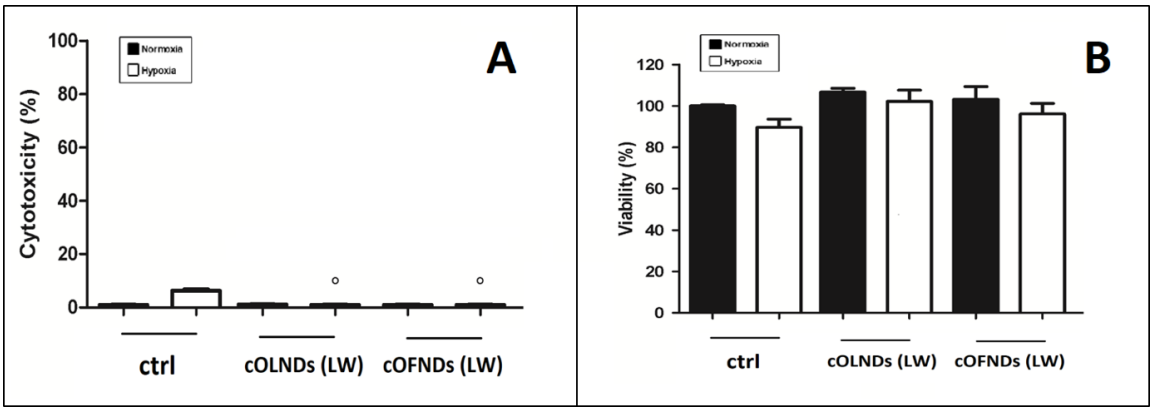

Fig. 38. Effects of hypoxia and LW chitosan nanodroplets on human fibroblast viability. HDF cells (5 x 10^5 cells/ml for LDH studies, 1.6 x 10^5 cells/ml for MTT studies) were left untreated or treated with LW cOLNDs and LW cOFNDs for 24 h in normoxia (20% O_2, black columns) or hypoxia (1% O_2, white columns). After collection of cell supernatants and lysates, cytotoxicity percentage was measured through LDH assay (panel A), whereas cell viability percentage was measured through MTT assay (panels B). Results are shown as means+ SEM from three independent experiments. Data were also evaluated for significance by ANOVA: ° vs hypoxic control cells, p<0.05.

4.3.5. Biocompatibility of low molecular weight chitosan nanodroplets with human endothelium

The biocompatibility of LW cOLNDs and LW cOFNDs with human HMEC-1 cell line was evaluated through LDH and MTT assays. In particular, treatment cytotoxicity was analysed by LDH assay while cell viability was checked by MTT assay. Endothelium (5 x 10^5 cells/ml for LDH assay, 1.6 x 10^5 cells/ml for MTT assay) was incubated for 24 h without or with 10% v/v LW cOLNDs and LW cOFNDs both in normoxic (20% O_2) and hypoxic (1% O_2) conditions.

According to results from analysis by LDH assay (Fig. 39, panel A), hypoxia mildly compromised the health of control cells, although it did not affect total cell viability, as emerged from investigation by MTT assay (Fig. 39, panel B). The treatment with LW cOFNDs appeared to be more toxic to cells compared to controls and reduced strongly their viability, both in normoxia and hypoxia. Encouragingly, LW cOLNDs appeared less toxic than LW cOFNDs, and the presence of oxygen within the nanodroplets seemed to be sufficient to counteract the loss of viability induced by nanodroplets themselves.

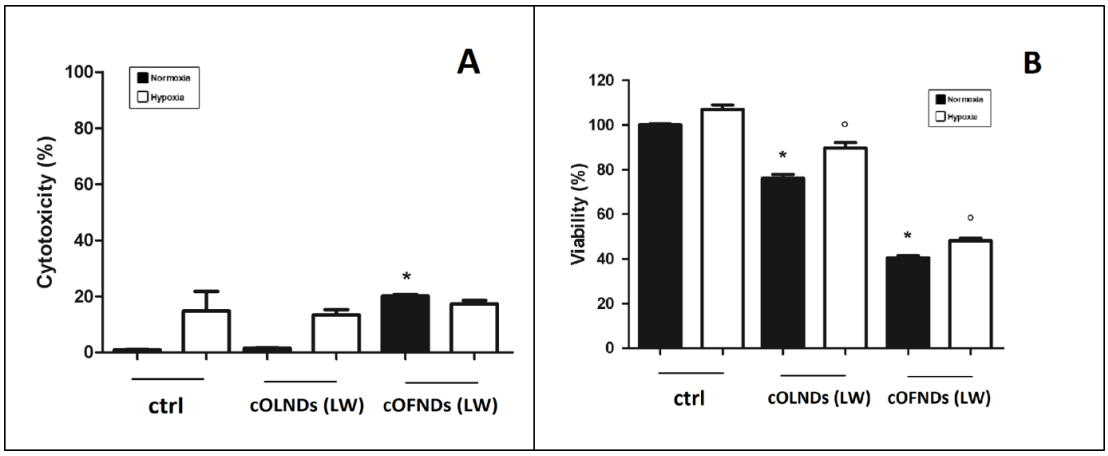

Fig. 39. Effects of hypoxia and LW chitosan nanodroplets on human endothelium viability. HMEC-1 endothelium (5 x 10^5 cells/ml for LDH studies, 1.6 x 10^5 cells/ml for MTT studies) were left untreated or treated with LW cOLNDs and LW cOFNDs for 24 h in normoxia (20% O_2, black columns) or hypoxia (1% O_2, white columns). After collection of cell supernatants and lysates, cytotoxicity percentage was measured through LDH assay (panel A), whereas cell viability percentage was measured through MTT assay (panels B). Results are shown as means+ SEM from three independent experiments. Data were also evaluated for significance by ANOVA: * vs normoxic control cells: $p<0.05$; ° vs hypoxic control cells $p<0.05$.

4.3.6. Effects of hypoxia and low molecular weight chitosan nanodroplets on the migration of human keratinocytes

The migration (and related wound healing abilities) of HaCaT cells treated with LW nanodroplets, as well as OSS, was evaluated through scratch assay under hypoxic conditions. Cells (3×10^5 cells/ml) were allowed to grow within cell culture inserts purposely made to generate a standardised cell-free gap within the well for 24 h. Then, human keratinocytes were incubated in absence or presence of 10% v/v LW cOLNDs, LW cOFNDs and OSS in normoxic and hypoxic conditions for 16 h.

As shown in Fig. 40, hypoxia slowed down the migration of human keratinocytes with respect to normoxic conditions. Additional treatment with LW cOLNDs fully abrogated hypoxia-dependent dysregulation of cell migration, whereas LW cOFNDs and OSS did not.

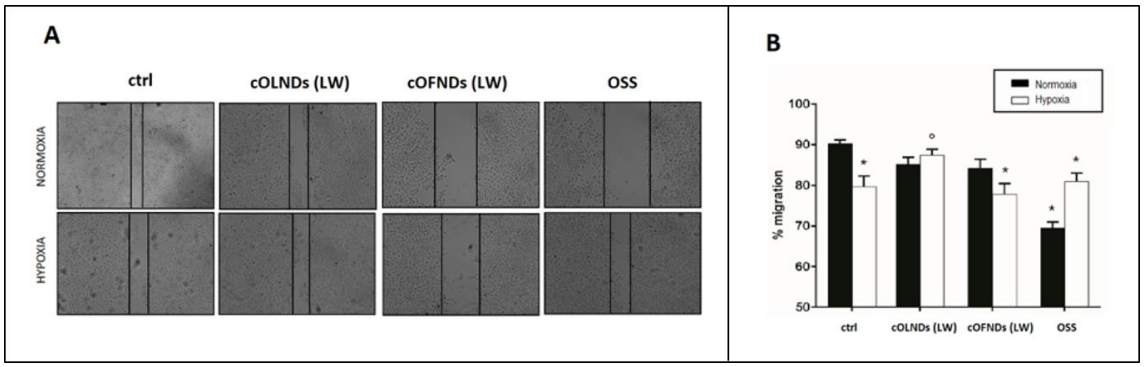

Fig. 40. Effects of hypoxia and LW chitosan nanodroplets on the migration and wound healing abilities of human keratinocytes. HaCaT cells (3 x 10^5 cells/ml) were seeded in two confluent monolayers, divided by a scratch of 500 µm, and incubated for 16 h in normoxia (20% O_2) or hypoxia (1% O_2) with/without 10% v/v LW cOLNDs, LW OFNDs or OSS. Thereafter, scratch lengths were photographed and measured. Panel A: representative images. Panel B: means + SEM of scratch lengths. Results are from three independent experiments performed in triplicates. Data were also evaluated for significance by ANOVA: * vs normoxic untreated cells: p<0.01; ° vs hypoxic untreated cells: p<0.01.

4.3.7. Effects of hypoxia and low molecular weight chitosan nanodroplets on the migration of human fibroblasts

The effects of hypoxia and LW chitosan nanodroplets, as well as OSS, on the migration (and related wound healing abilities) of hypoxic human fibroblasts were evaluated through scratch assay. Cells (3 x 10^5 cells/ml) were allowed to grow within cell culture inserts purposely made to generate a standardised cell-free gap within the well for 24 h. Then, HDF cells were incubated in absence or presence of 10% v/v LW cOLNDs, LW cOFNDs, and OSS in normoxic and hypoxic conditions for 16 h.

As shown in Fig. 41, hypoxia slowed down the migration of human fibroblasts with respect to normoxic conditions. Additional treatment with LW cOLNDs fully abrogated hypoxia-dependent dysregulation of cell migration, whereas LW cOFNDs and OSS did not.

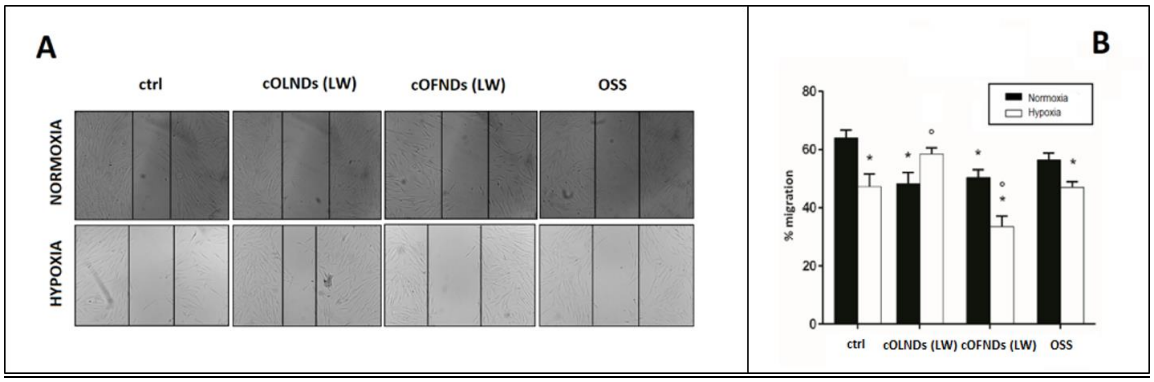

Fig. 41. Effects of hypoxia and LW chitosan nanodroplets on the migration and wound healing abilities of human fibroblasts. HDF cells (3 x 10^5 cells/ml) were seeded in two confluent monolayers, divided by a scratch of 500 µm, and incubated for 16 h in normoxia (20% O_2) or hypoxia (1% O_2) with/without 10% v/v LW cOLNDs, LW OFNDs, and OSS. Thereafter, scratch lengths were photographed and measured. Panel A: representative images. Panel B: means + SEM of scratch lengths. Results are from three independent experiments performed in triplicates. Data were also evaluated for significance by ANOVA: * vs normoxic untreated cells $p<0.01$; ° vs hypoxic untreated cells: $p<0.01$.

4.3.8. Effects of hypoxia and low molecular weight chitosan nanodroplets on the migration of human endothelium

The migration (and related wound healing abilities) of human endothelium treated with MW nanodroplets, as well as OSS, was evaluated through scratch assay under hypoxic conditions. HMEC-1 cells (3 x 10^5 cells/ml) were allowed to grow within cell culture inserts purposely made to generate a standardised cell-free gap within the well for 24 h. Then, cells were incubated in absence or presence of 10% v/v LW cOLNDs, LW cOFNDs, and OSS in normoxic and hypoxic conditions for 16 h.

As shown in Fig. 42, hypoxia strongly slowed down the migration of human HMEC-1 cells with respect to normoxic conditions. Additional treatment with LW cOLNDs fully abrogated hypoxia-dependent dysregulation of cell migration, whereas LW cOFNDs and OSS did not.

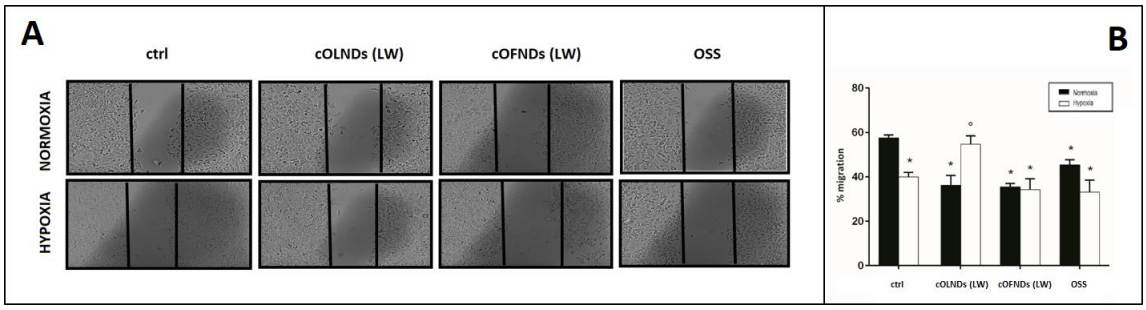

Fig. 42. Effects of hypoxia and LW chitosan nanodroplets on the migration and wound healing abilities of human endothelium. HMEC-1 endothelium (3 x 10^5 cells/ml) were seeded in two confluent monolayers, divided by a scratch of 500 µm, and incubated for 16 h in normoxia (20% O_2) or hypoxia (1% O_2) with/without 10% v/v LW cOLNDs, LW OFNDs or OSS. Thereafter, scratch lengths were photographed and measured. Panel A: representative images. Panel B: means + SEM of scratch lengths. Results are from three independent experiments performed in triplicates. Data were also evaluated for significance by ANOVA: * vs normoxic untreated cells: $p<0.01$; ° vs hypoxic untreated cells: $p<0.01$.

4.3.9. Mechanical interaction between low molecular weight chitosan nanodroplets and MRSA bacteria

The mechanical interaction between LW cOLNDs or LW cOFNDs and MRSA bacteria was investigated through analysis by confocal microscopy. MRSA bacteria (10^9 CFU/ml) were incubated without or with 10% v/v FITC-labelled LW cOLNDs or LW cOFNDs under normoxic conditions. After 3 h and 24 h, bacteria were fixed and stained with PI.

As shown in Fig. 43, both formulations appeared to have been avidly uptaken and internalised by bacteria already at the earlier observational time-point (3 h). Consistently, LW cOLND/OFND internalisation by bcteria was also observed at the later time-point (24 h) of incubation (data not shown).

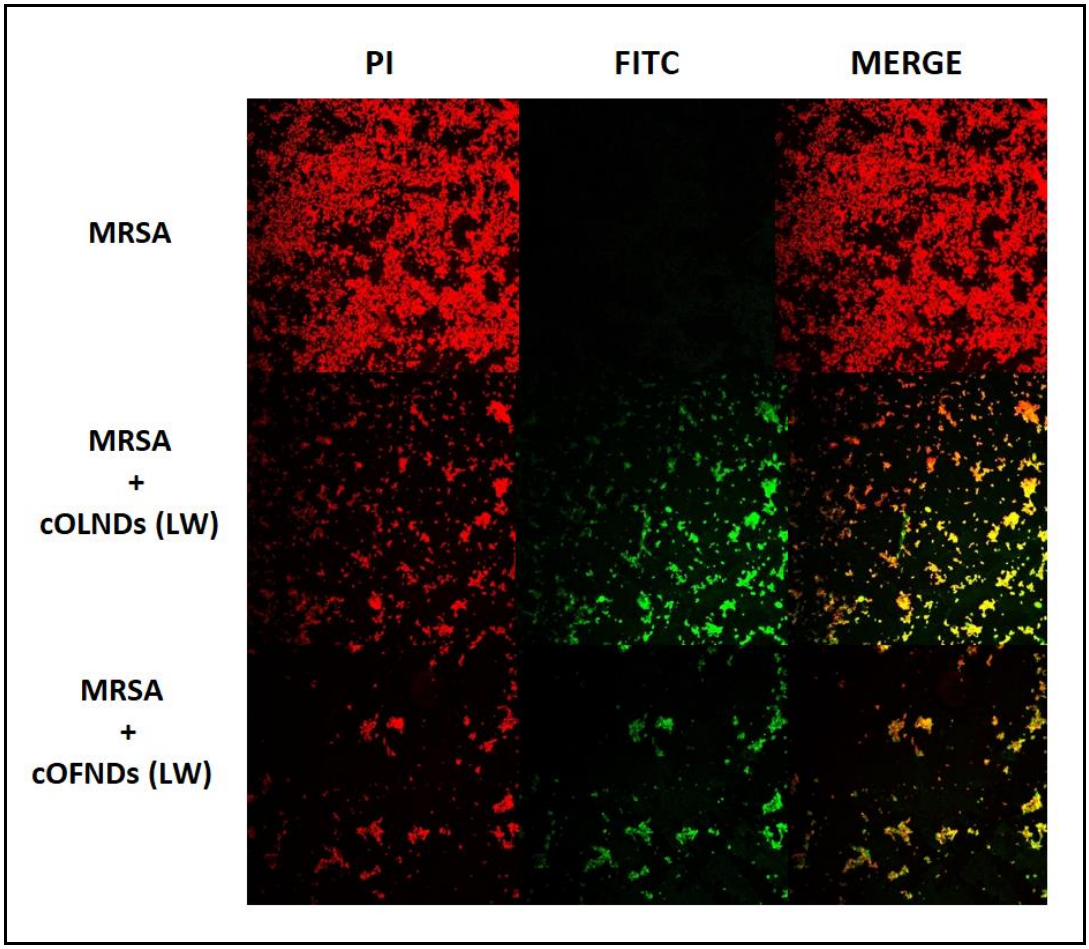

Fig. 43. LW chitosan nanodroplet internalisation by MRSA bacteria. MRSA bacteria (10^9 CFUs/ml) were left alone or incubated with 10% v/v FITC-labelled LW cOLNDs or LW cOFNDs for 3 h. After staining bacteria with PI, confocal fluorescent images were taken using FITC and TRITC filters. Data are shown as representative images from three independent experiments. Magnification: 100X. Red: PI. Green: FITC.

4.3.10. Antibacterial activity of low molecular weight chitosan nanodroplets on MRSA bacteria

The antibacterial properties of LW chitosan nanodroplets against MRSA were evaluated through a microbiological assay. MRSA bacteria (10^4 CFU/ml) were incubated without or with 10% v/v free LW chitosan solution (0.139% m/v), LW cOFNDs, and LW cOLNDs. The bacterial growth was monitored for 4, 6, and 24 h. As shown in Fig. 44, both LW cOLNDs and LW cOFNDs significantly inhibited bacterial growth up to 6 hours of incubation. At these observational timepoints, significant differences were observed among treatments with LW cOLNDs/cOFNDs and chitosan alone. LW cOLNDs and cOFNDs seem to be more effective against bacteria than LW chitosan solution.

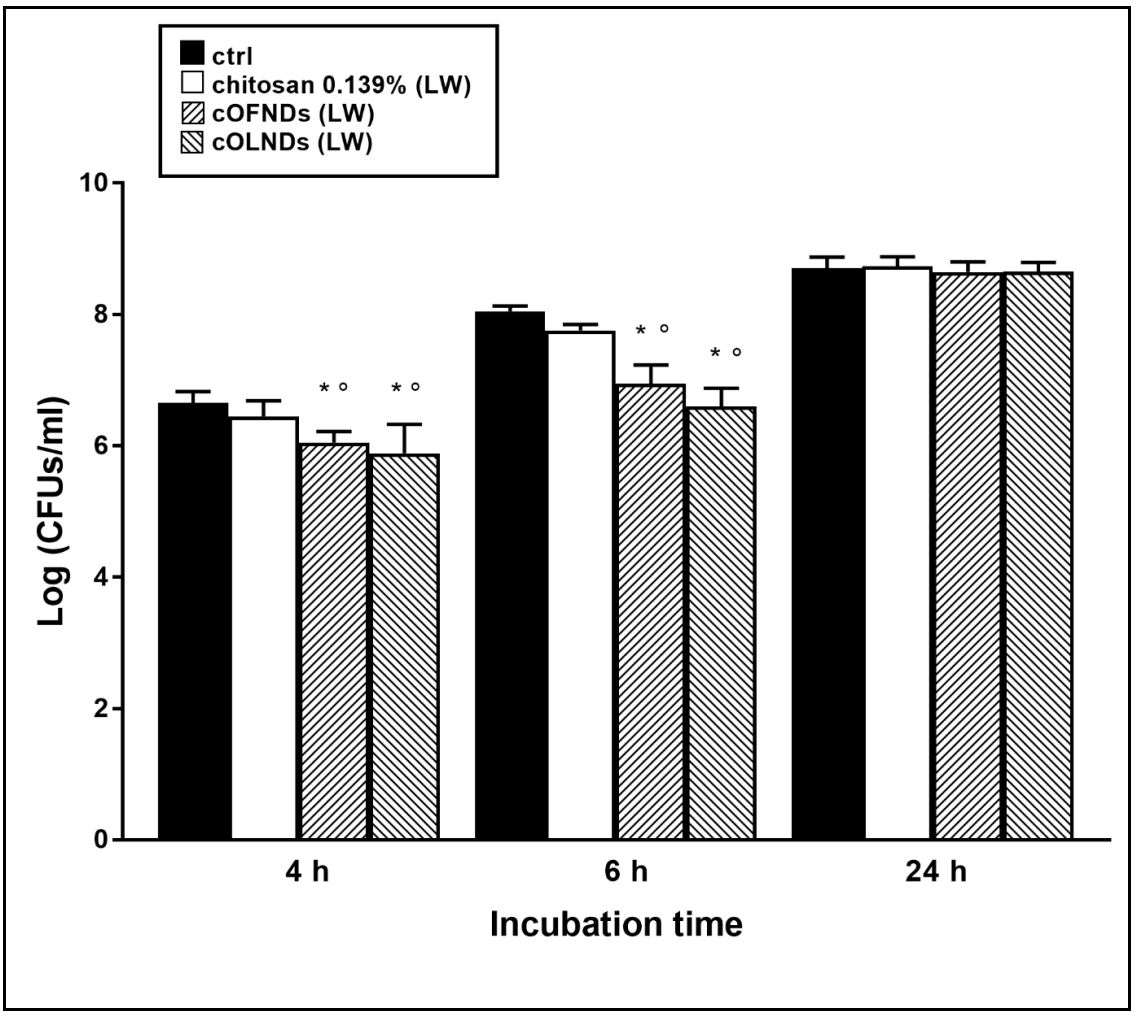

Fig. 44. Antibacterial activity of LW chitosan nanodroplets on MRSA bacteria. MRSA bacteria (10^4 CFUs/ml) were incubated alone or with 10% v/v OSS, free LW chitosan solution (0.139% m/v), LW cOFND suspension, and LW cOLND suspensions in sterile conditions at 37°C and their growth was monitored for 4, 6, and 24 h. At each incubation time, the samples were spread on TSA agar medium to determine the CFUs/ml. Results are shown as means + SEM from three independent experiments and expressed as Log CFUs/ml. Data were evaluated for significance by ANOVA: vs controls: 4-6 h, * p<0.0001; vs LW chitosan solution: 4-6 h, ° p<0.05.

4.3.11. Mechanical interaction between low molecular weight chitosan nanodroplets and *S. pyogenes* bacteria

The mechanical interaction between LW cOLNDs or LW cOFNDs and *S. pyogenes* bacteria was investigated through analysis by confocal microscopy. S. pyogenes bacteria (10^9 CFU/ml) were incubated without or with 10% v/v FITC-labelled LW cOLNDs or LW cOFNDs under normoxic conditions. After 3 h and 24 h, bacteria were fixed and stained with PI.

As shown in Fig. 45, both formulations appeared to have been uptaken and internalised by bacteria already at earlier observational time-point (3 h). Consistently, LW cOLND/cOFND internalisation by *S. pyogenes* bacteria was also observed at the later time-point (24 h) of incubation (data not shown).

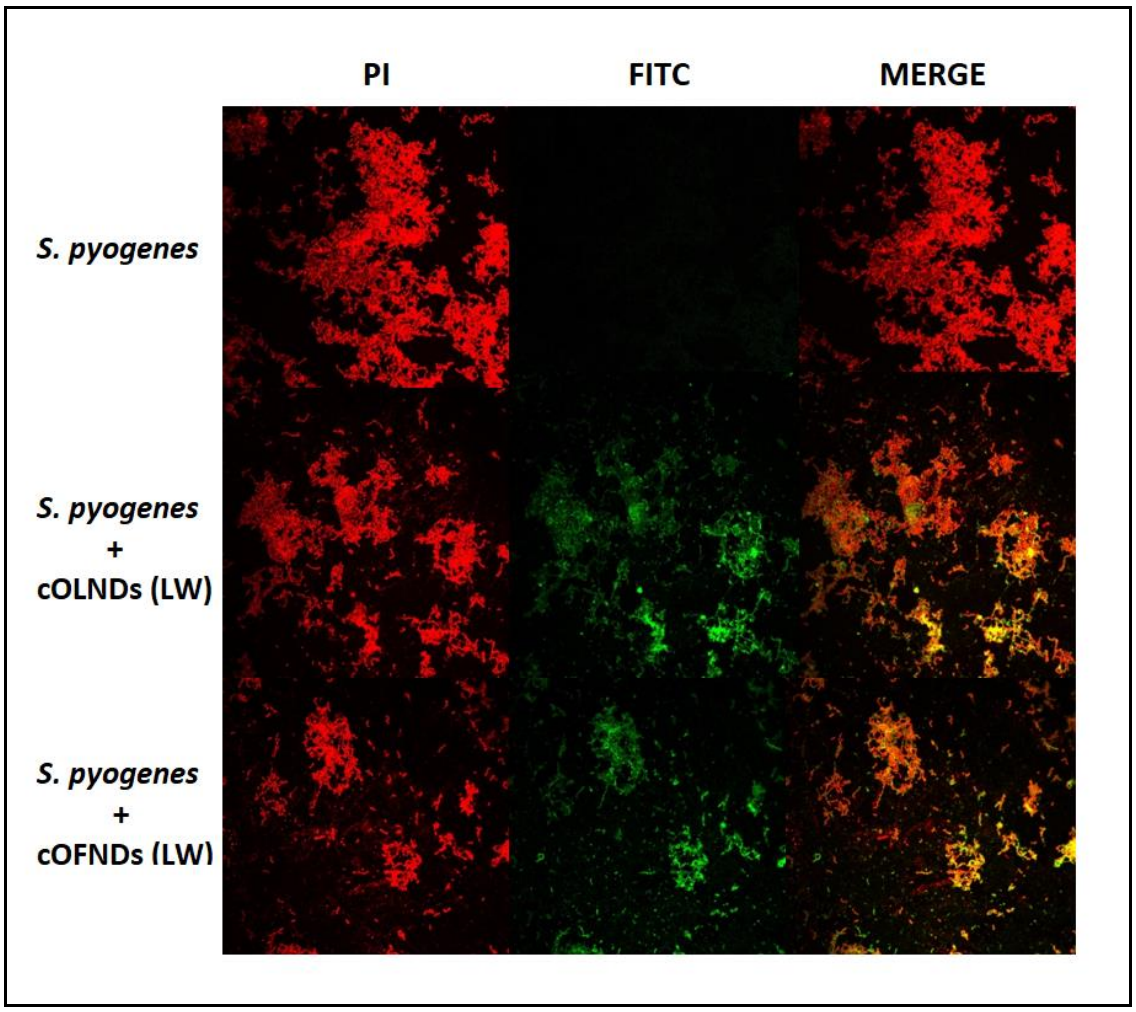

Fig. 45. LW chitosan nanodroplet internalisation by *S. pyogenes* bacteria. *S. pyogenes* bacteria (10^9 CFUs/ml) were left alone or incubated with 10% v/v FITC-labelled LW cOLNDs or LW cOFNDs for 3 h. After staining bacteria with PI, confocal fluorescent images were taken using FITC and TRITC filters. Data are shown as representative images from three independent experiments. Magnification: 100X. Red: PI. Green: FITC.

4.3.12. Antibacterial activity of low molecular weight chitosan nanodroplets on *S. pyogenes* bacteria

The antibacterial properties of LW chitosan nanodroplets against *S. pyogenes* bacteria were evaluated through a microbiological assay. *S. pyogenes* bacteria (10^4 CFU/ml) were incubated without or with 10% v/v free LW chitosan solution (0.139% m/v), LW cOFNDs and LW cOLNDs. The bacterial growth was monitored for 4 and 24 h.

As shown in Fig. 46, both LW cOLNDs and LW cOFNDs significantly inhibited *S. pyogenes* growth up to 24 hours of incubation, with no significant differences being observed between these two treatments at this observational timepoints. Moreover, after 24 h of incubation significant differences were observed between LW cOLNDs/cOFNDs and LW chitosan alone.

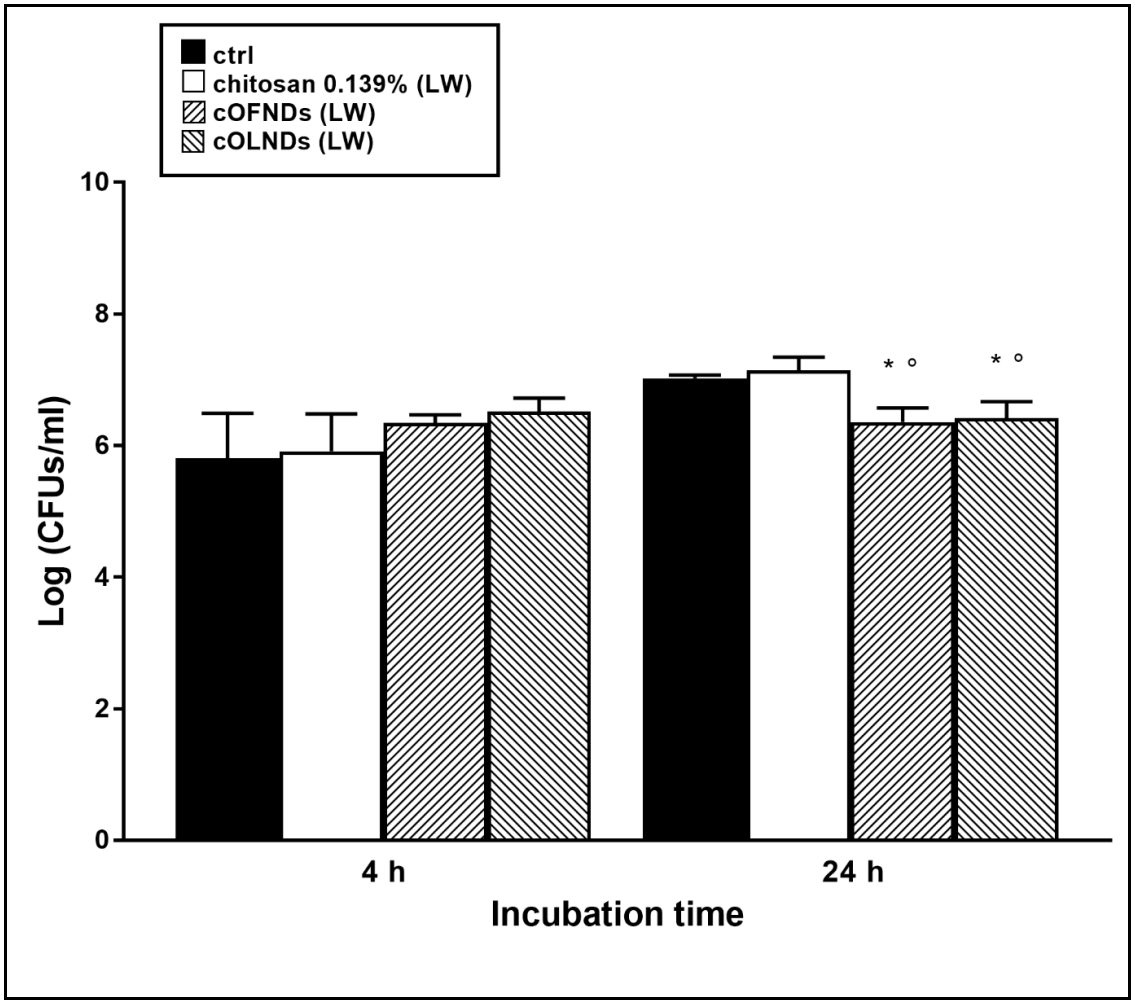

Fig. 46. Antibacterial activity of LW chitosan nanodroplets on *S. pyogenes* bacteria.
S. pyogenes bacteria (10^4 CFUs/ml) were incubated alone or with 10% v/v free LW chitosan solution (0.139% m/v), LW cOFND suspension, and LW cOLND suspension in sterile conditions at 37°C and their growth was monitored for 4 and 24 h. At each incubation time, the samples were spread on TODD agar medium to determine the CFUs/ml. Results are shown as means + SEM from three independent experiments and expressed as Log CFUs/ml.Data were evaluated for significance by ANOVA: vs controls: 24 h, * p<0.01; vs LW chitosan solution: 24 h, ° p<0.0001.

4.3.13. Mechanical interaction between low molecular weight chitosan nanodroplets and *C. albicans* yeasts

The mechanical interaction between LW cOLNDs or cOFNDs and *C. albicans* yeasts was investigated through analysis by confocal microscopy. *C. albicans* yeasts (10^8 CFUs/ml) were left untreated or treated with 10% v/v FITC-labelled LW cOLNDs or LW cOFNDs under normoxic conditions. After 3 h and 24 h, yeasts were fixed and stained with PI.

As shown in Fig. 47, both formulations appeared to have been avidly internalised by yeasts already at the earlier observational time-point (3 h). Consistently, cOLND/OFND internalisation by yeasts was also observed at the later time-point (24 h) of incubation (data not shown).

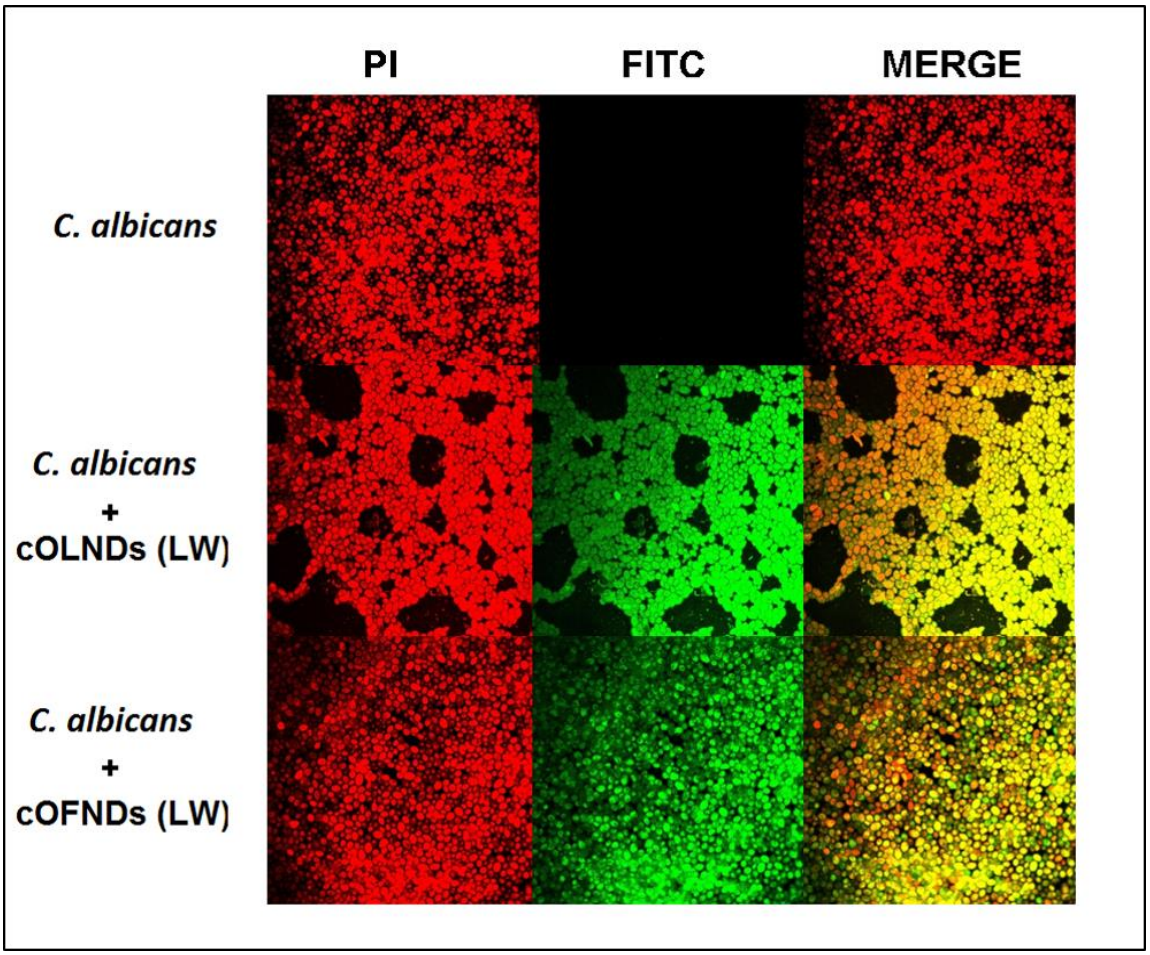

Fig. 47. LW chitosan nanodroplet internalisation by *C. albicans* yeasts. *C. albicans* yeasts (10^8 CFUs/ml) were left alone or incubated with 10% v/v FITC-labelled LW cOLNDs or LW cOFNDs for 3 h. After staining yeasts with PI, confocal fluorescent images were taken using FITC and TRITC filters. Data are shown as representative images from three independent experiments. Magnification: 100X. Red: PI. Green: FITC.

4.3.14. Antifungal activity of low molecular weight chitosan nanodroplets on *C. albicans* yeasts

The antifungal properties of LW chitosan nanodroplets against *C. albicans* were evaluated through a microbiological assay. *C. albicans* yeasts (10^5 CFUs/ml) were incubated alone or in presence of 10% v/v free LW chitosan solution (0.139% m/v), LW cOFNDs, or LW cOLNDs. The fungal growth was monitored for 4, 6 and 24 h.

Results are showed in Fig. 48. LW cOLNDs, LW cOFNDs, and free LW chitosan solution significantly inhibited fungal growth up to 24 hours of incubation, with free chitosan appearing less effective than nanodroplets at earlier timepoints. No significant differences among nanodroplet treatments were observed at any observational timepoint.

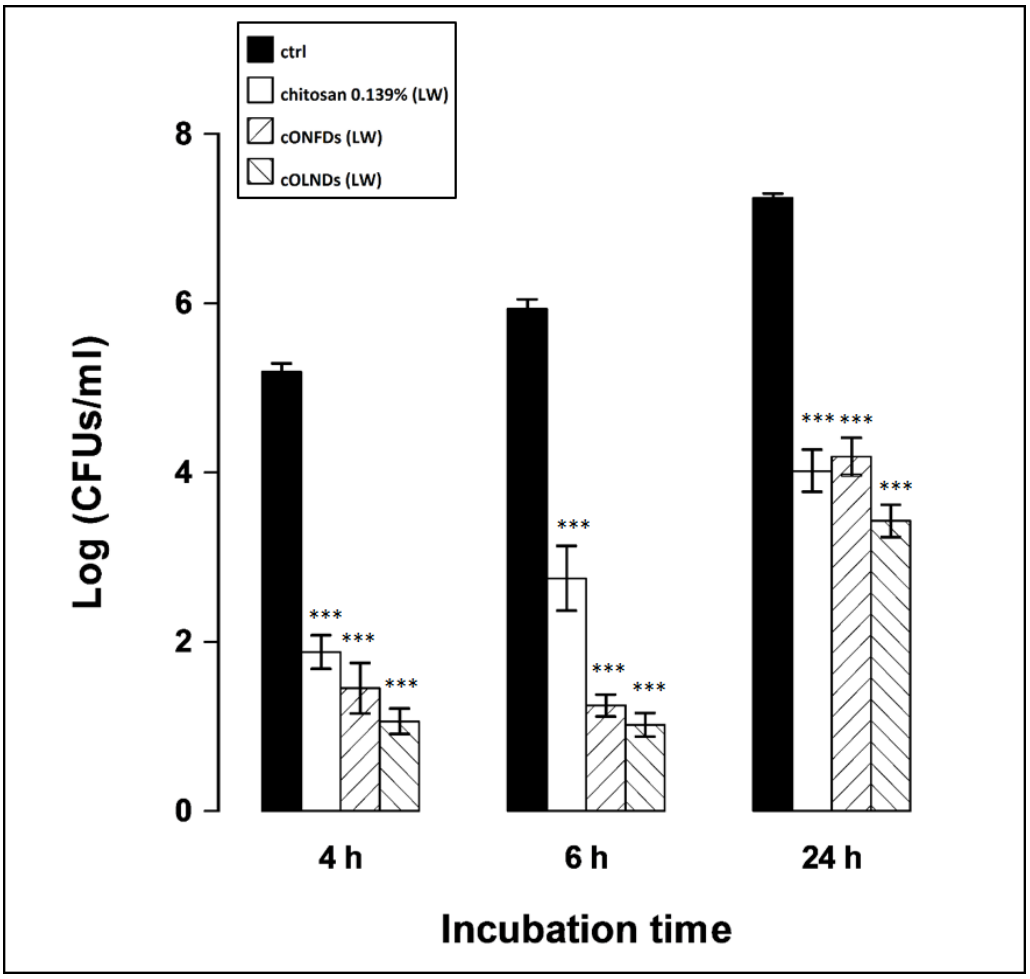

Fig. 48. Antifungal activity of LW chitosan nanodroplets on *C. albicans* yeasts.
C. albicans yeasts (10^5 CFUs/ml) were incubated alone or with 10% v/v free LW chitosan (0.139% m/v) solution, LW cOFND suspension, and LW cOLND suspension in sterile conditions at 37°C and their growth was monitored for 4, 6 and 24 h. At each incubation time, the samples were spread on SAB agar medium to determine the CFUs/ml. Results are shown as means ± SEM from three independent experiments and expressed as Log CFUs/ml. Data were evaluated for significance by ANOVA: vs controls, 4-6-24 h, *** p<0.0001.

4.3.15. Mechanical interaction between low molecular weight chitosan nanodroplets and *C. glabrata* yeasts

The mechanical interaction between LW cOLNDs or cOFNDs and *C. glabrata* yeasts was investigated through analysis by confocal microscopy. *C. glabrata* yeasts (10^8 CFUs/ml) were left untreated or treated with 10% v/v FITC-labelled LW cOLNDs or LW cOFNDs under normoxic conditions. After 3 h and 24 h, yeasts were fixed and stained with PI.

As shown in Fig. 49, both formulations appeared to have been avidly uptaken and internalised by yeasts already at the earlier observational time-point (3 h). Consistently, cOLND/OFND internalisation by yeasts was also observed at the later time-point (24 h) of incubation (data not shown).

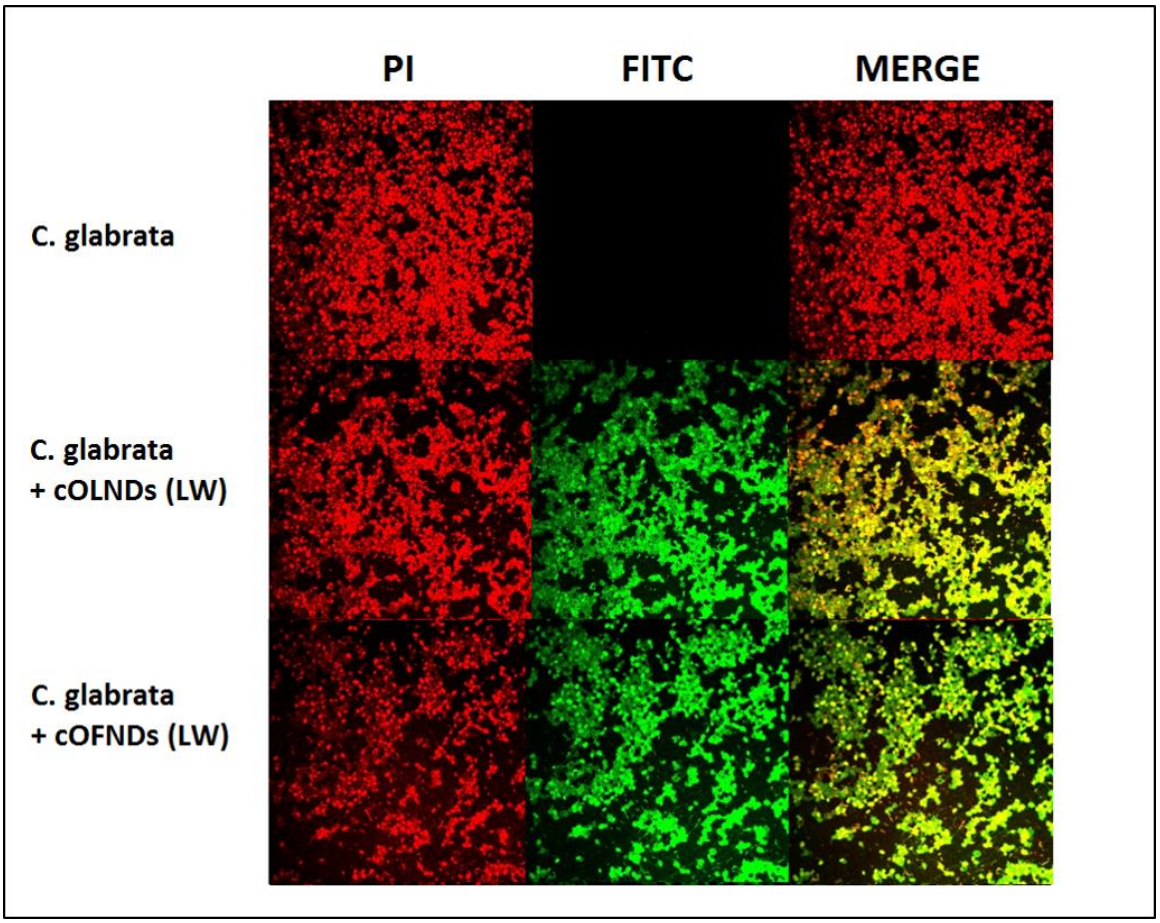

Fig. 49. LW chitosan nanodroplet internalisation by *C. glabrata* yeasts. *C. glabrata* yeasts (10^8 CFUs/ml) were left alone or incubated with 10% v/v FITC-labelled LW cOLNDs or LW cOFNDs for 3 h. After staining yeasts with PI, confocal fluorescent images were taken using FITC and TRITC filters. Data are shown as representative images from three independent experiments. Magnification: 100X. Red: PI. Green: FITC.

4.3.16. Antifungal activity of low molecular weight chitosan nanodroplets on *C. glabrata* yeasts

The antifungal properties of LW chitosan nanodroplets against *C. glabrata* were evaluated through a microbiological assay. *C. glabrata* yeasts (10^5 CFUs/ml) were incubated alone or in presence of 10% v/v free LW chitosan solution (0.139% m/v), LW cOFNDs, or LW cOLNDs. The fungal growth was monitored for 4, 6 and 24 h.

As shown in Fig. 50, LW cOLNDs and LW cOFNDs, as well as free LW chitosan solution, inhibited *C. glabrata* growth up to 24 hours of incubation. After 6 hours of treatment, LW chitosan nanodroplets strongly affected *C. glabrata* viability compared to chitosan alone.

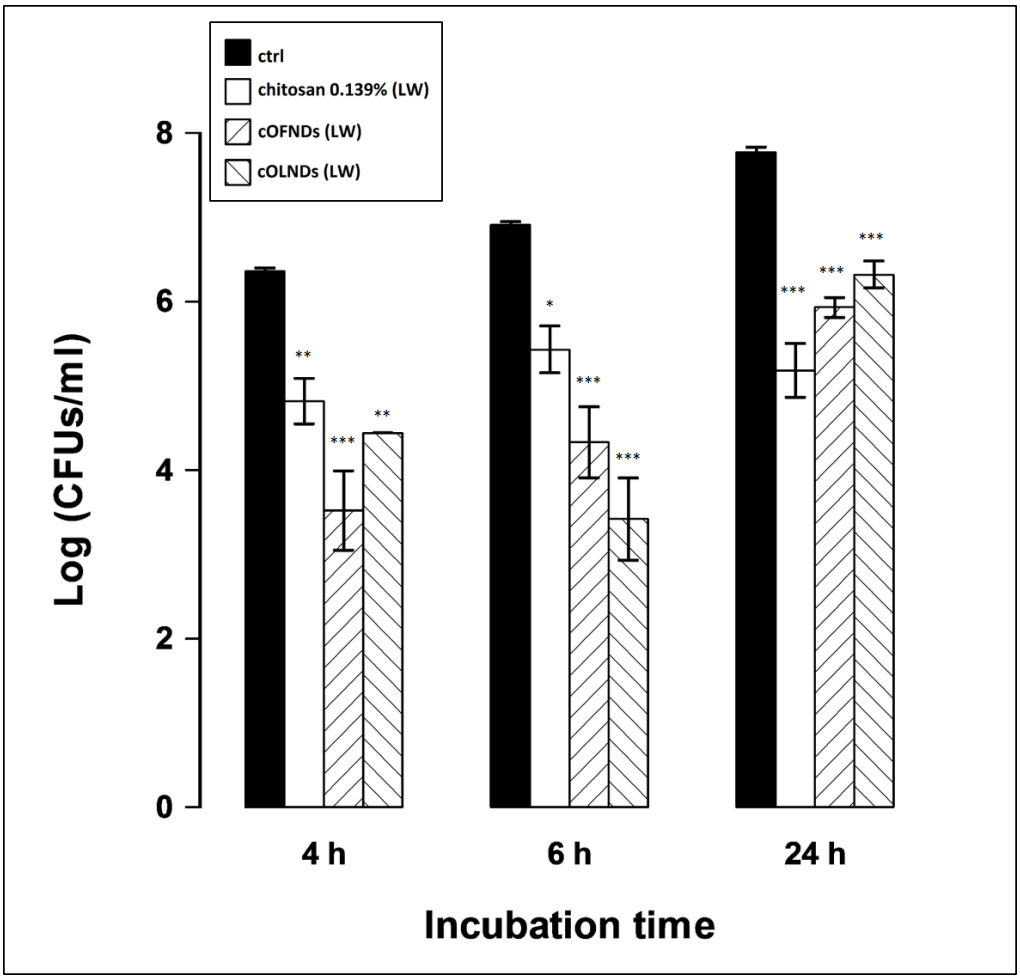

Fig. 50. Antifungal activity of LW chitosan nanodroplets against *C. glabrata* yeasts.
C. glabrata yeasts (10^5 CFUs/ml) were incubated alone or with 10% v/v free LW chitosan (0.139% m/v) solution, LW cOFND suspension, and LW cOLND suspension in sterile conditions at 37°C and their growth was monitored for 4, 6 and 24 h. At each incubation time, the samples were spread on SAB agar medium to determine the CFUs/ml. Results are shown as means ± SEM from three independent experiments and expressed as Log CFUs/ml. Data were evaluated for significance by ANOVA: vs controls: 4 h, *** p<0.0001; 6 h, ** p<0.001; 24 h, * p<0.01.

CHAPTER 5.
DISCUSSION

The present work aimed at developing, characterising and testing innovative and nonconventional platforms of oxygen nanocarriers with antimicrobial effects to potentially treat infected chronic wounds, an alarmingly spreading condition that affects worldwide the elderly especially.

The development of dextran- and chitosan- shelled nanobubbles (OLNBs) by our collaborative research network dates back to 2009[263,264]. From 2009 to 2014, a new platform of nanocarriers, named nanodroplets, was developed and characterised for its physico-chemical properties. Crucial studies on dextran and MW chitosan-shelled nanodroplets (OLNDs) were published during 2014 and 2015[326,336]. Nanodroplets were also patented in the same period[353]. Based on the current research interests, we recently aimed at developing nontoxic oxygen carriers with nanometric dimensions that could be able not only to abrogate hypoxia-related effects on human cells but also to counteract microbial infections. At the begining, dextran was employed for shell manufacturing[263]; however the use of natural antimicrobial polysaccharides, such as chitosan[354], represented the best option for our goals.

Firstly, MW chitosan nanobubbles (MW cOLNBs) were formulated, characterised and challenged for their biological effects on human keratinocytes, MRSA bacteria, and *C. albicans* yeasts as an effective model of antimicrobial oxygen-based nanocarrier. Then, MW chitosan nanodroplets (MW cOLNDs) were prepared and tested for their biocompatibility and antimicrobial activity not only using the above mentioned cell types but also expanding the study to additional cell populations (human dermal fibroblasts, human microvascular endothelium, *S. pyogenes* bacteria, and *C. glabrata* yeasts).

Based on the promising results obtained from MW cOLNDs, deeper investigation on such a promising platform of oxygen-based nanocarriers was conducted. Indeed, other biomaterials than MW chitosan were considered for shell manufacturing in order to improve nanodroplet phisico-chemistry, biocompatibility and effectiveness. Based on data obtained from preliminary studies on different chitosan species and derivatives[355] [MW, LW, glycol- (G), and methylglycol- (MG) chitosan], LW chitosan emerged as the best candidate for the abovementioned parameters and was chosen to be employed for manufacturing the outer shell of the nanodroplets employed in the present study. Therefore, new LW chitosan-

shelled nanodroplets were compared to formerly available MW chitosan-shelled nanodroplets for their biological properties on several human cells and yeasts.

Nanobubbles and nanodroplets were prepared as liquid formulations, suitable for *in vitro* studies. All nanocarriers were characterised by a typical shell-core structure, with a specific oxygen-binding fluorocarbon (PFP for nanobubbles and DFP for nanodroplets) in the inner core and two alternative chitosan species (MW chitosan either for nanobubbles or nanodroplets; LW chitosan for nanodroplets only) in the outer shell. These shell-core structured nanocarriers appear also suitable for further manipulation to conjugate different molecules such as dyes and antibiotics or antimycotics[263,264,326,327,336].

The choice of the fluorocarbon to be inserted within the core is crucial, as it can influence both physico-chemistry and effectiveness of the nanocarrier. The main advantages of nanobubbles and nanodroplets are related to the presence of PFP and DFP in the inner core, respectively. Both PFP and DFP are able to easily bind and release oxygen, greatly improving its delivery into hypoxic environments. However, PFP skeleton is characterised by twelve fluorine atoms whereas DFP carbon skeleton is surrounded by ten fluorine and two hydrogen atoms[331]. The advantage of using DFP is related to its ability to establish hydrogen bonds between hydrogen and oxygen atoms, in addition to dipole-dipole interactions between fluorine and oxygen atoms that can be also established by PFP. Based on this fact, oxygen releasing kinetics appear crucial in order to predict *in vitro* the effectiveness of formulations on cell cultures.

According to our studies, the replacement of PFP with DFP in the inner core did not affect nanoparticle stability, as shown by zeta potential values either of nanobubbles or nanodroplets. Zeta potential is a crucial parameter to predict the stability of a nanocarrier, as it measures charge repulsion or attraction among particles. Cationic zeta potentials higher than + 30 mV are usually required for stability of colloid systems[348]. Moreover, OLNDs have been reported to release *in vitro* higher amounts of oxygen in a more time-sustained manner than OLNBs and OSS[326,336]. Therefore, nanodroplets might be preferred to nanobubbles as a potential oxygen-based platform to be used in the future.

Clearly, the suitability of nanocarriers for specific applications is related to their size, composition and charge. In our nanobubbles and nanodroplets, MW chitosan

was firstly chosen as candidate polysaccharide for the preparation of the outer shell, due to its biocompatibility and antimicrobial properties[343]. Both MW cOLNBs and MW cOLNDs displayed nano-dimensions (~700 nm), however only their oxygen-free counterparts displayed the smallest diameters (~400 nm). Such a difference in size between oxygen-loaded and oxygen-free formulations appears as a direct consequence of oxygen presence or absence, respectively. Previous studies on dextran-shelled nanocarriers already suggested that oxygen in the inner core can change the interfacial layer structure, modify the surface tension, and lead to differences in the formulations hydrophobicity[263,326].

Positive values of charge of about + 40 mV for both nanocarriers confirm the stability and the presence of chitosan on the shell surfaces. In particular, cationic nanocarriers seem to be suitable for topical treatments as their positive charges interact strongly with anionic surface of the skin[356]. In an interesting study by Wu and colleagues[356], cationic fluorophore PMI-conjugated PS-NH_3^+ (amino-functionalised polystyrene latex nanoparticles) displayed brighter fluorescence at the skin surface than anionic PMI-conjugated PS-CO_2^-(carboxyl-functionalised polystyrene nanoparticles).

As mentioned previously, also other chitosan species and derivatives (LW, G, and MG chitosan) were considered for shell manufacturing[355]. According to the results obtained from preliminary investigation on the biocompatibility for each biomaterial, MG chitosan solution strongly reduced by 50% human keratinocyte viability and for this reason this polysaccharide was excluded from the subsequent studies. Either LW or G chitosan-shelled OLNDs displayed cationic surfaces and ≤ 500 nm average diameters, with LW chitosan-shelled OLNDs being the smallest ones and displaying higher stability. Based on these data, LW chitosan emerged as the best candidate molecule to be compared to MW chitosan for nanodroplet manufacturing.

Notably, the biocompatibility with human cells represents a crucial issue, since the potential use *in vivo* of oxygen nanocarriers is related to their toxicity to eukaryotic cells. Interestingly, LW chitosan (especially chitosan with molecular weight < 10000 Da) has been reported to be associated with lower toxicity and higher water solubility compared to chitosan molecules characterised by higher molecular weight[283]. Moreover, chitosan antimicrobial activity related to nanocarriers has been reported to depend on the molecular weight and degree of deacetylation of

the chitosan employed during formulation manufacturing[357,358]. Furthermore, chitosan with a proper molecular weight could be effectively employed as a carrier for renal targeting[359] and for oral delivery of paclitaxel[360]. These findings might be exploited in the future to develop antimicrobial-conjugated LW chitosan nanodroplets as adjuvant treatment for infected chronic wound management. In this context, vancomycin-loaded, erythromycin-loaded, and itraconazole-loaded LW chitosan nanodroplets have been also recently formulated and characterised by our group, with encouraging preliminary data[361,362] from biocompatibility studies and microbiological assays (unpublished data for vancomycin-loaded LW chitosan nanodroplets).

In the work described here, LW cOLNDs displayed spherical shape, shell-core structure, and average diameters of ~400 nm. Such sizes were similar to those of their oxygen-free counterparts and almost half of those previously measured in MW cOLNB/cOLND formulations. This evidence appears as a crucial element in the context of developing new effective nanocarriers for gas release. Indeed, according to the Law of Laplace for spherical surfaces, the difference between the outer and the inner gas pressure in bubbles (and droplets) is inversely proportional to their radius: therefore, the smaller the bubble's radius, the higher the differential pressure of the gas, and the faster the diffusion of the gas[323]. On the other hand, zeta potential values (+ 30 mV) confirmed LW cOLND stability.

The physico-chemical characteristics of nanocarriers are crucial as they will influence their interactions with cells. Moreover, during preclinical studies, their properties will influence the interactions with human skin and the rate and extent with which nanocarriers will be able to release the associated active molecules into the *stratum corneum*.

After manufacturing and physico-chemical characterisation, nanobubbles and nanodroplets underwent investigation on biocompatibility with human skin cells. Before any cell treatments, nanobubbles and nanodroplets were sterilised in order to avoid any contamination on cell cultures. UV-C irradiation was chosen as a sterilisation method. UV-C rays could alter fundamental cell molecules as DNA, lipids and protein leading to dramatic toxic effects on cells and pathology development[363]. Thus, MW cOLNBs, MW cOLNDs, and LW cOLNDs were checked for ozone and ROS production. The absence of ozone and singlet oxygen

production appears extremely comforting. Furthermore, nanobubbles and nanodroplets formulations were incubated up to 72 h in cell culture medium in order to check the absence of microbial contaminations.

Then, MW cOLNBs, MW cOLNDs, and LW cOLNDs were challenged for their biocompatibility with human skin cells and for their antimicrobial properties against selected bacteria and yeasts. Indeed, the main goal was to reach the lowest toxicity to human cells and the highest toxicity against pathogens. Furthermore, the concentration of nanocarrier formulations needed to be calibrated in order to deliver enough oxygen to counteract hypoxia without compromising cell viability. In a couple of former studies performed by our group, increasing concentrations of nanocarrier suspensions were tested on human keratinocytes, with 10% v/v emerging as the most effective and less toxic concentration to be used in the subsequent experiments[336,344]. Such a concentration was further validated also on fibroblasts and endothelial cells by other members of our collaborative network[355].

MW cOLNBs were firstly challenged for biocompatibility. HaCaT cell line, which has been immortalised from a 62-year old Caucasian male donor[349], was chosen as a source of human keratinocytes. Keratinocytes are the most represented cells (> 90%) in the skin epithelium, providing a physical barrier to limit fluid loss and to protect against pathogens, thus being crucial during all wound healing stages[37]. Interestingly, the production of keratinocytic MMPs, playing crucial roles during the remodelling phase of wound healing, was demonstrated to be altered by hypoxia and depend on the donor's age[364]. Thus, cell type and source appear to be critical in our context, since hypoxia-associated dermal pathologies are more common during the elderly. Based on these preconditions, HaCaT cells were chosen as the best candidate cells among available cell lines for our research purposes.

As expected, hypoxia affected human keratinocyte viability[343,344,365]. However, MW cOLNBs were not toxic to HaCaT cells both in normoxic and hypoxic conditions. These data are in accordance with evidence that perfluorocarbon emulsions are not toxic to human healthy cells, as erythrocytes for example[366]. Consistently, PFP was recently reported not to display any toxic effects on human keratinocytes when employed as inner core molecule of vancomycin-loaded dextran sulphate-shelled nanobubbles[327]. Moreover, these findings are in line with previous data on the lack of cytotoxicity effects of chitosan micro/nanobubbles on choriocarcinoma

cells[264,325]. Nevertheless, MW cOFNBs were slightly toxic to hypoxic human keratinocytes, opposite to MW cOLNBs. This evidence might suggest a protective role for oxygen, which has already been proposed in other studies on MW cOLNDs as adjuvant treatment for skin infections[343]. Indeed, oxygen could counteract through unknown mechanisms the cytotoxicity of chitosan, which has been reported to vary depending on its molecular weight and degree of deacetylation[367]. On the other hand, the difference in size between MW cOLNBs and MW cOFNBs cannot be excluded from the possible factors underlying the different toxicity of either nanocarrier. Nevertheless, these data showing MW cOLNB biocompatibility with human keratinocytes corroborate the available evidence on the key role of oxygen in nanobubble manufacturing for potential topical administration in future preclinical studies.

Thereafter, also MW and LW chitosan nanodroplets were challenged for their biocompatibility on HaCaT cells. Results obtained with MW chitosan nanodroplets were similar to those with MW chitosan nanobubbles. Indeed, MW cOLNDs did not affect the viability of human keratinocytes either in normoxia or in hypoxia, in contrast with MW cOFNDs, which were mildly toxic. On the other hand, the presence of LW chitosan in the shell of nanodroplets (either loaded or unloaded with oxygen) led to enhanced viability of human keratinocytes, confirming the dependence on chitosan molecular weight in biocompatibility with HaCaT cells[367].

Neverteheless, it should be noticed that keratinocytes are usually stronger than other cells involved in wound healing processes. For this reason, cells studies with MW and LW nanodroplets were extended to human dermal fibroblasts and microvascular dermal endothelium (HDF and HMEC-1 cell lines[350,351]). Encouragingly, MW or LW cOLNDs were not toxic to HDF cells and did not affect fibroblast viability either in normoxia or in hypoxia. However, biocompatibility studies on endothelium led to very different results. Hypoxia significantly compromised the health of endothelial cells, although it did not affect total cell viability, in line with data from literature[345,368]. However, MW chitosan nanodroplets strongly reduced endothelial cell viability. On the other hand, LW cOLNDs resulted significantly less toxic to endothelium compared to MW cOLNDs. These data from biocompatibility studies suggest that the treatment with LW chitosan nanodroplets should be preferred to MW chitosan nanocarriers in future studies.

As a next step, analyses by confocal microscopy were performed to discern the mechanisms of interaction between our nanocarriers and human cell surfaces (i.e. lack of contact, adhesion, or internalisation). According to the results, both MW cOLNBs and MW cOLNDs were avidly uptaken by HaCaT cells after 24 h of incubation. Studies on the mechanical interaction between LW cOLNDs and human keratinocytes, as well as all studies on fibroblasts and endothelial cells, are yet to be performed. Nevertheless, these preliminary data are in line with those obtained with dextran OLNBs in monkey fibroblastoid kidney cells (Vero)[263], as well as with dextran OLNDs in human keratinocytes[326], endothelial cells[345], and monocytes[346]. Besides, this approach was also widely chosen also to demonstrate the accumulation of LW chitosan in renal tubules[359] or chitosan/cyclodextrin nanoparticles internalisation by epithelial cells calu-3[369].

In general, after interacting with human cells, nanoparticles might be engulfed in invaginations of the cell membrane and then be internalised by cells through time-, concentration-, and energy-dependent pinocytic processes[370]. Macropinocytosis, clathrin-mediated endocytosis, caveolae-mediated endocytosis and mechanisms independent of clathrin and caveolin are examples of these uptake mechanisms[371,372]. These processes can activate several intracellular signalling pathways, thus paving the way for different cellular fates, from proliferation and survival to apoptosis and cell death[373,374]. Chitosan intracellular degradation has been hypotised to be associated to lysosomes[375]. Specific receptors for chitosan have not been reported to date, suggesting that the mechanism of chitosan's cellular binding might be a nonspecific electrostatic interaction with the negatively charged cell membrane. Keratinocytes have been reported to expose several anionic residues on their membranes[376], with dimensions ranging between 35 and 55 μm[377]. Therefore, evidence on MW cOLNB/cOLND cellular internalisation after adhering on cell plasma membrane is not surprising. Future studies aiming at elucidating the processes underlying cellular internalisation and trafficking of nanobubbles and nanodroplets are certainly required.

Cell migration is a critical process during wound healing[378]. Two processes are essential during wound repair for the lesion to heal successfully. First, keratinocytes should be able to detach from the underlying basal lamina. Second, keratinocytes must move and migrate through the new ECM within the wound.

This process is facilitated by MMPs and tissue inhibitors of metalloproteinases (TIMPs)[379]. All these processes are hampered by hypoxia.

In the present study, the effects of hypoxia as well as those of oxygen nanobubbles and/or nanodroplets on the migration of human keratinocytes, fibroblasts, and endothelial cells were evaluated *in vitro* by scratch assay. Hypoxia strongly impaired wound healing abilities in all three cell populations. However, either MW cOLNBs or MW cOLNDs restored a normoxia-like migratory phenotype in hypoxic human keratinocytes. MW cOLNDs also promoted the migration of hypoxic human fibroblasts. LW cOLNDs appeared to be the more effective nanocarriers, as they abrogated the effects of hypoxia, thus promoting normoxia-like migration, in all cell types: keratinocytes, fibroblasts, and endothelial cells. Interestingly, these effects were neither achieved by nanobubble/nanodroplet oxygen-free counterparts (OFNBs and OFNDs) nor by OSS, suggesting that not only oxygen presence was essential, but also its gradual release.

Cell migration during wound closure depends on tight regulation of balances between MMPs and TIMPs. Indeed, dysregulated MMP/TIMP ratio characterise chronic non healing wounds[380]. Normoxic HaCaT cells were shown to release MMP-2, MMP-9, TIMP-1, and TIMP-2, with hypoxia impairing MMP/TIMP balances by reducing MMP-2, MMP-9, and TIMP-2 release[344]. Interestingly, MW cOLNDs abrogated hypoxia-dependent dysregulation on MMP/TIMP secretion, an effect that was specifically due to oxygen delivering abilities of OLNDs[344]. Additionally, dextran-shelled OLNDs were reported to restore normoxia-like balances between MMP-2 and TIMP-2 as well as between MMP-9 and TIMP-1 also in hypoxic human microvascular endothelial cells[345], human monocytes[346], and human placenta explants[347].

Nanobubbles and nanodroplets were also able to interact with microbial cells. MW cOLNBs, as well as MW cOLNDs, where shown to physically interact with MRSA bacteria and *C. albicans* yeasts, although in a different manner. Indeed, both nanobubbles and nanodroplets just adhered to bacterial cell walls, whereas they were avidly uptaken only by yeasts. MW cOLNBs and MWcOLNDs have in common very similar diameters and the same polysaccharidic shell, therefore it is not surprising that the outcomes of the mechanical interaction between the nanocarriers and the cells vary depending on the cell type only. Bacteria present a

cell wall of peptidoglycans containing multiple glycine residues and lipoteichoic acids[381]. Although the exact molecular mechanisms have not yet been elucidated, positively charged chitosan residues (protonated amine groups) may bind to the negatively charged bacterial surface (lipoteichoic acid in Gram-positive bacteria), leading to altered membrane permeability[382]. On the other hand, *Candida* cell wall is thinner compared to that of bacteria and differs in composition for the presence of mainly mannoproteins and β-glucans[383]. In particular, Gram-positive bacteria differ greatly from yeasts in surface structure, and this difference can justify different interactions between nanocarriers and microbes.

These analyses were expanded to other microbes by using chitosan nanodroplets only, based on their formerly mentioned advantages in terms of biocompatibility with human cells. As for *C. albicans*, MW cOLNDs were also internalised by *C. glabrata* yeasts. However, MW cOLNDs were also avidly uptaken by *S. pyogenes* bacteria, in contrast to MRSA. Notably, MRSA bacteria are characterised by a complex cell wall[384], whereas *S. pyogenes* bacteria are covered by capsules with anti-phagocytic properties[169]. Therefore, either membrane is different in molecular composition, thus possibly justifying different interactions between chitosan nanocarriers and bacteria. However, the molecular mechanisms responsible for MW cOLND internalisation by *S. pyogenes* bacteria are yet to be elucidated.

When LW chitosan-shelled nanodroplets were employed, they were internalised by all four microbes (MRSA, *S. pyogenes*, *C. albicans*, and *C. glabrata*).

Based on these data on the physical interactions between nanocarriers and microbes, adhesion and internalisation were hypothesised to associate with short-term and long-term antimicrobial effects, respectively. This hypothesis was generally confirmed by the results obtained from microbiological assays, with one exception. Indeed, whenever nanobubbles or nanodroplets did adhere to MRSA cell wall, their antibacterial effects lasted up to 6 hours only. On the contrary, all tested oxygen nanocarriers displayed long-lasting (up to 24 hours) antimicrobial effects against *S. pyogenes*, *C. albicans*, and *C. glabrata* upon cell internalisation. The only exception to this pattern is represented by LW cOLND-treated MRSA: in this case, the antibacterial effects of nanodroplets lasted for 6 hours only, despite their internalisation by bacteria.

Specific adjustments to the protocol for microbiological assays, related to different characteristics among bacteria and yeasts, did not interfere with the experimental setting and data comparison among different microbes. Moreover, among the compounds employed for nanocarrier manufacturing, chitosan is the only molecule exerting cytostatic activity on microbes. The dependence of the antimicrobial properties of nanobubbles/nanodroplets on the presence of chitosan in their shells appears likely, as confirmed by data obtained with free chitosan solution alone, which were similar. Also, this hypothesis is also confirmed by evidence that the presence of different fluorocarbons as well as the presence or absence of oxygen molecules within the core on nanocarriers did not affect the effectiveness of nanobubbles and nanodroplets.

The mechanisms of interaction between nanodroplets and microbes can also result in leakage of intracellular constituents causing death of bacteria and yeasts. From literature on bacteria, experimental data obtained by Helander and colleagues provided evidence that chitosan disrupts the barrier properties of the outer membrane of Gram-negative bacteria under specif conditions[385]. Jeon and colleagues demonstrated that chitosan microparticles bactericidal activity is coupled with the binding activity to OmpA and LPS in *E. coli* O157:H7, leading to cell death, probably via two distinct mechanisms at neutral pH[386]. Although the strongest antimicrobial activity of chitosan was observed at acidic pH, antimicrobial effects of nanocarrier at neutral pH have been reported, according to data by Jeon and colleagues, showing that chitosan microparticles still had significant unexpected antimicrobial activity at pH 7[386]. In this context, Regiel-Futyra and colleagues described the effects of gold chitosan-based nanocomposites on *S. aureus* and *P. aeruginosa*, observing significant and progressive damage on the cell wall[387]. They underlined the importance of direct contact between materials and bacteria in order to achieve at least bacteriostatic effects. Furthermore, they stressed the issue that chitosan molecular weight might influence its different site of interaction with bacterial cells. MW chitosan exerts bacteriostatic effects which depend on the analysed bacterial strain, due to the interactions of nanodroplets with bacterial cell wall, according to the fact that medium molecular weight of the polymer seems to enable only surface interactions[388].

As far as it concerns chitosan fungistatic activity, the uptake of chitosan nanodroplets by yeasts may also cause cell wall permeabilisation resulting from binding of chitosan nanodroplets to the surface of *Candida* yeasts. According to Pena and colleagues, yeast permeabilisation might cause in turn the inhibition of main metabolic pathways, depriving cells of their energy sources[389]. Specific binding of nanocarriers to yeasts might promote K^+ efflux, extracellular acidification, inhibition of Rb^+ uptake, increased transmembrane potential difference, and increased uptake of Ca^{2+}, thus causing the inhibition of some metabolic pathways such as respiration and fermentation[389]. This modifications regarding ion homeostatis and metabolisms may be likely to occur also with our formulations. Nevertheless, specific antifungal molecular mechanisms triggered by nanodroplets are yet to be investigated.

CHAPTER 6.
CONCLUSION

In the present study, three different oxygen-based nanocarriers (MW cOLNBs, MW cOLNDs, and LW cOLNDs) were challenged for their physico-chemical characteristics, oxygen releasing abilities, mechanical interaction with human and microbial cells, biocompatibility with human cells, abilities to promote wound healing, and antimicrobial properties.

Nanobubbles and nanodroplets displayed spherical morphology, cationic surfaces, and diameters in the nanometer range (with LW cOLNDs being the smallest ones). However, *in* vitro oxygen release from OLNDs appeared higher and more sustained over time than from OLNBs[149,189]. Based on these data, nanodroplets might be preferred to nanobubbles as an oxygen-releasing platform.

The substitution of MW with LW chitosan in the outer shell did not affect oxygen release from OLNDs. Additionally, LW cOLNDs displayed lower toxicity to human cells (especially to endothelium) than MW cOLNDs. Compared to MW cOLNBs and MW cOLNDs, LW cOLNDs displayed greater effectiveness in promoting wound healing during hypoxia and in counteracting microbial growth in a long-term manner as a consequence of early cellular internalisation. Based on these findings, LW cOLNDs appear to be the most promising oxygen nanocarriers among those tested as nonconventional and cost-effective antimicrobial and oxygenating adjuvant treatment in the context of chronic wound managment.

In the future, *in vitro* studies are going to be performed on co-cultures of wound healing-related cell populations, which were already tested here singularly. Preclinical studies will be performed using *in vitro* models of human reconstructed epidermis that will be specifically treated with appropriated doses of LW chitosan nanodroplets. Furthermore, *in vivo* studies with gel formulations of chitosan nanodroplets in the absence or presence of US will be encouraged to optimise nanodroplet delivery throughout the skin. Future researches will aim at improving the effectiveness of these nanocarrier by drugs conjugation. Antibodies might also be added during manufacturing in order to enhance specific targeting of the nanocarriers. Finally, LW chitosan nanodroplets might be coupled with porphyrins to assess the potential advantages of photodynamic therapies (PDT) in the context of antimicrobial chronic wound management.

CHAPTER 7.
ACKNOWLEDGEMENTS

The studies described here were performed at Università degli Studi di Torino (UNITO), in collaboration with Istituto Nazionale di Ricerca Metrologica (INRIM) and Università degli Studi di Milano (UNIMI).
The research was supported by funds from: Compagnia di San Paolo to C. Guiot, R. Cavalli, and A. Troia (2012-2014) and to A. M. Cuffini, G. Banche, G. Giribaldi, and V. Tullio (2015-2017); Fondazione Cariplo to M. Prato, N. Basilico, and M. Dell'Agli (2016-2018).
Special thanks are due to my Supervisor G. Giribaldi and Co-Supervisor M. Prato, who gave me the possibility to study and to work on such an interesting research project.
Thanks are due to A. Troia and C. Magnetto for suggestions on nanodroplet manufacturing and characterisation and to M. Argenziano and R. Cavalli for help with preparation and characterisation of nanobubbles. I also thank A. Khadjavi, G.R. Gulino, and E. Gazzano for tips on LDH and MTT experiments, as well as T. Genova and E. Zicola for help with ATP assay and scratch assay experiments. Thanks are due to N. Basilico, M. Dell'Agli, S. D'Alessandro, M. Fumagalli, and E. Sangiovanni for collaborating in studies with endothelial and fibroblast cells. I also want to thank A. Luganini for help with confocal microscopy analyses on prokaryotic and eukaryotic cells. Furthermore, thanks are due to G. Banche and N. Mandras for help with bacterial and fungal cultures, and to A.M. Cuffini for hosting me in her Microbiology Lab at the beginning of my doctoral course. It was an honour for me.
Finally, thanks are due to V. Allizond, D. Scalas, J. Roana, M. Soster, I. Fenoglio, I. Rivolta, A. Panariti, C. Costamagna, G. Gribaudo, C. Guiot, V. Tullio, S. Turini and B. Bressan.

Thanks are due to my husband because he did the most important work during these years: he loves me everyday.
Loving thanks are also due to my lab friends G. Piersigilli, N. Collino, R. La Grotta, E. Mungo, I. C. Salaroglio, G. Mandili, E. Mazza, S. De Lucia, J. Kopechka, E. Gazzano, and V. Gallo.

CHAPTER 8.
REFERENCES

1. Scuderi, N. & Toth, B. A. International Textbook of Aesthetic Surgery. (Springer, 2016).
2. Tortora, G. J. & Derrickson, B. H. Principles of Anatomy and Physiology. (John Wiley & Sons, 2008).
3. Watt, F. M. Mammalian skin cell biology: at the interface between laboratory and clinic. Science **346,** 937–940 (2014).
4. Arda, O., Goksugur, N. & Tuzun, Y. Basic histological structure and functions of facial skin. Clin. Dermatol. **32,** 3–13 (2014).
5. Rittie, L. & Fisher, G. J. Natural and sun-induced aging of human skin. Cold Spring Harb. Perspect. Med. **5,** a015370 (2015).
6. Hao, J., Bonnet, C., Amsalem, M., Ruel, J. & Delmas, P. Transduction and encoding sensory information by skin mechanoreceptors. Pflugers Arch. **467,** 109–119 (2015).
7. Peng, Y. et al. Systematic review focusing on the excretion and protection roles of sweat in the skin. Dermatol. Basel Switz. **228,** 115–120 (2014).
8. Kim, E. J. et al. UV modulation of subcutaneous fat metabolism. J. Invest. Dermatol. **131,** 1720–1726 (2011).
9. Baroni, A. et al. Structure and function of the epidermis related to barrier properties. Clin. Dermatol. **30,** 257–262 (2012).
10. Natsuga, K. Epidermal barriers. Cold Spring Harb. Perspect. Med. **4,** a018218 (2014).
11. Kenneth, S. & Saladin, D. Human Anatomy. (McGraw-Hill Education, 2016).
12. Roberts, N. & Horsley, V. Developing stratified epithelia: lessons from the epidermis and thymus. Wiley Interdiscip. Rev. Dev. Biol. **3,** 389–402 (2014).
13. Zelickson, A. S. & Hartmann, J. F. An electron microscopic study of human epidermis. J. Invest. Dermatol. **36,** 65–72 (1961).
14. Hänel, K. H., Cornelissen, C., Lüscher, B. & Baron, J. M. Cytokines and the Skin Barrier. Int. J. Mol. Sci. **14,** 6720–6745 (2013).
15. Griffiths, C., Barker, J., Bleiker, T., Chalmers, R. & Creamer, D. Rook's textbook of dermatology. (John Wiley & Sons, 2016).
16. Odland, G. F. A submicroscopic granular component in human epidermis. J. Invest. Dermatol. **34,** 11–15 (1960).
17. Simpson, C. L., Patel, D. M. & Green, K. J. Deconstructing the skin: cytoarchitectural determinants of epidermal morphogenesis. Nat. Rev. Mol. Cell Biol. **12,** 565 (2011).
18. Kern, F., Niault, T. & Baccarini, M. Ras and Raf pathways in epidermis development and carcinogenesis. Br. J. Cancer **104,** 229–234 (2011).
19. McMillan, J. R., Akiyama, M. & Shimizu, H. Epidermal basement membrane zone components: ultrastructural distribution and molecular interactions. J. Dermatol. Sci. **31,** 169–177 (2003).
20. Koster, M. I. & Roop, D. R. Mechanisms regulating epithelial stratification. Annu. Rev. Cell Dev. Biol. **23,** 93–113 (2007).
21. Nagarajan, P., Romano, R.-A. & Sinha, S. Transcriptional control of the differentiation program of interfollicular epidermal keratinocytes. Crit. Rev. Eukaryot. Gene Expr. **18,** 57–79 (2008).
22. Freinkel, R. K. & Woodley, D. T. The Biology of the Skin. (Taylor & Francis, 2001).
23. Harper, R. A. & Grove, G. Human skin fibroblasts derived from papillary and reticular dermis: differences in growth potential in vitro. Science **204,** 526–527 (1979).
24. Holbrook, K. A., Byers, P. H. & Pinnell, S. R. The structure and function of dermal connective tissue in normal individuals and patients with inherited connective tissue disorders. Scan. Electron Microsc. 1731–1744 (1982).
25. Montagna, W. The structure and function of skin. (Elsevier, 2012).

*26. Kanitakis, J. Anatomy, histology and immunohistochemistry of normal human skin. Eur. J. Dermatol. EJD **12,** 390-9; quiz 400–1 (2002).*
*27. Wysocki, A. Skin anatomy, physiology, and pathophysiology. Nurs. Clin. North Am. **34,** 777–97, v (1999).*
*28. Khavkin, J. & Ellis, D. A. F. Aging skin: histology, physiology, and pathology. Facial Plast. Surg. Clin. N. Am. **19,** 229–234 (2011).*
*29. Singer, A. J. & Clark, R. A. Cutaneous wound healing. N. Engl. J. Med. **341,** 738–746 (1999).*
*30. Martin, P. Wound healing-aiming for perfect skin regeneration. Science **276,** 75–81 (1997).*
*31. Gurtner, G. C., Werner, S., Barrandon, Y. & Longaker, M. T. Wound repair and regeneration. Nature **453,** 314–321 (2008).*
*32. You, H.-J. & Han, S.-K. Cell therapy for wound healing. J. Korean Med. Sci. **29,** 311–319 (2014).*
*33. Hunt, T. K. & Hopf, H. W. Wound healing and wound infection. What surgeons and anesthesiologists can do? Surg. Clin. North Am. **77,** 587–606 (1997).*
*34. Dudas, M., Wysocki, A., Gelpi, B. & Tuan, T.-L. Memory encoded throughout our bodies: molecular and cellular basis of tissue regeneration. Pediatr. Res. **63,** 502–512 (2008).*
*35. Takeo, M., Lee, W. & Ito, M. Wound healing and skin regeneration. Cold Spring Harb. Perspect. Med. **5,** a023267 (2015).*
*36. Li, J., Chen, J. & Kirsner, R. Pathophysiology of acute wound healing. Clin. Dermatol. **25,** 9–18 (2007).*
37. Wang, P.-H., Huang, B.-S., Horng, H.-C., Yeh, C.-C. & Chen, Y.-J. Wound healing. J. Chin. Med. Assoc. JCMA (2017). doi:10.1016/j.jcma.2017.11.002
*38. Guo, S. al & DiPietro, L. A. Factors affecting wound healing. J. Dent. Res. **89,** 219–229 (2010).*
39. Molnar, M. D. Nutrition and Wound Healing. (CRC Press, 2006).
*40. Ruberg, R. L. Role of nutrition in wound healing. Surg. Clin. North Am. **64,** 705–714 (1984).*
*41. Thiruvoth, F. M., Mohapatra, D. P., Sivakumar, D. K., Chittoria, R. K. & Nandhagopal, V. Current concepts in the physiology of adult wound healing. 2015 **2,** 250–6 (2015).*
*42. Broughton, G. 2nd, Janis, J. E. & Attinger, C. E. The basic science of wound healing. Plast. Reconstr. Surg. **117,** 12S–34S (2006).*
*43. Pool, J. G. Normal hemostatic mechanisms: a review. Am. J. Med. Technol. **43,** 776–780 (1977).*
*44. Kim, W. J.-H., Gittes, G. K. & Longaker, M. T. Signal transduction in wound pharmacology. Arch. Pharm. Res. **21,** 487–495 (1998).*
*45. Diegelmann, R. F. & Evans, M. C. Wound healing: an overview of acute, fibrotic and delayed healing. Front Biosci **9,** 283–289 (2004).*
*46. Henry, G. & Garner, W. L. Inflammatory mediators in wound healing. Surg. Clin. **83,** 483–507 (2003).*
*47. Mahdavian Delavary, B., van der Veer, W. M., van Egmond, M., Niessen, F. B. & Beelen, R. H. J. Macrophages in skin injury and repair. Immunobiology **216,** 753–762 (2011).*
48. Clark, R. A. F. Wound Repair. In The Molecular and Cellular Biology of Wound Repair (ed. Clark, R. A. F.) 3–50 (Springer US, 1988).
*49. Berton, G. & Lowell, C. A. Integrin signalling in neutrophils and macrophages. Cell. Signal. **11,** 621–635 (1999).*
*50. Chazaud, B. Macrophages: supportive cells for tissue repair and regeneration. Immunobiology **219,** 172–178 (2014).*

51. Leibovich, S. J. & Ross, R. The role of the macrophage in wound repair. A study with hydrocortisone and antimacrophage serum. Am. J. Pathol. ***78,*** *71–100 (1975).*
52. Evans, N. D., Oreffo, R. O. C., Healy, E., Thurner, P. J. & Man, Y. H. Epithelial mechanobiology, skin wound healing, and the stem cell niche. J. Mech. Behav. Biomed. Mater. ***28,*** *397–409 (2013).*
53. Coulombe, P. A. Towards a molecular definition of keratinocyte activation after acute injury to stratified epithelia. Biochem. Biophys. Res. Commun. ***236,*** *231–238 (1997).*
54. Freedberg, I. M., Tomic-Canic, M., Komine, M. & Blumenberg, M. Keratins and the keratinocyte activation cycle. J. Invest. Dermatol. ***116,*** *633–640 (2001).*
55. Santoro, M. M. & Gaudino, G. Cellular and molecular facets of keratinocyte reepithelization during wound healing. Exp. Cell Res. ***304,*** *274–286 (2005).*
56. Huang, X., Wu, J., Spong, S. & Sheppard, D. The integrin alphavbeta6 is critical for keratinocyte migration on both its known ligand, fibronectin, and on vitronectin. J. Cell Sci. ***111 (Pt 15),*** *2189–2195 (1998).*
57. Szabo, I., Simon, M. J. & Hunyadi, J. Plasmin promotes keratinocyte migration and phagocytic-killing accompanied by suppression of cell proliferation which may facilitate re-epithelialization of wound beds. Clin. Dev. Immunol. ***11,*** *233–240 (2004).*
58. Raja, Sivamani, K., Garcia, M. S. & Isseroff, R. R. Wound re-epithelialization: modulating keratinocyte migration in wound healing. Front. Biosci. J. Virtual Libr. ***12,*** *2849–2868 (2007).*
59. Tonnesen, M. G., Feng, X. & Clark, R. A. F. Angiogenesis in Wound Healing. J. Investig. Dermatol. Symp. Proc. ***5,*** *40–46*
60. Grøndahl-Hansen, J., Lund, L. R., Ralfkiær, E., Ottevanger, V. & Danø, K. Urokinase- and tissue-type plasminogen activators in keratinocytes during wound reepithelialization in vivo. J. Invest. Dermatol. ***90,*** *790–795 (1988).*
61. Litjens, S. H. M., de Pereda, J. M. & Sonnenberg, A. Current insights into the formation and breakdown of hemidesmosomes. Trends Cell Biol. ***16,*** *376–383 (2006).*
62. Li, J., Zhang, Y.-P. & Kirsner, R. S. Angiogenesis in wound repair: Angiogenic growth factors and the extracellular matrix. Microsc. Res. Tech. ***60,*** *107–114 (2003).*
63. Sinno, H. & Prakash, S. Complements and the wound healing cascade: an updated review. Plast. Surg. Int. ***2013,*** *146764 (2013).*
64. Laurens, N., Koolwijk, P. & de Maat, M. P. M. Fibrin structure and wound healing. J. Thromb. Haemost. JTH ***4,*** *932–939 (2006).*
65. Becker, J. C., Domschke, W. & Pohle, T. Biological in vitro effects of fibrin glue: fibroblast proliferation, expression and binding of growth factors. Scand. J. Gastroenterol. ***39,*** *927–932 (2004).*
66. Allen Jr., R. J. et al. Combination therapy accelerates diabetic wound closure. PLoS ONE ***9,*** *e92667 (2014).*
67. Robson, M. C. et al. The safety and effect of topically applied recombinant basic fibroblast growth factor on the healing of chronic pressure sores. Ann. Surg. ***216,*** *401–408 (1992).*
68. Li, B. & Wang, J. H.-C. Fibroblasts and myofibroblasts in wound healing: Force generation and measurement. J. Tissue Viability ***20,*** *108–120*
69. Xue, M. & Jackson, C. J. Extracellular matrix reorganization during wound healing and its impact on abnormal scarring. Adv. Wound Care ***4,*** *119–136 (2015).*
70. Tomasek, J. J., Gabbiani, G., Hinz, B., Chaponnier, C. & Brown, R. A. Myofibroblasts and mechano-regulation of connective tissue remodelling. Nat. Rev. Mol. Cell Biol. ***3,*** *349 (2002).*
71. Reinke, J. M. & Sorg, H. Wound repair and regeneration. Eur. Surg. Res. Eur. Chir. Forsch. Rech. Chir. Eur. ***49,*** *35–43 (2012).*

*72. Korting, H. C., Schollmann, C. & White, R. J. Management of minor acute cutaneous wounds: importance of wound healing in a moist environment. J. Eur. Acad. Dermatol. Venereol. JEADV **25,** 130–137 (2011).*
*73. Hong, W. X. et al. The role of hypoxia-inducible factor in wound healing. Adv. Wound Care **3,** 390–399 (2014).*
*74. Han, G. & Ceilley, R. Chronic Wound Healing: A review of current management and treatments. Adv. Ther. **34,** 599–610 (2017).*
*75. Pendsey, S. P. Understanding diabetic foot. Int. J. Diabetes Dev. Ctries. **30,** 75–79 (2010).*
*76. Suresh, D. H., Suryanarayan, S., Sarvajnamurthy, S. & Puvvadi, S. Treatment of a non-healing diabetic foot ulcer with platelet-rich plasma. J. Cutan. Aesthetic Surg. **7,** 229–231 (2014).*
*77. Fahey, T. J. 3rd et al. Diabetes impairs the late inflammatory response to wound healing. J. Surg. Res. **50,** 308–313 (1991).*
*78. Falanga, V. Wound healing and its impairment in the diabetic foot. The Lancet **366,** 1736–1743 (2005).*
*79. Tredget, E. E., Nedelec, B., Scott, P. G. & Ghahary, A. Hypertrophic scars, keloids, and contractures. The cellular and molecular basis for therapy. Surg. Clin. North Am. **77,** 701–730 (1997).*
*80. Saed, G. M. et al. Analysis of p53 gene mutations in keloids using polymerase chain reaction-based single-strand conformational polymorphism and DNA sequencing. Arch. Dermatol. **134,** 963–967 (1998).*
*81. Machesney, M., Tidman, N., Waseem, A., Kirby, L. & Leigh, I. Activated keratinocytes in the epidermis of hypertrophic scars. Am. J. Pathol. **152,** 1133–1141 (1998).*
*82. Sen, C. K. et al. Human skin wounds: a major and snowballing threat to public health and the economy. Wound Repair Regen. Off. Publ. Wound Heal. Soc. Eur. Tissue Repair Soc. **17,** 763–771 (2009).*
*83. Gottrup, F., Holstein, P., Jorgensen, B., Lohmann, M. & Karlsmar, T. A new concept of a multidisciplinary wound healing center and a national expert function of wound healing. Arch. Surg. **136,** 765–772 (2001).*
*84. McGuckin, M. et al. Validation of venous leg ulcer guidelines in the United States and United Kingdom. Am. J. Surg. **183,** 132–137 (2002).*
*85. Brem, H. et al. Healing of elderly patients with diabetic foot ulcers, venous stasis ulcers, and pressure ulcers. Surg. Technol. Int. **11,** 161–167 (2003).*
*86. Järbrink, K. et al. The humanistic and economic burden of chronic wounds: a protocol for a systematic review. Syst. Rev. **6,** 15 (2017).*
*87. Chen, W. Y. J. & Rogers, A. A. Recent insights into the causes of chronic leg ulceration in venous diseases and implications on other types of chronic wounds. Wound Repair Regen. Off. Publ. Wound Heal. Soc. Eur. Tissue Repair Soc. **15,** 434–449 (2007).*
*88. Gordon, M. D., Gottschlich, M. M., Helvig, E. I., Marvin, J. A. & Richard, R. L. Review of evidenced-based practice for the prevention of pressure sores in burn patients. J. Burn Care Rehabil. **25,** 388–410 (2004).*
*89. Kuhn, B. A. & Coulter, S. J. Balancing the pressure ulcer cost and quality equation. Nurs. Econ. **10,** 353–359 (1992).*
*90. Pereira, S. G., Moura, J., Carvalho, E. & Empadinhas, N. Microbiota of chronic diabetic wounds: ecology, impact, and potential for innovative treatment strategies. Front. Microbiol. **8,** 1791 (2017).*
*91. Naves, C. C. The Diabetic Foot: A historical overview and gaps in current treatment. Adv. Wound Care **5,** 191–197 (2016).*
*92. Rice, J. B. et al. Burden of venous leg ulcers in the United States. J. Med. Econ. **17,** 347–356 (2014).*

*93. Sargen, M. R., Hoffstad, O. & Margolis, D. J. Geographic variation in Medicare spending and mortality for diabetic patients with foot ulcers and amputations. J. Diabetes Complications **27,** 128–133 (2013).*
*94. Greenwald, L. M. Medicare part D data: major changes on the horizon. Med. Care **45,** S9-12 (2007).*
*95. Home, P., Mant, J., Diaz, J. & Turner, C. Management of type 2 diabetes: summary of updated NICE guidance. BMJ **336,** 1306–1308 (2008).*
*96. Hossain, P., Kawar, B. & El Nahas, M. Obesity and diabetes in the developing world--a growing challenge. N. Engl. J. Med. **356,** 213–215 (2007).*
*97. Suleman, L. Extracellular bacterial proteases in chronic wounds: a potential therapeutic target? Adv. Wound Care **5,** 455–463 (2016).*
*98. McCarty, S. M. & Percival, S. L. Proteases and delayed wound healing. Adv. Wound Care **2,** 438–447 (2013).*
*99. Zhao, R., Liang, H., Clarke, E., Jackson, C. & Xue, M. Inflammation in chronic wounds. Int. J. Mol. Sci. **17,** (2016).*
*100. Thackham, J. A., McElwain, D. L. S. & Long, R. J. The use of hyperbaric oxygen therapy to treat chronic wounds: a review. Wound Repair Regen. Off. Publ. Wound Heal. Soc. Eur. Tissue Repair Soc. **16,** 321–330 (2008).*
*101. Richard, J.-L., Sotto, A. & Lavigne, J.-P. New insights in diabetic foot infection. World J. Diabetes **2,** 24–32 (2011).*
*102. Dietz, I., Jerchel, S., Szaszak, M., Shima, K. & Rupp, J. When oxygen runs short: the microenvironment drives host-pathogen interactions. Microbes Infect. **14,** 311–316 (2012).*
*103. Sancineto, L. et al. Diphenyl diselenide derivatives inhibit microbial biofilm formation involved in wound infection. BMC Microbiol. **16,** 220 (2016).*
*104. Gurtner, G. C. & Chapman, M. A. Regenerative medicine: charting a new course in wound healing. Adv. Wound Care **5,** 314–328 (2016).*
*105. Mulaj, R. R., Muhlstadt, M. & Barouti, N. Antisepsis of wounds: when and what?. Rev. Med. Suisse **11,** 773–4, 776–778 (2015).*
*106. Robson, M. C., Mannari, R. J., Smith, P. D. & Payne, W. G. Maintenance of wound bacterial balance. Am. J. Surg. **178,** 399–402 (1999).*
*107. Williams, D. T., Hilton, J. R. & Harding, K. G. Diagnosing foot infection in diabetes. Clin. Infect. Dis. **39,** S83–S86 (2004).*
*108. Ki, V. & Rotstein, C. Bacterial skin and soft tissue infections in adults: a review of their epidemiology, pathogenesis, diagnosis, treatment and site of care. Can. J. Infect. Dis. Med. Microbiol. **19,** 173–184 (2008).*
*109. Gjodsbol, K. et al. Multiple bacterial species reside in chronic wounds: a longitudinal study. Int. Wound J. **3,** 225–231 (2006).*
*110. Giacometti, A. et al. Epidemiology and microbiology of surgical wound infections. J. Clin. Microbiol. **38,** 918–922 (2000).*
*111. Lazaro, J. L. et al. Elevated levels of matrix metalloproteinases and chronic wound healing: an updated review of clinical evidence. J. Wound Care **25,** 277–287 (2016).*
*112. Schultz, D. R. & Miller, K. D. Elastase of Pseudomonas aeruginosa: inactivation of complement components and complement-derived chemotactic and phagocytic factors. Infect. Immun. **10,** 128–135 (1974).*
*113. Laarman, A. J. et al. Staphylococcus aureus metalloprotease aureolysin cleaves complement C3 to mediate immune evasion. J. Immunol. Baltim. Md 1950 **186,** 6445–6453 (2011).*
*114. Schmidtchen, A., Holst, E., Tapper, H. & Bjorck, L. Elastase-producing Pseudomonas aeruginosa degrade plasma proteins and extracellular products of human skin and fibroblasts, and inhibit fibroblast growth. Microb. Pathog. **34,** 47–55 (2003).*

115. McCarty, S. M., Cochrane, C. A., Clegg, P. D. & Percival, S. L. The role of endogenous and exogenous enzymes in chronic wounds: a focus on the implications of aberrant levels of both host and bacterial proteases in wound healing. Wound Repair Regen. Off. Publ. Wound Heal. Soc. Eur. Tissue Repair Soc. ***20,*** *125–136 (2012).*
116. Shoham, S. & Marwaha, S. Invasive fungal infections in the ICU. J. Intensive Care Med. ***25,*** *78–92 (2010).*
117. Ballard, J. et al. Positive fungal cultures in burn patients: a multicenter review. J. Burn Care Res. Off. Publ. Am. Burn Assoc. ***29,*** *213–221 (2008).*
118. Kourkoumpetis, T. et al. Candida infection and colonization among non-trauma emergency surgery patients. Virulence ***1,*** *359–366 (2010).*
119. Naglik, J. R., Challacombe, S. J. & Hube, B. Candida albicans secreted aspartyl proteinases in virulence and pathogenesis. Microbiol. Mol. Biol. Rev. MMBR ***67,*** *400–428, table of contents (2003).*
120. Pfaller, M. A. & Diekema, D. J. Epidemiology of invasive candidiasis: a persistent public health problem. Clin. Microbiol. Rev. ***20,*** *133–163 (2007).*
121. Papon, N., Courdavault, V., Clastre, M. & Bennett, R. J. Emerging and emerged pathogenic Candida species: beyond the Candida albicans paradigm. PLoS Pathog. ***9,*** *e1003550 (2013).*
122. Mlinaric Missoni, E. et al. Fungal infection in diabetic foot ulcers. Diabet. Med. J. Br. Diabet. Assoc. ***22,*** *1124–1125 (2005).*
123. Beck-Sague, C. & Jarvis, W. R. Secular trends in the epidemiology of nosocomial fungal infections in the United States, 1980-1990. National Nosocomial Infections Surveillance System. J. Infect. Dis. ***167,*** *1247–1251 (1993).*
124. Kim, J. & Sudbery, P. Candida albicans, a major human fungal pathogen. J. Microbiol. Seoul Korea ***49,*** *171–177 (2011).*
125. Turner, S. A. & Butler, G. The Candida pathogenic species complex. Cold Spring Harb. Perspect. Med. ***4,*** *a019778 (2014).*
126. D'enfert, C. Hidden killers: persistence of opportunistic fungal pathogens in the human host. Curr. Opin. Microbiol. ***12,*** *358–364 (2009).*
127. Malani, A. et al. Candida glabrata fungemia: experience in a tertiary care center. Clin. Infect. Dis. Off. Publ. Infect. Dis. Soc. Am. ***41,*** *975–981 (2005).*
128. Nucci, M. & Marr, K. A. Emerging fungal diseases. Clin. Infect. Dis. Off. Publ. Infect. Dis. Soc. Am. ***41,*** *521–526 (2005).*
129. Maertens, J., Vrebos, M. & Boogaerts, M. Assessing risk factors for systemic fungal infections. Eur. J. Cancer Care (Engl.) ***10,*** *56–62 (2001).*
130. Pappas, P. G. Invasive candidiasis. Infect. Dis. Clin. North Am. ***20,*** *485–506 (2006).*
131. Sievert, D. M. et al. Antimicrobial-resistant pathogens associated with healthcare-associated infections: summary of data reported to the National Healthcare Safety Network at the Centers for Disease Control and Prevention, 2009-2010. Infect. Control Hosp. Epidemiol. ***34,*** *1–14 (2013).*
132. Wisplinghoff, H. et al. Nosocomial bloodstream infections in US hospitals: analysis of 24,179 cases from a prospective nationwide surveillance study. Clin. Infect. Dis. Off. Publ. Infect. Dis. Soc. Am. ***39,*** *309–317 (2004).*
133. Yapar, N. Epidemiology and risk factors for invasive candidiasis. Ther. Clin. Risk Manag. ***10,*** *95–105 (2014).*
134. Gudlaugsson, O. et al. Attributable mortality of nosocomial candidemia, revisited. Clin. Infect. Dis. Off. Publ. Infect. Dis. Soc. Am. ***37,*** *1172–1177 (2003).*
135. Dunyach-Remy, C., Ngba Essebe, C., Sotto, A. & Lavigne, J.-P. Staphylococcus aureus toxins and diabetic foot ulcers: role in pathogenesis and interest in diagnosis. Toxins ***8,*** *(2016).*

136. Stapleton, P. D. & Taylor, P. W. Methicillin resistance in Staphylococcus aureus: mechanisms and modulation. Sci. Prog. ***85,*** *57–72 (2002).*
137. Blair, E. B., Emerson, J. S. & Tull, A. H. A new medium, salt mannitol plasma agar, for the isolation of Staphylococcus aureus. Am. J. Clin. Pathol. ***47,*** *30–39 (1967).*
138. Miller, L. S. & Cho, J. S. Immunity against Staphylococcus aureus cutaneous infections. Nat. Rev. Immunol. ***11,*** *505–518 (2011).*
139. Krishna, S. & Miller, L. S. Host-pathogen interactions between the skin and Staphylococcus aureus. Curr. Opin. Microbiol. ***15,*** *28–35 (2012).*
140. McCaig, L. F., McDonald, L. C., Mandal, S. & Jernigan, D. B. Staphylococcus aureus-associated skin and soft tissue infections in ambulatory care. Emerg. Infect. Dis. ***12,*** *1715–1723 (2006).*
141. Rigby, K. M. & DeLeo, F. R. Neutrophils in innate host defense against Staphylococcus aureus infections. Semin. Immunopathol. ***34,*** *237–259 (2012).*
142. Thammavongsa, V., Kim, H. K., Missiakas, D. & Schneewind, O. Staphylococcal manipulation of host immune responses. Nat. Rev. Microbiol. ***13,*** *529–543 (2015).*
143. Patti, J. M., Allen, B. L., McGavin, M. J. & Hook, M. MSCRAMM-mediated adherence of microorganisms to host tissues. Annu. Rev. Microbiol. ***48,*** *585–617 (1994).*
144. Clarke, S. R. et al. Identification of in vivo-expressed antigens of Staphylococcus aureus and their use in vaccinations for protection against nasal carriage. J. Infect. Dis. ***193,*** *1098–1108 (2006).*
145. Weidenmaier, C. et al. Role of teichoic acids in Staphylococcus aureus nasal colonization, a major risk factor in nosocomial infections. Nat. Med. ***10,*** *243–245 (2004).*
146. Burian, M. et al. Temporal expression of adhesion factors and activity of global regulators during establishment of Staphylococcus aureus nasal colonization. J. Infect. Dis. ***201,*** *1414–1421 (2010).*
147. Cho, S. H., Strickland, I., Boguniewicz, M. & Leung, D. Y. Fibronectin and fibrinogen contribute to the enhanced binding of Staphylococcus aureus to atopic skin. J. Allergy Clin. Immunol. ***108,*** *269–274 (2001).*
148. Lijnen, H. R. et al. On the mechanism of fibrin-specific plasminogen activation by staphylokinase. J. Biol. Chem. ***266,*** *11826–11832 (1991).*
149. Barber, M. & Rozwadowska-Dowzenko, M. Infection by penicillin-resistant staphylococci. Lancet ***2,*** *641–644 (1948).*
150. Rammelkamp, C. & Maxon, T. Resistance of Staphylococcus aureus to the action of penicillin. Proc Soc Exp Biol Med ***51,*** *386–389 (1942).*
151. Dougherty, T. J. & Pucci, M. J. Antibiotic discovery and development. (Springer US, 2011).
152. Jevons, M. P., Coe, A. W. & Parker, M. T. Methicillin resistance in staphylococci. Lancet ***1,*** *904–907 (1963).*
153. Deurenberg, R. H. et al. The molecular evolution of methicillin-resistant Staphylococcus aureus. Clin. Microbiol. Infect. Off. Publ. Eur. Soc. Clin. Microbiol. Infect. Dis. ***13,*** *222–235 (2007).*
154. van Loo, I. et al. Emergence of methicillin-resistant Staphylococcus aureus of animal origin in humans. Emerg. Infect. Dis. ***13,*** *1834–1839 (2007).*
155. Kock, R. et al. Methicillin-resistant Staphylococcus aureus (MRSA): burden of disease and control challenges in Europe. Euro Surveill. Bull. Eur. Sur Mal. Transm. Eur. Commun. Dis. Bull. ***15,*** *19688 (2010).*
156. Deresinski, S. Methicillin-Resistant Staphylococcus aureus: an evolutionary, epidemiologic, and therapeutic odyssey. Clin. Infect. Dis. ***40,*** *562–573 (2005).*

157. van Hal, S. J. & Fowler, V. G. Is it time to replace vancomycin in the treatment of methicillin-resistant Staphylococcus aureus infections? Clin. Infect. Dis. Off. Publ. Infect. Dis. Soc. Am. ***56,*** *1779–1788 (2013).*
158. Moellering, R. C. The specter of glycopeptide resistance: current trends and future considerations. Am. J. Med. ***104,*** *3S–6S (1998).*
159. Sakoulas, G. & Moellering, R. C. Increasing antibiotic resistance among methicillin-resistant Staphylococcus aureus strains. Clin. Infect. Dis. Off. Publ. Infect. Dis. Soc. Am. ***46 Suppl 5,*** *S360-367 (2008).*
160. Shin, D.-Y. et al. Isolation of a potent anti-MRSA sesquiterpenoid quinone from Ulmus davidiana var. japonica. Chem. Pharm. Bull. (Tokyo) ***48,*** *1805–1806 (2000).*
161. Nascimento, J. S. et al. Bacteriocins as alternative agents for control of multiresistant staphylococcal strains. Lett. Appl. Microbiol. ***42,*** *215–221 (2006).*
162. Kokai-Kun, J. F., Walsh, S. M., Chanturiya, T. & Mond, J. J. Lysostaphin cream eradicates Staphylococcus aureus nasal colonization in a cotton rat model. Antimicrob. Agents Chemother. ***47,*** *1589–1597 (2003).*
163. Peschel, A. & Collins, L. V. Staphylococcal resistance to antimicrobial peptides of mammalian and bacterial origin. Peptides ***22,*** *1651–1659 (2001).*
164. Zanetti, M., Gennaro, R., Skerlavaj, B., Tomasinsig, L. & Circo, R. Cathelicidin peptides as candidates for a novel class of antimicrobials. Curr. Pharm. Des. ***8,*** *779–793 (2002).*
165. Sulakvelidze, A., Alavidze, Z. & Morris, J. G. J. Bacteriophage therapy. Antimicrob. Agents Chemother. ***45,*** *649–659 (2001).*
166. Jori, G. & Brown, S. B. Photosensitized inactivation of microorganisms. Photochem. Photobiol. Sci. Off. J. Eur. Photochem. Assoc. Eur. Soc. Photobiol. ***3,*** *403–405 (2004).*
167. Otto, M. Targeted immunotherapy for staphylococcal infections : focus on anti-MSCRAMM antibodies. BioDrugs Clin. Immunother. Biopharm. Gene Ther. ***22,*** *27–36 (2008).*
168. Hayes, C. S. & Williamson, H. J. Management of Group A beta-hemolytic streptococcal pharyngitis. Am. Fam. Physician ***63,*** *1557–1564 (2001).*
169. Patterson, M. J. Streptococcus. Medical Microbiology (ed. Baron, S.) (University of Texas Medical Branch at Galveston, 1996).
170. Pancholi, V. & Caparon, M. Streptococcus pyogenes metabolism. Streptococcus pyogenes : Basic Biology to Clinical Manifestations (eds. Ferretti, J. J., Stevens, D. L. & Fischetti, V. A.) (University of Oklahoma Health Sciences Center, 2016).
171. Lancefield, R. C. A serological differentiation of human and other groups of hemolytic Streptococci. J. Exp. Med. ***57,*** *571–595 (1933).*
172. Vallalta Morales, M. et al. Group A streptococcal bacteremia: outcome and prognostic factors. Rev. Espanola Quimioter. Publicacion Of. Soc. Espanola Quimioter. ***19,*** *367–375 (2006).*
173. Cunningham, M. W. Pathogenesis of Group A Streptococcal Infections. Clin. Microbiol. Rev. ***13,*** *470–511 (2000).*
174. Walker, M. J. et al. Disease manifestations and pathogenic mechanisms of group A Streptococcus. Clin. Microbiol. Rev. ***27,*** *264–301 (2014).*
175. Mitchell, T. J. The pathogenesis of streptococcal infections: from tooth decay to meningitis. Nat. Rev. Microbiol. ***1,*** *219–230 (2003).*
176. Kreikemeyer, B., McIver, K. S. & Podbielski, A. Virulence factor regulation and regulatory networks in Streptococcus pyogenes and their impact on pathogen-host interactions. Trends Microbiol. ***11,*** *224–232 (2003).*
177. Abachi, S., Lee, S. & Rupasinghe, H. P. V. Molecular mechanisms of inhibition of Streptococcus species by phytochemicals. Mol. Basel Switz. ***21,*** *(2016).*

178. Tarlow, M. J. Macrolides in the management of streptococcal pharyngitis/tonsillitis. Pediatr. Infect. Dis. J. ***16,*** *444–448 (1997).*
179. Stevens, D. L. et al. Practice guidelines for the diagnosis and management of skin and soft tissue infections: 2014 update by the Infectious Diseases Society of America. Clin. Infect. Dis. Off. Publ. Infect. Dis. Soc. Am. ***59,*** *e10-52 (2014).*
180. Cormican, M. G. & Jones, R. N. Emerging resistance to antimicrobial agents in Gram-Positive Bacteria. Drugs ***51,*** *6–12 (1996).*
181. Ayer, V. et al. Tetracycline resistance in group A Streptococci: emergence on a global scale and influence on multiple-drug resistance. Antimicrob. Agents Chemother. ***51,*** *1865–1868 (2007).*
182. Cattoir, V. Mechanisms of antibiotic resistance. (2016).
183. Malbruny, B. et al. Resistance to macrolides in clinical isolates of Streptococcus pyogenes due to ribosomal mutations. J. Antimicrob. Chemother. ***49,*** *935–939 (2002).*
184. Varaldo, P. E., Montanari, M. P. & Giovanetti, E. Genetic elements responsible for erythromycin resistance in Streptococci. Antimicrob. Agents Chemother. ***53,*** *343–353 (2009).*
185. Montagnani, F. et al. Erythromycin resistance in Streptococcus pyogenes and macrolide consumption in a central Italian region. Infection ***37,*** *353–7 (2009).*
186. Neville, B. A., d'Enfert, C. & Bougnoux, M.-E. Candida albicans commensalism in the gastrointestinal tract. FEMS Yeast Res. ***15,*** *(2015).*
187. Schulze, J. & Sonnenborn, U. Yeasts in the gut: from commensals to infectious agents. Dtsch. Arzteblatt Int. ***106,*** *837–842 (2009).*
188. Montagna, M. T. et al. Epidemiology of invasive fungal infections in the intensive care unit: results of a multicenter Italian survey (AURORA Project). Infection ***41,*** *645–653 (2013).*
189. Tortorano, A. M. et al. A 1-year prospective survey of candidemia in Italy and changing epidemiology over one decade. Infection ***41,*** *655–662 (2013).*
190. Richardson, M. & Lass-Florl, C. Changing epidemiology of systemic fungal infections. Clin. Microbiol. Infect. Off. Publ. Eur. Soc. Clin. Microbiol. Infect. Dis. ***14 Suppl 4,*** *5–24 (2008).*
191. Samaranayake, D. P. & Hanes, S. D. Milestones in Candida albicans gene manipulation. Fungal Genet. Biol. FG B ***48,*** *858–865 (2011).*
192. Duhring, S. et al. Host-pathogen interactions between the human innate immune system and Candida albicans-understanding and modeling defense and evasion strategies. Front. Microbiol. ***6,*** *625 (2015).*
193. Kabir, M. A., Hussain, M. A. & Ahmad, Z. Candida albicans: a model organism for studying fungal pathogens. ISRN Microbiol. ***2012,*** *15 (2012).*
194. Thompson, D. S., Carlisle, P. L. & Kadosh, D. Coevolution of morphology and virulence in Candida species. Eukaryot. Cell ***10,*** *1173–1182 (2011).*
195. Morschhauser, J. Regulation of white-opaque switching in Candida albicans. Med. Microbiol. Immunol. (Berl.) ***199,*** *165–172 (2010).*
196. Huang, G. Regulation of phenotypic transitions in the fungal pathogen Candida albicans. Virulence ***3,*** *251–261 (2012).*
197. Liu, H. Transcriptional control of dimorphism in Candida albicans. Curr. Opin. Microbiol. ***4,*** *728–735 (2001).*
198. Jacobsen, I. D. et al. Candida albicans dimorphism as a therapeutic target. Expert Rev. Anti Infect. Ther. ***10,*** *85–93 (2012).*
199. Liu, Y. & Filler, S. G. Candida albicans Als3, a multifunctional adhesin and invasin. Eukaryot. Cell ***10,*** *168–173 (2011).*
200. Phan, Q. T. et al. Als3 is a Candida albicans invasin that binds to cadherins and induces endocytosis by host cells. PLoS Biol. ***5,*** *e64 (2007).*

201. Moreno-Ruiz, E. et al. Candida albicans internalization by host cells is mediated by a clathrin-dependent mechanism. Cell. Microbiol. ***11,*** *1179–1189 (2009).*
202. Wachtler, B. et al. Candida albicans-epithelial interactions: dissecting the roles of active penetration, induced endocytosis and host factors on the infection process. PloS One ***7,*** *e36952 (2012).*
203. Zhu, W. et al. EGFR and HER2 receptor kinase signaling mediate epithelial cell invasion by Candida albicans during oropharyngeal infection. Proc. Natl. Acad. Sci. U. S. A. ***109,*** *14194–14199 (2012).*
204. Jackson, A. P. et al. Comparative genomics of the fungal pathogens Candida dubliniensis and Candida albicans. Genome Res. ***19,*** *2231–2244 (2009).*
205. Cowen, L. E. et al. Evolution of drug resistance in experimental populations of Candida albicans. J. Bacteriol. ***182,*** *1515–1522 (2000).*
206. Selmecki, A. M., Dulmage, K., Cowen, L. E., Anderson, J. B. & Berman, J. Acquisition of aneuploidy provides increased fitness during the evolution of antifungal drug resistance. PLoS Genet. ***5,*** *e1000705 (2009).*
207. Berman, J. & Hadany, L. Does stress induce (para)sex? Implications for Candida albicans evolution. Trends Genet. TIG ***28,*** *197–203 (2012).*
208. Forche, A. et al. The parasexual cycle in Candida albicans provides an alternative pathway to meiosis for the formation of recombinant strains. PLoS Biol. ***6,*** *e110 (2008).*
209. Perepnikhatka, V. et al. Specific chromosome alterations in fluconazole-resistant mutants of Candida albicans. J. Bacteriol. ***181,*** *4041–4049 (1999).*
210. Hill, J. A., Ammar, R., Torti, D., Nislow, C. & Cowen, L. E. Genetic and genomic architecture of the evolution of resistance to antifungal drug combinations. PLoS Genet. ***9,*** *e1003390 (2013).*
211. Cannon, R. D. et al. Efflux-mediated antifungal drug resistance. Clin. Microbiol. Rev. ***22,*** *291–321, Table of Contents (2009).*
212. Vandeputte, P., Ferrari, S. & Coste, A. T. Antifungal resistance and new strategies to control fungal infections. Int. J. Microbiol. ***2012,*** *713687 (2012).*
213. Saravolatz, L. D., Ostrosky-Zeichner, L., Marr, K. A., Rex, J. H. & Cohen, S. H. Amphotericin B: time for a new 'gold standard'. Clin. Infect. Dis. ***37,*** *415–425 (2003).*
214. Hughes, C. E. & Beggs, W. H. Action of fluconazole (UK-49,858) in relation to other systemic antifungal azoles. J. Antimicrob. Chemother. ***19,*** *171–174 (1987).*
215. Sohnle, P. G., Hahn, B. L. & Erdmann, M. D. Effect of fluconazole on viability of Candida albicans over extended periods of time. Antimicrob. Agents Chemother. ***40,*** *2622–2625 (1996).*
216. Hitchcock, C. A., Dickinson, K., Brown, S. B., Evans, E. G. V. & Adams, D. J. Interaction of azole antifungal antibiotics with cytochrome P-450-dependent 14α-sterol demethylase purified from Candida albicans. Biochem. J. ***266,*** *475 (1990).*
217. Ghannoum, M. A. & Rice, L. B. Antifungal agents: mode of action, mechanisms of resistance, and correlation of these mechanisms with bacterial resistance. Clin. Microbiol. Rev. ***12,*** *501–517 (1999).*
218. Vanden Bossche, H. et al. Cytochrome P-450: target for itraconazole. Drug Dev. Res. ***8,*** *287–298 (1986).*
219. Saag, M. S. & Dismukes, W. E. Azole antifungal agents: emphasis on new triazoles. Antimicrob. Agents Chemother. ***32,*** *1–8 (1988).*
220. Stricker, B. H. C., Blok, A. P. R., Bronkhorst, F. B., Van Parys, G. E. & Desmet, V. J. Ketoconazole-associated hepatic injury. J. Hepatol. ***3,*** *399–406*
221. Yu, D. T., Peterson, J. F., Seger, D. L., Gerth, W. C. & Bates, D. W. Frequency of potential azole drug–drug interactions and consequences of potential fluconazole drug interactions. Pharmacoepidemiol. Drug Saf. ***14,*** *755–767 (2005).*
222. Chen, S. C. & Sorrell, T. C. Antifungal agents. Med. J. Aust. ***187,*** *404 (2007).*

223. Janknegt, R., de Marie, S., Bakker-Woudenberg, I. A. & Crommelin, D. J. Liposomal and lipid formulations of amphotericin B. Clinical pharmacokinetics. Clin. Pharmacokinet. ***23,*** *279–291 (1992).*
224. Chapman, S. W., Sullivan, D. C. & Cleary, J. D. In search of the holy grail of antifungal therapy. Trans. Am. Clin. Climatol. Assoc. ***119,*** *197-215; discussion 215-216 (2008).*
225. Perlin, D. S. Current perspectives on echinocandin class drugs. Future Microbiol. ***6,*** *441–457 (2011).*
226. Denning, D. W. Echinocandin antifungal drugs. Lancet Lond. Engl. ***362,*** *1142–1151 (2003).*
227. Kurtz, M. B. & Douglas, C. M. Lipopeptide inhibitors of fungal glucan synthase. J. Med. Vet. Mycol. Bi-Mon. Publ. Int. Soc. Hum. Anim. Mycol. ***35,*** *79–86 (1997).*
228. Sanglard, D. Emerging threats in antifungal-resistant fungal pathogens. Front. Med. ***3,*** *11 (2016).*
229. Nadig, S. et al. A relationship between salivary flow rates and Candida counts in patients with xerostomia. J. Oral Maxillofac. Pathol. ***21,*** *316–316 (2017).*
230. Anderson, H. W. Yeast-like fungi of the human intestinal tract. J. Infect. Dis. 341–386 (1917).
231. Fidel, P. L. J., Vazquez, J. A. & Sobel, J. D. Candida glabrata: review of epidemiology, pathogenesis, and clinical disease with comparison to C. albicans. Clin. Microbiol. Rev. ***12,*** *80–96 (1999).*
232. Just, G. et al. Change of causative organisms under antifungal treatment in immunosuppressed patients with HIV-infections. Mycoses ***32 Suppl 2,*** *47–51 (1989).*
233. Hazen, K. C. New and emerging yeast pathogens. Clin. Microbiol. Rev. ***8,*** *462–478 (1995).*
234. Arendrup, M. C. et al. Semi-national surveillance of fungaemia in Denmark 2004-2006: increasing incidence of fungaemia and numbers of isolates with reduced azole susceptibility. Clin. Microbiol. Infect. Off. Publ. Eur. Soc. Clin. Microbiol. Infect. Dis. ***14,*** *487–494 (2008).*
235. Horn, D. L. et al. Epidemiology and outcomes of candidemia in 2019 patients: data from the prospective antifungal therapy alliance registry. Clin. Infect. Dis. Off. Publ. Infect. Dis. Soc. Am. ***48,*** *1695–1703 (2009).*
236. Perlroth, J., Choi, B. & Spellberg, B. Nosocomial fungal infections: epidemiology, diagnosis, and treatment. Med. Mycol. ***45,*** *321–346 (2007).*
237. Dujon, B. et al. Genome evolution in yeasts. Nature ***430,*** *35–44 (2004).*
238. Wong, S., Fares, M. A., Zimmermann, W., Butler, G. & Wolfe, K. H. Evidence from comparative genomics for a complete sexual cycle in the 'asexual' pathogenic yeast Candida glabrata. Genome Biol. ***4,*** *R10–R10 (2003).*
239. Magee, P. & Chibana, H. The genomes of Candida albicans and other Candida species. Candida Candidiasis (2002).
240. Kaur, R., Domergue, R., Zupancic, M. L. & Cormack, B. P. A yeast by any other name: Candida glabrata and its interaction with the host. Curr. Opin. Microbiol. ***8,*** *378–384 (2005).*
241. Sudbery, P. E. Growth of Candida albicans hyphae. Nat. Rev. Microbiol. ***9,*** *737–748 (2011).*
242. Ahmad, K. M. et al. Genome structure and dynamics of the yeast pathogen Candida glabrata. FEMS Yeast Res. ***14,*** *529–535 (2014).*
243. Kurtzman, C. P. Phylogenetic circumscription of Saccharomyces, Kluyveromyces and other members of the Saccharomycetaceae, and the proposal of the new genera Lachancea, Nakaseomyces, Naumovia, Vanderwaltozyma and Zygotorulaspora. FEMS Yeast Res. ***4,*** *233–245 (2003).*

244. Kaur, R., Ma, B. & Cormack, B. P. A family of glycosylphosphatidylinositol-linked aspartyl proteases is required for virulence of Candida glabrata. Proc. Natl. Acad. Sci. U. S. A. ***104,*** *7628–7633 (2007).*
245. Rai, M. N., Balusu, S., Gorityala, N., Dandu, L. & Kaur, R. Functional genomic analysis of Candida glabrata-macrophage interaction: role of chromatin remodeling in virulence. PLoS Pathog. ***8,*** *e1002863 (2012).*
246. Roetzer, A., Gratz, N., Kovarik, P. & Schuller, C. Autophagy supports Candida glabrata survival during phagocytosis. Cell. Microbiol. ***12,*** *199–216 (2010).*
247. Seider, K. et al. The facultative intracellular pathogen Candida glabrata subverts macrophage cytokine production and phagolysosome maturation. J. Immunol. Baltim. Md 1950 ***187,*** *3072–3086 (2011).*
248. Lee, I. et al. Risk factors for fluconazole-resistant Candida glabrata bloodstream infections. Arch. Intern. Med. ***169,*** *379–383 (2009).*
249. Abi-Said, D. et al. The epidemiology of hematogenous candidiasis caused by different Candida species. Clin. Infect. Dis. Off. Publ. Infect. Dis. Soc. Am. ***24,*** *1122–1128 (1997).*
250. Lee, I. et al. Clinical and economic outcomes of decreased fluconazole susceptibility in patients with Candida glabrata bloodstream infections. Am. J. Infect. Control ***38,*** *740–745 (2010).*
251. Castilla, D. M., Liu, Z.-J. & Velazquez, O. C. Oxygen: implications for wound healing. Adv. Wound Care ***1,*** *225–230 (2012).*
252. Sen, C. K. Wound healing essentials: let there be oxygen. Wound Repair Regen. Off. Publ. Wound Heal. Soc. Eur. Tissue Repair Soc. ***17,*** *1–18 (2009).*
253. Allen, D. B. et al. Wound hypoxia and acidosis limit neutrophil bacterial killing mechanisms. Arch. Surg. Chic. Ill 1960 ***132,*** *991–996 (1997).*
254. Broussard, C. L. Hyperbaric oxygenation and wound healing. J. Wound Ostomy Cont. Nurs. Off. Publ. Wound Ostomy Cont. Nurses Soc. ***30,*** *210–216 (2003).*
255. Rodriguez, P. G., Felix, F. N., Woodley, D. T. & Shim, E. K. The role of oxygen in wound healing: a review of the literature. Dermatol. Surg. Off. Publ. Am. Soc. Dermatol. Surg. Al ***34,*** *1159–1169 (2008).*
256. Castro, C. I. & Briceno, J. C. Perfluorocarbon-based oxygen carriers: review of products and trials. Artif. Organs ***34,*** *622–634 (2010).*
257. Kairuz, E., Upton, Z., Dawson, R. A. & Malda, J. Hyperbaric oxygen stimulates epidermal reconstruction in human skin equivalents. Wound Repair Regen. Off. Publ. Wound Heal. Soc. Eur. Tissue Repair Soc. ***15,*** *266–274 (2007).*
258. Dimitrijevich, S. D., Paranjape, S., Wilson, J. R., Gracy, R. W. & Mills, J. G. Effect of hyperbaric oxygen on human skin cells in culture and in human dermal and skin equivalents. Wound Repair Regen. Off. Publ. Wound Heal. Soc. Eur. Tissue Repair Soc. ***7,*** *53–64 (1999).*
259. Williams, R. L. Hyperbaric oxygen therapy and the diabetic foot. J. Am. Podiatr. Med. Assoc. ***87,*** *279–292 (1997).*
260. Kalliainen, L. K., Gordillo, G. M., Schlanger, R. & Sen, C. K. Topical oxygen as an adjunct to wound healing: a clinical case series. Pathophysiol. Off. J. Int. Soc. Pathophysiol. ***9,*** *81–87 (2003).*
261. Wu, S. C., Marston, W. & Armstrong, D. G. Wound care: the role of advanced wound-healing technologies. J. Am. Podiatr. Med. Assoc. ***100,*** *385–394 (2010).*
262. Hampson, N. & Atik, D. Central nervous system oxygen toxicity during routine hyperbaric oxygen therapy. Undersea Hyperb. Med. J. Undersea Hyperb. Med. Soc. Inc ***30,*** *147–153 (2003).*
263. Cavalli, R. et al. Preparation and characterization of dextran nanobubbles for oxygen delivery. Int. J. Pharm. ***381,*** *160–165 (2009).*
264. Cavalli, R. et al. Ultrasound-mediated oxygen delivery from chitosan nanobubbles. Int. J. Pharm. ***378,*** *215–217 (2009).*

265. Kent, K. M. et al. Reduction of myocardial ischemia during percutaneous transluminal coronary angioplasty with oxygenated Fluosol®1. Am. J. Cardiol. ***66,*** *279–284*
266. Percival, S. L., Hill, K. E., Malic, S., Thomas, D. W. & Williams, D. W. Antimicrobial tolerance and the significance of persister cells in recalcitrant chronic wound biofilms. Wound Repair Regen. Off. Publ. Wound Heal. Soc. Eur. Tissue Repair Soc. ***19,*** *1–9 (2011).*
267. Naik, A., Kalia, Y. N., & Guy, R. H. Transdermal drug delivery: overcoming the skin's barrier function. Pharm. Sci. Technol. Today ***3,*** *318–326 (2000).*
268. Ventola, C. L. The antibiotic resistance crisis: part 1: causes and threats. Pharm. Ther. ***40,*** *277–283 (2015).*
269. Bush, K. et al. Tackling antibiotic resistance. Nat. Rev. Microbiol. ***9,*** *894–896 (2011).*
270. Chopra, I. The 2012 Garrod lecture: discovery of antibacterial drugs in the 21st century. J. Antimicrob. Chemother. ***68,*** *496–505 (2013).*
271. Roberts, R. R. et al. Hospital and societal costs of antimicrobial-resistant infections in a Chicago teaching hospital: implications for antibiotic stewardship. Clin. Infect. Dis. Off. Publ. Infect. Dis. Soc. Am. ***49,*** *1175–1184 (2009).*
272. Levison, M. E. & Levison, J. H. Pharmacokinetics and pharmacodynamics of antibacterial agents. Infect. Dis. Clin. North Am. ***23,*** *791–vii (2009).*
273. Savjani, K. T., Gajjar, A. K. & Savjani, J. K. Drug Solubility: Importance and Enhancement Techniques. ISRN Pharm. ***2012,*** *195727 (2012).*
274. Jin, J., Sklar, G. E., Min Sen Oh, V. & Chuen Li, S. Factors affecting therapeutic compliance: A review from the patient's perspective. Ther. Clin. Risk Manag. ***4,*** *269–286 (2008).*
275. Dusing, R., Weisser, B., Mengden, T. & Vetter, H. Changes in antihypertensive therapy--the role of adverse effects and compliance. Blood Press. ***7,*** *313–315 (1998).*
276. Cramer JA, Mattson RH, Prevey ML, Scheyer RD & Ouellette VL. How often is medication taken as prescribed? A novel assessment technique. JAMA ***261,*** *3273–3277 (1989).*
277. Seil, J. T. & Webster, T. J. Antimicrobial applications of nanotechnology: methods and literature. Int. J. Nanomedicine ***7,*** *2767–2781 (2012).*
278. Nath, D. & Banerjee, P. Green nanotechnology - a new hope for medical biology. Environ. Toxicol. Pharmacol. ***36,*** *997–1014 (2013).*
279. Li, D., Diao, J., Zhang, J. & Liu, J. Fabrication of new chitosan-based composite sponge containing silver nanoparticles and its antibacterial properties for wound dressing. J. Nanosci. Nanotechnol. ***11,*** *4733–4738 (2011).*
280. Gao, P., Nie, X., Zou, M., Shi, Y. & Cheng, G. Recent advances in materials for extended-release antibiotic delivery system. J. Antibiot. (Tokyo) ***64,*** *625–634 (2011).*
281. Chen, L., Liu, X. & Wong, K.-H. Novel nanoparticle materials for drug/food delivery-polysaccharides. ***2016,*** *(2016).*
282. Kim, K. et al. Physicochemical characterizations of self-assembled nanoparticles of glycol chitosan-deoxycholic acid conjugates. Biomacromolecules ***6,*** *1154–1158 (2005).*
283. Park, J. H., Saravanakumar, G., Kim, K. & Kwon, I. C. Targeted delivery of low molecular drugs using chitosan and its derivatives. Adv. Drug Deliv. Rev. ***62,*** *28–41 (2010).*
284. Blecher, K., Nasir, A. & Friedman, A. The growing role of nanotechnology in combating infectious disease. Virulence ***2,*** *395–401 (2011).*
285. Kohanski, M. A., Dwyer, D. J. & Collins, J. J. How antibiotics kill bacteria: from targets to networks. Nat. Rev. Microbiol. ***8,*** *423–435 (2010).*

286. Piras, A. M. et al. Chitosan nanoparticles loaded with the antimicrobial peptide temporin B exert a long-term antibacterial activity in vitro against clinical isolates of Staphylococcus epidermidis. Front. Microbiol. ***6,*** *372 (2015).*
287. Trotta, F., Dianzani, C., Caldera, F., Mognetti, B. & Cavalli, R. The application of nanosponges to cancer drug delivery. Expert Opin. Drug Deliv. ***11,*** *931–941 (2014).*
288. Duchene, D., Cavalli, R. & Gref, R. Cyclodextrin-based Polymeric Nanoparticles as Efficient Carriers for Anticancer Drugs. Curr. Pharm. Biotechnol. ***17,*** *248–255 (2016).*
289. Cavalli, R., Bisazza, A. & Lembo, D. Micro- and nanobubbles: a versatile non-viral platform for gene delivery. Int. J. Pharm. ***456,*** *437–445 (2013).*
290. Cavalli, R. et al. New chitosan nanobubbles for ultrasound-mediated gene delivery: preparation and in vitro characterization. Int. J. Nanomedicine ***7,*** *3309–3318 (2012).*
291. Fattal, E. & Bochot, A. Ocular delivery of nucleic acids: antisense oligonucleotides, aptamers and siRNA. Adv. Drug Deliv. Rev. ***58,*** *1203–1223 (2006).*
292. Farjo, R., Skaggs, J., Quiambao, A. B., Cooper, M. J. & Naash, M. I. Efficient non-viral ocular gene transfer with compacted DNA nanoparticles. PloS One ***1,*** *e38 (2006).*
293. Hassan, S. et al. Evolution and clinical translation of drug delivery Nanomaterials. Nano Today ***15,*** *91–106 (2017).*
294. Dutta, P. K., Dutta, J. & Tripathi, V. S. Chitin and chitosan: chemistry, properties and applications. (2004).
295. Domard, A. & Domard, M. Chitosan: structure-properties relationship and biomedical applications. Polym. Biomater. ***2,*** *187–212 (2001).*
296. Rinaudo, M. Chitin and chitosan: properties and applications. Prog. Polym. Sci. ***31,*** *603–632 (2006).*
297. Qinna, N. A. et al. Influence of molecular weight and degree of deacetylation of low molecular weight chitosan on the bioactivity of oral insulin preparations. Mar. Drugs ***13,*** *1710–1725 (2015).*
298. Park, B. K. & Kim, M.-M. Applications of chitin and its derivatives in biological medicine. Int. J. Mol. Sci. ***11,*** *5152–5164 (2010).*
299. Periayah, M. H., Halim, A. S. & Saad, A. Z. M. Chitosan: a promising marine polysaccharide for biomedical research. Pharmacogn. Rev. ***10,*** *39–42 (2016).*
300. Kim, S. J., Kim, S. S. & Lee, Y. M. Synthesis and characterization of ether-type chitin derivatives. Macromol. Chem. Phys. ***195,*** *1687–1693 (1994).*
301. Zhang, J. et al. Chitosan modification and pharmaceutical/biomedical applications. Mar. Drugs ***8,*** *1962–1987 (2010).*
302. Key, J. et al. Multicomponent, peptide-targeted glycol chitosan nanoparticles containing ferrimagnetic iron oxide nanocubes for bladder cancer multimodal imaging. Int. J. Nanomedicine ***11,*** *4141–4155 (2016).*
303. Dumont, V. C. et al. Glycol chitosan/nanohydroxyapatite biocomposites for potential bone tissue engineering and regenerative medicine. Int. J. Biol. Macromol. ***93,*** *1465–1478 (2016).*
304. Kingkaew, J., Jatupaiboon, N., Sanchavanakit, N., Pavasant, P. & Phisalaphong, M. Biocompatibility and growth of human keratinocytes and fibroblasts on biosynthesized cellulose-chitosan film. J. Biomater. Sci. Polym. Ed. ***21,*** *1009–1021 (2010).*
305. Howling, G. I. et al. The effect of chitin and chitosan on fibroblast-populated collagen lattice contraction. Biotechnol. Appl. Biochem. ***36,*** *247–253 (2002).*
306. Dai, T., Tanaka, M., Huang, Y.-Y. & Hamblin, M. R. Chitosan preparations for wounds and burns: antimicrobial and wound-healing effects. Expert Rev. Anti Infect. Ther. ***9,*** *857–879 (2011).*

*307. Pangburn, S. H., Trescony, P. V. & Heller, J. Lysozyme degradation of partially deacetylated chitin, its films and hydrogels. Biomaterials **3,** 105–108 (1982).*
*308. Li, X. et al. Chitin, chitosan, and glycated chitosan regulate immune responses: the novel adjuvants for cancer vaccine. Clin. Dev. Immunol. **2013,** 387023 (2013).*
*309. Raafat, D., Sahl, H.-G. Chitosan and its antimicrobial potential – a critical literature survey. Microb. Biotechnol. **2,** 186–201 (2009).*
*310. Kato, Y., Onishi, H., Machida, Y. Contribution of chitosan and its derivatives to cancer chemotherapy. In Vivo **19,** 301–310 (2005).*
*311. Schlievert, P. M. Chitosan Malate Inhibits Growth and Exotoxin Production of Toxic Shock Syndrome-Inducing Staphylococcus aureus Strains and Group A Streptococci. Antimicrob. Agents Chemother. **51,** 3056–3062 (2007).*
*312. Kulikov, S. N. et al. Antifungal activity of oligochitosans (short chain chitosans) against some Candida species and clinical isolates of Candida albicans: molecular weight-activity relationship. Eur. J. Med. Chem. **74,** 169–178 (2014).*
*313. Jayakumar, R., Menon, D., Manzoor, K., Nair, S. V. & Tamura, H. Biomedical applications of chitin and chitosan based nanomaterials-a short review. Carbohydr. Polym. **82,** 227–232 (2010).*
*314. Chen, F.-M. & Liu, X. Advancing biomaterials of human origin for tissue engineering. Prog. Polym. Sci. **53,** 86–168 (2016).*
*315. Lauto, A. Integration of extracellular matrix with chitosan adhesive film for sutureless tissue fixation. Lasers Surg. Med. **41,** 366–371 (2009).*
316. Takei, T. et al. Autoclavable physically-crosslinked chitosan cryogel as a wound dressing. J. Biosci. Bioeng. (2017). doi:10.1016/j.jbiosc.2017.10.015
*317. Comblain, F., Rocasalbas, G., Gauthier, S. & Henrotin, Y. Chitosan: a promising polymer for cartilage repair and viscosupplementation. Biomed. Mater. Eng. **28,** S209–S215 (2017).*
*318. Hirano, S., Tobetto, K. & Noishiki, Y. SEM ultrastructure studies of N-acyl- and N-benzylidene-chitosan and chitosan membranes. J. Biomed. Mater. Res. **15,** 903–911 (1981).*
*319. Jiang, H. et al. Optical waveguiding and morphology of chitosan thin films. J. Appl. Polym. Sci. **61,** 1163–1171 (1996).*
*320. de Campos, A. M., Diebold, Y., Carvalho, E. L. S., Sanchez, A. & Alonso, M. J. Chitosan nanoparticles as new ocular drug delivery systems: in vitro stability, in vivo fate, and cellular toxicity. Pharm. Res. **21,** 803–810 (2004).*
*321. De Campos, A. M., Sanchez, A., Gref, R., Calvo, P. & Alonso, M. J. The effect of a PEG versus a chitosan coating on the interaction of drug colloidal carriers with the ocular mucosa. Eur. J. Pharm. Sci. Off. J. Eur. Fed. Pharm. Sci. **20,** 73–81 (2003).*
*322. Spinner, J. L. et al. Methylglycol chitosan and a synthetic TLR4 agonist enhance immune responses to influenza vaccine administered sublingually. Vaccine **33,** 5845–5853 (2015).*
*323. Sanfeld, A., Sefiane, K., Benielli, D. & Steinchen, A. Does capillarity influence chemical reaction in drops and bubbles? A thermodynamic approach. Adv. Colloid Interface Sci. **86,** 153–193 (2000).*
*324. Cavalli, R., Soster, M. & Argenziano, M. Nanobubbles: a promising efficient tool for therapeutic delivery. Ther. Deliv. **7,** 117–138 (2016).*
*325. Bisazza, A. et al. Microbubble-mediated oxygen delivery to hypoxic tissues as a new therapeutic device. 30th Annu. Int. IEEE EMBS Conf. **2008,** 2067–2070 (2008).*
*326. Prato, M. et al. 2H,3H-decafluoropentane-based nanodroplets: new perspectives for oxygen delivery to hypoxic cutaneous tissues. PloS One **10,** e0119769 (2015).*
*327. Argenziano, M. et al. Vancomycin-loaded nanobubbles: a new platform for controlled antibiotic delivery against methicillin-resistant Staphylococcus aureus infections. Int. J. Pharm. **523,** 176–188 (2017).*

*328. Faithfull, N. S. Fluorocarbons. Current status and future applications. Anaesthesia **42,** 234–242 (1987).*
*329. Sargent, J. W. & Seffl, R. J. Properties of perfluorinated liquids. Fed. Proc. **29,** 1699–1703 (1970).*
*330. Yokoyama, K., Yamanouchi, K., Murashima, R. Excretion of perfluorochemicals after intravenous injection of their emulsion. Chem. Pharm. Bull. (Tokyo) **23,** 1368–1373 (1975).*
*331. Tsai, W.-T. Environmental hazards and health risk of common liquid perfluoro-n-alkanes, potent greenhouse gases. Environ. Int. **35,** 418–424 (2009).*
*332. Moller, S., Weisser, J., Bischoff, S. & Schnabelrauch, M. Dextran and hyaluronan methacrylate based hydrogels as matrices for soft tissue reconstruction. Biomol. Eng. **24,** 496–504 (2007).*
*333. Guiot, C. et al. Thermal response of contrast agent microbubbles: preliminary results from physico-chemical and US-imaging characterization. Ultrasonics **44 Suppl 1,** e127-130 (2006).*
*334. Salari, A. et al. Shrinking microbubbles with microfluidics: mathematical modelling to control microbubble sizes. Soft Matter **13,** 8796–8806 (2017).*
*335. Blau, R., Krivitsky, A., Epshtein, Y., Satchi-Fainaro, R. Are nanotheranostics and nanodiagnostics-guided drug delivery stepping stones towards precision medicine? Drug Resist. Updat. **27,** 39–58 (2016).*
*336. Magnetto, C. et al. Ultrasound-activated decafluoropentane-cored and chitosan-shelled nanodroplets for oxygen delivery to hypoxic cutaneous tissues. RSC Adv. **4,** 38433–38441 (2014).*
*337. Cote, M., Rogueda, P. G. A. & Griffiths, P. C. Effect of molecular weight and end-group nature on the solubility of ethylene oxide oligomers in 2H, 3H-decafluoropentane and its fully fluorinated analogue, perfluoropentane. J. Pharm. Pharmacol. **60,** 593–599 (2008).*
*338. Ridder, K. B., Davies-Cutting, C. J. & Kellaway, I. W. Surfactant solubility and aggregate orientation in hydrofluoroalkanes. Int. J. Pharm. **295,** 57–65 (2005).*
*339. Riess, J. G. & Krafft, M. P. Fluorinated materials for in vivo oxygen transport (blood substitutes), diagnosis and drug delivery. Biomaterials **19,** 1529–1539 (1998).*
*340. Ita, K. Recent progress in transdermal sonophoresis. Pharm. Dev. Technol. **22,** 458–466 (2017).*
*341. Sivakumar, M. et al. Transdermal drug delivery using ultrasound-theory, understanding and critical analysis. Cell Mol Biol **51,** OL767-OL784 (2005).*
*342. Capece, S. et al. Complex interfaces in 'phase-change' contrast agents. Phys. Chem. Chem. Phys. PCCP **18,** 8378–8388 (2016).*
*343. Banche, G. et al. Antimicrobial chitosan nanodroplets: new insights for ultrasound-mediated adjuvant treatment of skin infection. Future Microbiol. **10,** 929–939 (2015).*
*344. Khadjavi, A. et al. Chitosan-shelled oxygen-loaded nanodroplets abrogate hypoxia dysregulation of human keratinocyte gelatinases and inhibitors: New insights for chronic wound healing. Toxicol. Appl. Pharmacol. **286,** 198–206 (2015).*
*345. Basilico, N. et al. Dextran-shelled oxygen-loaded nanodroplets reestablish a normoxia-like pro-angiogenic phenotype and behavior in hypoxic human dermal microvascular endothelium. Toxicol. Appl. Pharmacol. **288,** 330–338 (2015).*
*346. Gulino, G. R. et al. Oxygen-loaded nanodroplets effectively abrogate hypoxia dysregulating effects on secretion of MMP-9 and TIMP-1 by human monocytes. Mediators Inflamm. **2015,** 964838 (2015).*
*347. Prato, M. et al. Effects of oxygen tension and dextran-shelled/2H,3H-decafluoropentane-cored oxygen-loaded nanodroplets on secretion of gelatinases and their inhibitors in term human placenta. Biosci. Biotechnol. Biochem. **80,** 466–472 (2016).*

348. Sze, A., Erickson, D., Ren, L. & Li, D. Zeta-potential measurement using the Smoluchowski equation and the slope of the current-time relationship in electroosmotic flow. J. Colloid Interface Sci. ***261,*** *402–410 (2003).*
349. Boukamp, P. et al. Normal keratinization in a spontaneously immortalized aneuploid human keratinocyte cell line. J. Cell Biol. ***106,*** *761–771 (1988).*
350. Almqvist, S. et al. Evaluation of a near-senescent human dermal fibroblast cell line and effect of amelogenin. Br. J. Dermatol. ***160,*** *1163–1171 (2009).*
351. Ades, E. W. et al. HMEC-1: establishment of an immortalized human microvascular endothelial cell line. J. Invest. Dermatol. ***99,*** *683–690 (1992).*
352. Cumming, G., Fidler, F. & Vaux, D. L. Error bars in experimental biology. J. Cell Biol. ***177,*** *7–11 (2007).*
353. Cavalli, R., Guiot, C., Prato, M. & Troia, A. A nanostructure for the vehiculation of gas and/or active ingredients and/or contrast agents and uses thereof. Patent number: WO2015/028901 A1 (2015).
354. Kong, M., Chen, X. G., Xing, K. & Park, H. J. Antimicrobial properties of chitosan and mode of action: a state of the art review. Int. J. Food Microbiol. ***144,*** *51–63 (2010).*
355. Argenziano, M. et al. Comparative evaluation of different chitosan species and derivatives as candidate biomaterials for oxygen-loaded nanodroplet formulations to treat chronic wounds. 10th International Conference on Advanced Nano Materials (ANM2017) University of Surrey, Guildford, UK, 11-13/09/2017. Abstract book, page 376. (2017).
356. Wu, X., Landfester, K., Musyanovych, A. & Guy, R. H. Disposition of charged nanoparticles after their topical application to the skin. Skin Pharmacol. Physiol. ***23,*** *117–123 (2010).*
357. Seyfarth, F., Schliemann, S., Elsner, P. & Hipler, U.-C. Antifungal effect of high- and low-molecular-weight chitosan hydrochloride, carboxymethyl chitosan, chitosan oligosaccharide and N-acetyl-D-glucosamine against Candida albicans, Candida krusei and Candida glabrata. Int. J. Pharm. ***353,*** *139–148 (2008).*
358. No, H. K., Park, N. Y., Lee, S. H. & Meyers, S. P. Antibacterial activity of chitosans and chitosan oligomers with different molecular weights. Int. J. Food Microbiol. ***74,*** *65–72 (2002).*
359. Yuan, Z.-X. et al. Randomly 50% N-acetylated low molecular weight chitosan as a novel renal targeting carrier. J. Drug Target. ***15,*** *269–278 (2007).*
360. Lee, E. et al. Conjugated chitosan as a novel platform for oral delivery of paclitaxel. J. Med. Chem. ***51,*** *6442–6449 (2008).*
361. Banche, G. et al. Low molecular weight chitosan nanodroplets as promising strategy for controlled antibiotic delivery against Streptococcus pyogenes skin infections. 28th European Congress on Clinical Microbiology and Infectious Diseases (ECCMID) 2018. Madrid, Spain, 21-24/04/2018 (2018).
362. Mandras, N. et al. Itraconazole-loaded chitosan-shelled nanodroplets as new nonconventional antifungal strategy against Candida albicans and C.glabrata infections in hypoxic chronic wounds. 28th European Congress on Clinical Microbiology and Infectious Diseases (ECCMID) 2018. Madrid, Spain, 21-24/04/2018 (2018).
363. Fenoglio, I. et al. Singlet oxygen plays a key role in the toxicity and DNA damage caused by nanometric TiO2 in human keratinocytes. Nanoscale ***5,*** *6567–76 (2013).*
364. Xia, X., Zhao, Y., Chen, A. & Mustoe, T. Differential activation of migration by hypoxia in keratinocytes isolated from donors of increasing age: implication for chronic wounds in the elderly. J Invest Dermatol ***116,*** *50–6 (2001).*
365. Kwon, J.-Y. et al. Remifentanil protects human keratinocytes against hypoxia-reoxygenation injury through activation of autophagy. PloS One ***10,*** *e0116982 (2015).*

366. Fang, J.-Y., Hung, C.-F., Hua, S.-C. & Hwang, T.-L. Acoustically active perfluorocarbon nanoemulsions as drug delivery carriers for camptothecin: drug release and cytotoxicity against cancer cells. Ultrasonics **49,** 39–46 (2009).
367. Wiegand, C., Winter, D. & Hipler, U.-C. Molecular-weight-dependent toxic effects of chitosans on the human keratinocyte cell line HaCaT. Skin Pharmacol. Physiol. **23,** 164–170 (2010).
368. Bianco, S., Mancardi, D., Merlino, A., Bussolati, B. & Munaron, L. Hypoxia and hydrogen sulfide differentially affect normal and tumor-derived vascular endothelium. Redox Biol. **12,** 499–504 (2017).
369. Teijeiro-Osorio, D., Remunan-Lopez, C. & Alonso, M. J. Chitosan/cyclodextrin nanoparticles can efficiently transfect the airway epithelium in vitro. Eur. J. Pharm. Biopharm. Off. J. Arbeitsgemeinschaft Pharm. Verfahrenstechnik EV **71,** 257–263 (2009).
370. Shang, L., Nienhaus, K., Nienhaus, G. U. Engineered nanoparticles interacting with cells: size matters. J. Nanobiotechnology **12,** 5–5 (2014).
371. Xie, S. et al. Biodegradable nanoparticles for intracellular delivery of antimicrobial agents. J. Control. Release Off. J. Control. Release Soc. **187,** 101–117 (2014).
372. Treuel, L., Jiang, X. & Nienhaus, G. U. New views on cellular uptake and trafficking of manufactured nanoparticles. J. R. Soc. Interface **10,** 20120939 (2013).
373. Johannes, L., Lamaze, C., Clathrin-dependent or not: is it still the question? Traffic Cph. Den. **3,** 443–451 (2002).
374. Ivanov, A. I. Pharmacological inhibition of endocytic pathways: is it specific enough to be useful? Methods Mol. Biol. Clifton NJ **440,** 15–33 (2008).
375. Thibault, M., Nimesh, S., Lavertu, M. & Buschmann, M. D. Intracellular trafficking and decondensation kinetics of chitosan-pDNA polyplexes. Mol. Ther. J. Am. Soc. Gene Ther. **18,** 1787–1795 (2010).
376. Schuler, G., Pohlin, G. & Fritsch, P. O. Differences of cell surface label distribution and redistribution patterns between mammalian keratinocytes and melanocytes in culture. J. Invest. Dermatol. **77,** 347–352 (1981).
377. Lulevich, V., Yang, H., Isseroff, R. R. & Liu, G. Single cell mechanics of keratinocyte cells. Ultramicroscopy **110,** 1435–1442 (2010).
378. Gill, S. E. & Parks, W. C. Metalloproteinases and their inhibitors: regulators of wound healing. Int. J. Biochem. Cell Biol. **40,** 1334–1347 (2008).
379. Nagase, H., Visse, R. & Murphy, G. Structure and function of matrix metalloproteinases and TIMPs. Cardiovasc. Res. **69,** 562–573 (2006).
380. Caley, M. P., Martins, V. L. & O'Toole, E. A. Metalloproteinases and wound healing. Adv. Wound Care **4,** 225–234 (2015).
381. Navarre, W. W. & Schneewind, O. Surface proteins of Gram-Positive bacteria and mechanisms of their targeting to the cell wall envelope. Microbiol. Mol. Biol. Rev. MMBR **63,** 174–229 (1999).
382. Liu, H., Du, Y., Wang, X. & Sun, L. Chitosan kills bacteria through cell membrane damage. Int. J. Food Microbiol. **95,** 147–155 (2004).
383. Chaffin, W. L., López-Ribot, J. L., Casanova, M., Gozalbo, D. & Martínez, J. P. Cell wall and secreted proteins of Candida albicans: identification, function, and expression. Microbiol. Mol. Biol. Rev. **62,** 130–180 (1998).
384. Brown, S., Santa Maria, J. P. & Walker, S. Wall teichoic acids of Gram-Positive bacteria. Annu. Rev. Microbiol. **67,** 10.1146/annurev-micro-092412-155620 (2013).
385. Helander, I. M., Nurmiaho-Lassila, E. L., Ahvenainen, R., Rhoades, J. & Roller, S. Chitosan disrupts the barrier properties of the outer membrane of Gram-Negative bacteria. Int. J. Food Microbiol. **71,** 235–244 (2001).

386. Jeon, S. J., Oh, M., Yeo, W.-S., Galvao, K. N. & Jeong, K. C. Underlying mechanism of antimicrobial activity of chitosan microparticles and implications for the treatment of infectious diseases. PloS One ***9,*** *e92723 (2014).*
387. Regiel-Futyra, A. et al. Development of noncytotoxic chitosan-gold nanocomposites as efficient antibacterial materials. ACS Appl. Mater. Interfaces ***7,*** *1087–1099 (2015).*
388. Rai, A., Prabhune, A. & Perry, C. C. Antibiotic mediated synthesis of gold nanoparticles with potent antimicrobial activity and their application in antimicrobial coatings. J. Mater. Chem. ***20,*** *6789–6798 (2010).*
389. Pena, A., Sanchez, N. S. & Calahorra, M. Effects of chitosan on Candida albicans: conditions for its antifungal activity. BioMed Res. Int. ***2013,*** *527549 (2013).*

SITOGRAPHY:
226. www.eo$_2$.com

CHAPTER 9.
PUBLICATIONS

Publications

- Full articles

  2017

  ARGENZIANO M., BANCHE G., LUGANINI A., **FINESSO N**., ALLIZOND V., GULINO G.R., KHADJAVI A., SPAGNOLO R., TULLIO V., GIRIBALDI G., GUIOT C., CUFFINI A.M., PRATO M., CAVALLI R. (2017). Vancomycin-loaded nanobubbles: A new platform for controlled antibiotic delivery against methicillin-resistant Staphylococcus aureus infections. International Journal of Pharmacology 523(1):176-188.

  2015

  BANCHE G., PRATO M., MAGNETTO C., ALLIZOND V., GIRIBALDI G., ARGENZIANO M., KHADJAVI A., GULINO G. R., **FINESSO N.**, MANDRAS N., TULLIO V., CAVALLI R., GUIOT C., CUFFINI A. M. (2015). Antimicrobial chitosan nanodroplets: new insights for ultrasound-mediated adjuvant treatment of skin infection. Future Microbiology 10: 929-939.

- Abstracts

  - Oral communications

    2017

    ARGENZIANO M., **FINESSO N.**, D'ALESSANDRO S., FUMAGALLI M., SANGIOVANNI E., GENOVA T., ZICOLA E., TROIA A., GIRIBALDI G., GUIOT C., CUFFINI A.M., DELL'AGLI M., BASILICO N., CAVALLI R., PRATO M. (2017). Comparative evaluation of different chitosan species and derivatives as candidate biomaterials for oxygen-loaded nanodroplet formulations to treat chronic wounds. 10th International Conference of Advanced Nano Materials (ANM2017) (Nanomedicine session) in Guildford (University of Surrey), UK, 11-13/09/2017. Abstract book, page 376.

2016

FINESSO N., LUGANINI A., BANCHE G., ALLIZOND V., GULINO G.R., GENOVA T., MAGNETTO C., TULLIO V., GIRIBALDI G., CUFFINI A.M., PRATO M. (2016). Antimicrobial oxygen-loaded nanobubbles as promising tools to promote wound healing in hypoxic human keratinocytes."Hypoxia 2016" in Nantes, France, 06-07/10/2016. Abstract book, pages 56-57.

FINESSO N., LUGANINI A., BANCHE G., ALLIZOND V., GULINO G.R., GENOVA T., MAGNETTO C., TULLIO V., GIRIBALDI G., CUFFINI A.M., PRATO M. (2016). Oxygen-loaded chitosan/perfluoropentane nanobubbles as promising antimicrobial devices to promote wound healing. 4th International Conference on Antimicrobial Research (ICAR2016) in Torremolinos-Malaga, Spain, 30/06-01/07/2016. Abstract book, page 129.

PRATO M., ARGENZIANO M., BANCHE G., **FINESSO N.**, LUGANINI A., ALLIZOND V., GULINO G.R., KHADJAVI A., SOSTER M., GIRIBALDI G., GUIOT C., CUFFINI A.M., CAVALLI R. (2016). Vancomycin-loaded dextran sulfate/perfluoropentane nanobubbles for controlled drug release against methicillin-resistant Staphylococcus aureus infections. 4th International Conference on Antimicrobial Research (ICAR2016) in Torremolinos-Malaga, Spain, 30/06-01/07/2016. Abstract book, page 246.

2015

ARGENZIANO M., SOSTER M., PRATO M., BANCHE G., **FINESSO N.**, ALLIZOND V., LUGANINI A., KHADJAVI A., GIRIBALDI G., CUFFINI A. M., GUIOT C., CAVALLI R. (2015). Vancomycin-loaded dextran sulfate-shelled/perfluoropentane-cored nanobubbles for antibiotic transdermal delivery. Crossing Biological Barriers - Advances in Nanocarrier Design for Targeted Drug Delivery in Dresden, Germany, 9-11/11/2015. Abstract book page 55.

- Poster communications

2018

BANCHE G., ALLIZOND V., **FINESSO N.**, ARGENZIANO M., LUGANINI A., TROIA A., GIRIBALDI G., KHADJAVI A., IANNANTUONI M.R., TULLIO V., MANDRAS N., PRATO M., CAVALLI R., CUFFINI A.M. (2018). Low molecular weight chitosan nanodroplets as promising strategy for controlled antibiotic delivery against *Streptococcus pyogenes* skin infections. 28th European Congress of Clinical Microbiology and Infectious Diseases (ECCMID2018) in Madrid, Spain, 21-24/04/2018.

MANDRAS N., ARGENZIANO M., ROANA J., SCALAS D., **FINESSO N.**, LUGANINI A., GIRIBALDI G., FUMAGALLI M., SANGIOVANNI E., D'ALESSANDRO S., BASILICO N., DELL'AGLI M., BANCHE G., ALLIZOND V., CAVALLI R., PRATO M., CUFFINI A.M., TULLIO V. (2018). Itraconazole-loaded chitosan-shelled nanodroplets as new nonconventional antifungal strategy against *Candida albicans* and *C.glabrata* infections in hypoxic chronic wounds. 28th European Congress of Clinical Microbiology and Infectious Diseases (ECCMID2018) in Madrid, Spain, 21-24/04/2018.

2017

PIAZZA S., FUMAGALLI M., PRATO M., SANGIOVANNI E., **FINESSO N.**, TROIA A., GIRIBALDI G., BASILICO N., DELL'AGLI M. (2017). Cutaneous hypoxia: effect of oxygen-loaded nanodroplets in human keratinocytes and fibroblasts. 38th National Congress of the Italian Society of Farmacology in Rimini, Italy, 25-28 October 2017.

BANCHE G., **FINESSO N.**, ALLIZOND V., PRATO M., LUGANINI A., TROIA A., GIRIBALDI G., KHADJAVI A., TULLIO V., MANDRAS N., ARGENZIANO M., CAVALLI R., GUIOT C., CUFFINI A.M. (2017). Antibacterial activity of chitosan-shelled oxygen-loaded nanobubbles and nanodroplets against MRSA in chronic wounds. 45th National

Congress of the Italian Society of Microbiology in Genova, Italy, 27-30/9/2017.

ARGENZIANO M., BANCHE G., LUGANINI A., **FINESSO N.**, ALLIZOND V., GULINO G.R., KHADJAVI A., SPAGNOLO R., TULLIO V., GIRIBALDI G., GUIOT C., CUFFINI A.M., PRATO M., CAVALLI R. (2017). Vancomycin-loaded nanobubbles as innovative and effective nanocarriers for controlled topical antibiotic delivery against methicillin-resistant Staphylococcus aureus infections. 21th International Symposium on Microencapsulation in Faro, Portugal, 27-29/9/2017.

FINESSO N., G. BANCHE, V. ALLIZOND, M. PRATO, A. LUGANINI, A. TROIA, G. GIRIBALDI, A. KHADJAVI, V. TULLIO, N. MANDRAS, R. CAVALLI, C. GUIOT, A.M. CUFFINI. (2017). Chitosan-shelled oxygen-loaded nanobubble and nanodroplet comparison: new insights into infected chronic wounds caused by MRSA. 27th European Congress of Clinical Microbiology and Infectious Diseases (ECCMID2017) in Vienna, Austria, 22-25/04/2017.

2016

FINESSO N., LUGANINI A., BANCHE G., MANDRAS N., ALLIZOND V., ARGENZIANO M., MAGNETTO C., SCALAS D., ROANA J., GIRIBALDI G., GUIOT C., CAVALLI R., TROIA A., TULLIO V., CUFFINI A.M., PRATO M. (2016). Confocal microscopy as a promising tool to predict the antimicrobial efficacy of chitosan nanodroplets. 2nd Microscopy Congress" in London, UK, 14-15/11/2016. Abstract book, P6, page no.9.

FINESSO N., PRATO M., BANCHE G., ALLIZOND V., MAGNETTO C., ARGENZIANO M., LUGANINI A., KHADJAVI A., TROIA A., GIRIBALDI G., CAVALLI R., GUIOT C., CUFFINI A.M. (2016). Chitosan/2H,3H-decafluoropentane nanodroplets as anti-bacterial and skin-friendly devices for ultrasound-triggered transdermal

delivery. 4th International Conference on Antimicrobial Research (ICAR2016) in Torremolinos-Malaga, Spain, 30/06-01/07/2016. Abstract book, page 187.

PRATO M., **FINESSO N.**, MANDRAS N., SCALAS D., ROANA J., MAGNETTO C., LUGANINI A., GULINO G.R., GENOVA T., TROIA A., GIRIBALDI G., CUFFINI A.M., TULLIO V. (2016). Oxygen-loaded chitosan/2H,3H-decafluoropentane nanodroplets as anti-fungal devices to promote wound healing. 4th International Conference on Antimicrobial Research (ICAR2016) in Torremolinos-Malaga, Spain, 30/06-01/07/2016. Abstract book, page 204.

2015

FINESSO N., BANCHE G., LUGANINI A., MAGNETTO C., ARGENZIANO M., SOSTER M., ALLIZOND V., GRIBAUDO G., TULLIO V., GUIOT C., CAVALLI R., CUFFINI A. M., PRATO M., GIRIBALDI G. (2015). Antimicrobial effects against MRSA and C. albicans of chitosan-shelled oxygenloaded nanobubbles and nanodroplets. 27th National Meeting "A. Castellani" of Biochemistry PhD Students in Brallo di Pregola (PV), Italy, 8-12/6/2015.

PRATO M., BANCHE G., MAGNETTO C., ALLIZOND V., GIRIBALDI G., ARGENZIANO M., KHADJAVI A., GULINO G.R., **FINESSO N**., MANDRAS N., TULLIO V., CAVALLI R., GUIOT C., CUFFINI A.M. (2015). Chitosan-shelled oxygen-loaded nanodroplets as innovative and nonconventional antimicrobial tools against methicillin-resistant Staphylococcus aureus and Candida albicans: new perspectives for an ultrasound-mediated adjuvant treatment of infected chronic wounds. 25th European Congress of Clinical Microbiology and Infectious Diseases (ECCMID2015) in Copenhagen, Denmark, 25-28/04/2015 (P1373).